

THE MONTREAL OPEN CLUSTERS AND ASSOCIATIONS (MOCA) DATABASE: A CENSUS OF NEARBY ASSOCIATIONS, OPEN CLUSTERS, AND YOUNG SUBSTELLAR OBJECTS WITHIN 500 pc OF THE SUN

JONATHAN GAGNÉ,^{1, 2} LESLIE MORANTA,^{1, 2, 3} JACQUELINE K. FAHERTY,³ JASON LEE CURTIS,^{4, 3} THOMAS P. BICKLE,⁵ DOMINIC COUTURE,^{1, 2} AMÉLIE CHIASSON DAVID,^{1, 2} KATIE CHRISTIE,^{1, 2} SAMANTHA LAMBIE,^{6, 7} ELISE LECLERC,^{1, 2} LIVIA POLIQUIN,^{1, 2} DANIKA BELZILE,¹ AND ERIC E. MAMAJEK⁸

¹Planétarium de Montréal, Espace pour la Vie, 4801 av. Pierre-de Coubertin, Montréal, Québec, Canada

²Trottier Institute for Research on Exoplanets, Université de Montréal, Département de Physique, C.P. 6128 Succ. Centre-ville, Montréal, QC H3C 3J7, Canada

³Department of Astrophysics, American Museum of Natural History, Central Park West, New York, NY, USA

⁴Department of Astronomy, Columbia University, 550 West 120th Street, New York, NY 10027, USA

⁵School of Physical Sciences, The Open University, Milton Keynes, MK7 6AA, UK

⁶Department of Physics and Astronomy, The University of Western Ontario, 1151 Richmond St, London, Ontario, N6A 3K7, Canada

⁷Institute for Earth and Space Exploration, The University of Western Ontario, 1151 Richmond St, London, Ontario, N6A 3K7, Canada

⁸Jet Propulsion Laboratory, California Institute of Technology, 4800 Oak Grove Drive, Pasadena, CA 91109, USA

Submitted to ApJS

ABSTRACT

We present the Montreal Open Clusters and Associations database (MOCAdb), a public MySQL database with a Python interface. MOCAdb provides a census of memberships for 10259 associations and open clusters within 500 pc of the Sun, with a comprehensive compilation of literature measurements such as spectral types, kinematics, rotation periods, activity indices, spectral indices, and photometry. All known substellar objects are cataloged in MOCAdb, along with 2943 public spectra, to enable the characterization of substellar association members. MOCAdb also features periodically updated calculations such as Galactic UVW space velocities. We use this compilation to construct mappings between independent association definitions, and to update the BANYAN Σ membership classification tool, which now includes 8125 associations. The BANYAN Σ model construction is improved to account for heterogeneous and correlated errors and to capture complex association shapes using Gaussian mixture models. Combined with Gaia DR3, this enabled us to identify 11535 yet unrecognized candidate members of young associations within 500 pc, mostly M dwarfs. Our results corroborate a recent observation that systematics up to $\approx 4 \text{ km s}^{-1}$ remain in Gaia DR3 radial velocities for A-type stars. We present an updated census of age-calibrated exoplanets and substellar objects: 134 age-calibrated exoplanet systems (plus 121 TESS exoplanet candidates), 99 of which did not appear to have known memberships so far, and 455 substellar (L0 or later) candidate members of young associations, 196 of which appear newly recognized. We bring the total of candidate isolated planetary-mass objects to 101, 53 of which are newly recognized candidate members.

Keywords: Brown dwarfs (185) — Exoplanets (498) — Free floating planets (549) — Open star clusters (1160) — Stellar ages (1581) — Stellar associations (1582)

1. INTRODUCTION

Young stellar associations near the Sun are valuable laboratories to study stellar evolution and refine age-dating methods because they contain groups of stars

spanning a wide range of masses that formed from the same molecular cloud within a short time period (e.g., Zuckerman & Song 2004; Torres et al. 2008). The associations closest to the Sun (within ≈ 70 pc) are particularly valuable because their members appear brighter,

but it also causes them to spread over larger areas of the sky, making their initial identification less straightforward than distant associations (Moranta et al. 2022). Obtaining reliable lists of members with low contamination by unrelated field stars is challenging and typically requires measuring the six-dimensional position and space velocity of each member. As these stars typically formed from a single molecular cloud, they share the same velocities typically within $\lesssim 1 \text{ km s}^{-1}$, allowing us to distinguish them from most field stars.

The study of nearby young stars recently benefited from a tremendous influx of data, in large part due to the highly successful Gaia mission (Gaia Collaboration et al. 2016b) which measured high-precision proper motions and parallaxes for more than a billion stars and heliocentric radial velocities for a subset of 33.8 million stars as of the third data release (Gaia Collaboration et al. 2023). This makes it possible to calculate the three-dimensional Galactic position and space velocities for a sample of stars much larger than was previously possible. These new data have led to the discovery of many new nearby young associations (e.g., see Oh et al. 2017; Kounkel & Covey 2019; Kounkel et al. 2020; Moranta et al. 2022; Meingast et al. 2019), new coronae around known open clusters (e.g., see Meingast & Alves 2019; Meingast et al. 2021), and a significant refinement in the shape and substructure of many star-forming complexes (e.g., see Kerr et al. 2021, 2022b,a; Liu et al. 2021; Kerr et al. 2023; Ratzenböck et al. 2023).

The coalescing of available data has also become a gradually more demanding task given the increasing number of available data sets. The construction of young star samples that benefit from the best available measurements is becoming ever more powerful, yet also a longer process; this situation will only become more pronounced with upcoming data releases from existing missions and imminent releases from the Vera Rubin Observatory (Ivezić et al. 2019) and the EUCLID mission (Laureijs et al. 2011).

In this paper, we present the Montreal Open Clusters and Associations (MOCA) database, whose objective is to coalesce currently available data for (1) all nearby associations within 500 pc of the Sun and (2) all currently known nearby substellar objects. This database was built with the intended goal of facilitating the age-dating of astrophysical objects in the Solar neighborhood, and the identification of age-calibrated exoplanet systems and substellar objects down into the planetary-mass regime.

Section 2 describes the starting samples of members of young associations that were used to construct a list of stars, associations, and substellar objects. Section 3

describes the structure of the MOCA database and its main tables. Section 4 describes a set of calculated quantities that are included in the MOCA database and will be periodically updated as new data come in. Section 5 presents a discussion based on the contents of the MOCA database. This includes an overview of the hierarchical relationships between nearby young associations, a refreshed version of the BANYAN Σ tool for membership classification based on improved models, empirical age-calibrated color magnitude diagrams, a search for new candidate members of known associations using Hipparcos and Gaia DR3 and more. A presentation of the user-accessible MOCAdb website is presented in Section 6, and this work is concluded in Section 7.

2. SAMPLE

This section describes the input sample of young associations and their members that were used to build the MOCA database.

2.1. Young Associations and open Clusters

We extended the initial list of members in nearby young associations, compiled in the BANYAN paper series (Malo et al. 2013; Gagné et al. 2014, 2018e) with a series of recent young association surveys based on the Gaia mission. These include papers from the SPYGLASS series and other studies of substructures in young stellar formation regions (Kerr et al. 2021, 2022b,a, 2023; Ratzenböck et al. 2023; Liu et al. 2021), clustering searches for new associations (Oh et al. 2017; Kounkel & Covey 2019; Kounkel et al. 2020; Moranta et al. 2022; Meingast et al. 2019), recent discoveries of nearby open cluster coronae (Meingast & Alves 2019; Meingast et al. 2021), and recent open cluster catalogs and surveys (Kharchenko et al. 2005; Platais et al. 1998; Castro-Ginard et al. 2020; Cantat-Gaudin & Anders 2020; Prisinzano et al. 2022; Hunt & Reffert 2023; Qin et al. 2023). We have also included associations that are currently not thought to be coeval or even physical (e.g., Hercules-Lyra of Gaidos 1998, and the Castor moving group of Barrado y Navascués 1998, see Mamajek 2015 for more details) for completeness, but those are marked with a special flag `is_real=0`.

The 10259 associations that we have considered are listed in Table 1 with some of their basic properties, and are stored in the database table `moca_associations` as described in Section 3.

2.2. Brown Dwarfs

We included all objects from the Ultracoolsheet (Best et al. 2024a)⁹ in the database, with their spectral types, memberships to young associations when available, and their kinematics in the MOCAdb. The Ultracoolsheet systematically includes all ultracool dwarfs (spectral types L0 and later) at distances up to ≈ 100 pc. Although most of the brown dwarfs in this list show no signs of youth or known memberships in young associations, we decided to include them all to facilitate future searches for brown dwarfs of intermediate ages (≈ 200 , Myr and older) and cold, young brown dwarfs (spectral types T0 and later, ie, ≈ 1300 , K and cooler) for which the signatures of low surface gravity (a consequence of youth) are not immediately obvious from low resolution spectroscopy.

3. DATABASE STRUCTURE

The MOCA database compiles not only young associations, their members, and substellar objects, but also a number of literature properties of individual stars, as well as calculations that are performed using a set of custom IDL and Python libraries which automatically update measurements when new data becomes available.

The MOCA database currently includes 147 tables, divided into six categories, from which the table name prefixes are determined.

- **moca_**: Tables containing unique identifiers used across the MOCA database along with their basic information (e.g., `moca_associations`),
- **cat_**: Tables containing subsets of astronomical catalogs, usually imported from an external database, linked with a MOCA object identifier (e.g., `cat_gaiadr3`),
- **data_**: Tables containing raw data, usually imported from the scientific literature or a `cat_` table (e.g., `data_radial_velocities`),
- **calc_**: Tables containing calculations performed as part of the MOCAdb infrastructure (e.g., `calc_radial_velocities_combined`),
- **mechanics_**: Other tables containing quantities necessary to the functioning of MOCAdb features (e.g., `mechanics_memberships_propagated`),
- **summary_**: Summary tables (or views) allowing users to quickly access a number of useful quantities (e.g., `summary_all_members`). Some summary tables are precomputed for efficiency.

Most of the foreign keys connecting the MOCAdb tables have column names starting with `moca_`, to indicate a database-wide identifier. Some of these identifiers are listed below:

- **moca_oid**: Unique identifier for a single star or substellar object,
- **moca_aid**: Unique identifier for a young association,
- **moca_pid**: Unique identifier for a publication’s bibliographic entry,
- **moca_psid**: Unique identifier for a photometric system,

The `moca_aid` keys are defined with a unique string identifier that is only composed of alphanumeric characters and underscore symbols (e.g., the β Pic Moving Group is linked with the keyword `BPMG`).

All MOCAdb tables are listed in Table 3 with their total number of columns and approximate numbers of rows at the time of publication, and detailed column descriptions can be found at <https://mocadb.ca/schema>.

A simplified flow chart that presents the mechanisms by which the MOCAdb tables are updated is shown in Figure 1. Membership lists are gathered from literature papers, from which unique `moca_oid` stars are imported, and cross-matched with a series of astronomical databases as described in Section 3.1. A set of various raw measurements are then derived from these astronomical databases (and from scientific papers directly), and form the base for various calculations performed in MOCAdb as described in Section 5.

Each table starting with the `data_` prefix includes a column `object_designation`, containing the identifier for the star listed in the original science paper or astronomical database where the data were obtained from. These unique identifiers are matched to a unique `moca_oid` identifier in the `mechanics_all_designations` table, which contains a list of all known identifiers for each unique star. All known designations are downloaded from the CDS service (Wenger et al. 2000) for stars with known CDS identifiers, and those additional designations are included in the `mechanics_all_designations` table. After all rows of the `data_memberships` table have been connected to a `moca_oid` identifier, those without a match in the `mechanics_all_designations` table are added to the database with Simbad or the relevant database matching their designation (e.g., Gaia DR3) along all of their CDS identifiers.

⁹ A persistent and versioned copy of the Ultracoolsheet is available on Zenodo at [doi:10.5281/zenodo.4169084](https://doi.org/10.5281/zenodo.4169084)

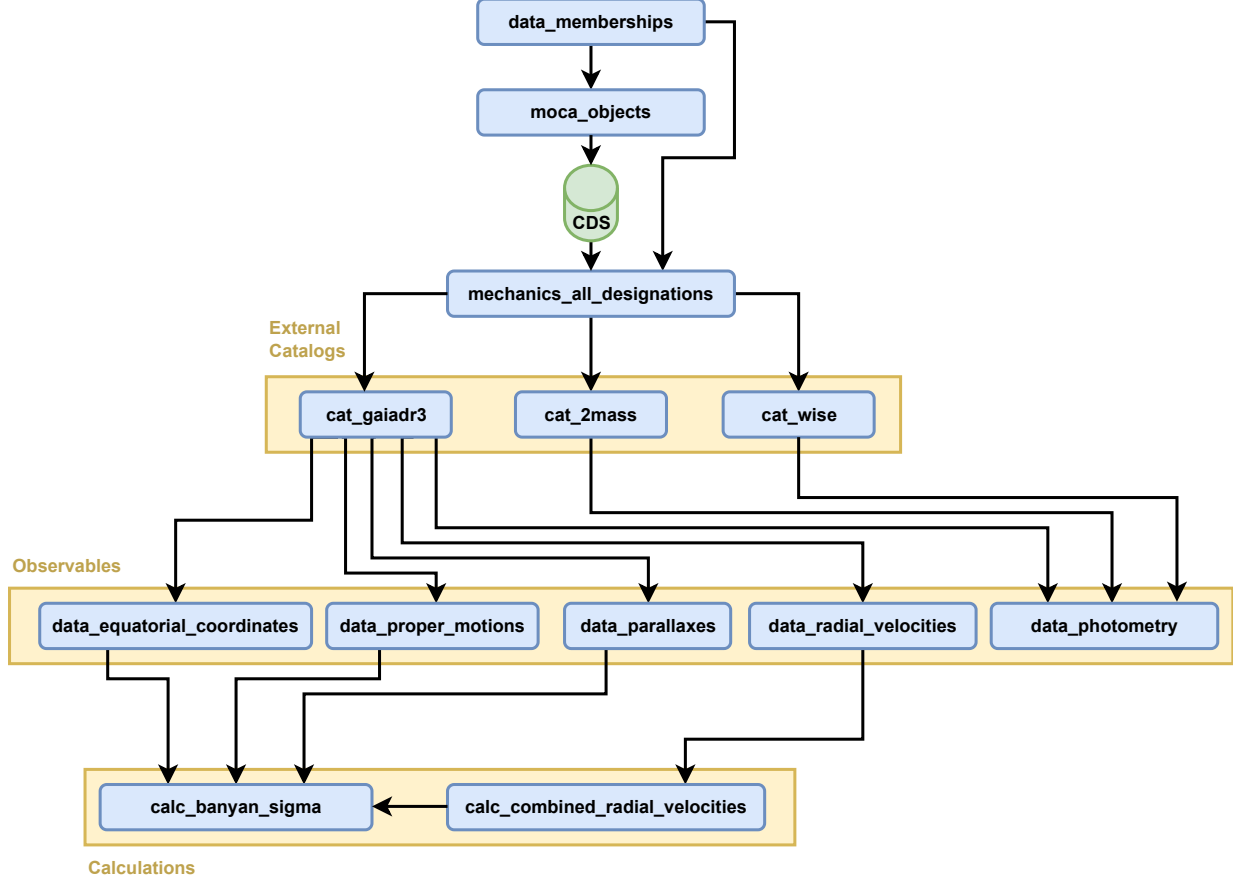


Figure 1. Flow chart of update algorithm in MOCAdb. Black arrows represent dependencies for calculations or data transfer. Astrophysical objects are mostly inserted into MOCAdb starting from the `data_memberships` table using the designations from the original paper. They are then cross-matched using CDS to compile all of their designations – the main designation is added to the `moca_objects` table with a new unique `moca_oid` integer identifier assigned by the database. These `moca_oid` identifiers are propagated back to the `data_memberships` table, and all alternate designations are ported to the table `mechanics_all_designations`. All designations relevant to one of the known online databases (such as Gaia DR3) are then used to download the relevant rows from the corresponding database into the corresponding `cat_` table, and MySQL procedures then port several observable quantities (such as radial velocities and proper motions) in the corresponding `data_` table in MOCAdb. These newly available observables trigger changes in the MD5 hashes used for calculations, and trigger a recalculations of the relevant properties for the `moca_oid` objects which gained new data. See Section 3 for more detail.

3.1. Cross-Matching and Catalog Data

All stars listed in the `moca_objects` table were automatically cross-matched to a set of 10 external astronomical databases using a set of custom libraries: Simbad, Gaia DR1, DR2 and DR3, Hipparcos, the The GALactic Archaeology with HERMES (GALAH) DR3, the Apache Point Observatory Galactic Evolution Experiment (APOGEE) DR11, the Radial Velocity Experiment (RAVE) DR6, ROSAT, and GALEX as described below, unless a designation specific to the catalog was already listed in Simbad, in which case that specific match was assigned. Catalog data were also downloaded for any source with a 2MASS, WISE, AllWISE, or CatWISE designation in Simbad.

All sources without a Gaia DR3 entry (mostly sub-stellar objects) and without a corresponding existing Simbad match were cross-matched with an additional set of 23 visible, red, or near-infrared catalogs: 2MASS, WISE, AllWISE, CatWISE, the Dark Energy Survey (DES) DR2, the Noirlab Souce Catalog (NSC) DR2, Pan-STARRS1 DR2, the Sloan Digital Sky Survey (SDSS) DR17, the UKIRT Hemisphere Survey (UHS) DR3, the VISTA Hemisphere Survey (VHS) DR6, the VISTA survey of the Magellanic Clouds system (VMC) DR5, VISTA Variables in The Via Lactea (VVV) DR5, the VVV Infrared Astrometric Catalogue (VIRAC) DR4, the SkyMapper Southern Survey (SMSS) DR4, the Southern Photometric Local Universe Survey (S-PLUS)

DR4, DENIS DR3, the DECam Plane Survey (DECAPS) DR2, the VISTA Kilo-degree Infrared Galaxy Survey (VIKING) DR4, the VISTA Deep Extragalactic Observations (VIDEO) DR5, and four DR11PLUS UKIRT InfraRed Deep Sky Surveys (UKIDSS; Deep Extragalactic Survey, DXS; Large Area Survey, LAS; Galactic Clusters Survey, GCS; and Galactic Plane Survey, GPS). All catalogs are listed in Table 5 with their references.

When a Gaia identifier is available, the ARI Gaia services¹⁰ are used to cross-match 2MASS (Skrutskie et al. 2006) or AllWISE (Kirkpatrick et al. 2014) designations with ARI’s `gaiadr2.tmass_best_neighbour`, `gaiadr2.allwise_best_neighbour`, `gaiadr3.tmass_psc_xsc_best_neighbour`, `gaiadr3.allwise_best_neighbour`, and `gaiadr3.dr2_neighbourhood` tables.

When no matches are found, cross-matches that account for the most accurate Gaia proper motion (when available) are made¹¹. Once all combinations of cross-matches have been exhausted, another SIMBAD query is performed with each of the available identifiers, and any resulting match is used to gather additional related identifiers. Data from the SIMBAD database, such as coordinates, spectral types, kinematics, photometry and object types are also automatically downloaded and included in the `cat_simbad` database table.

Individual designations that were identified for the 2MASS, WISE, AllWISE, CatWISE, Gaia DR1, Gaia DR2, Gaia DR3 (Skrutskie et al. 2006; Wright et al. 2010; Kirkpatrick et al. 2014; Marocco et al. 2021; Gaia Collaboration et al. 2016a, 2018, 2023) catalogs are used to automatically query the relevant entries of these catalogs, using the IRSA¹² and ARI¹³ servers, and are included to the MOCAdb tables `cat_2mass`, `cat_wise`, `cat_allwise`, `cat_catwise`, `allwise`, `gaiadr1`, `gaiadr2`, and `gaiadr3`, respectively. The Hipparcos table of van Leeuwen (2007) was included in its entirety in the `cat_hipparcos` table due to its modest size. Data from the ROSAT all-sky survey (Voges et al. 1999) was included in the `cat_rosat` table with automatic queries of the ViZieR tables IX/29/rass_fsc, IX/10A/1rxs, and IX/10A/1rxs_cor, with a 15” cross-match radius to account for the low astrometric precision of ROSAT. The best-available

proper motions were used to project the reference MOCAdb coordinate to the average ROSAT epoch (1995 ± 5 yr) to perform this cross-match, and the resulting astrometric uncertainty in the expected coordinates were added in quadrature to the base 15” cross-match radius.

A manual cross-match was performed with the `GALEXDR6PlusDR7` table (Bianchi et al. 2014) hosted at the Mikulski Archive for Space Telescopes (MAST)¹⁴, using the best available Gaia proper motion to the average GALEX epoch (2005.5) with a 30” cross-match radius: this accounts for both the limited astrometric precision of GALEX (5”), and a further 25” for the range of GALEX epochs (2003–2008) with proper motions as large as 8.3 as yr^{-1} . Once all possible matches have been identified with a database source star, only those that match within the uncertainty of proper motions and GALEX epoch (2.5 yr) were identified, and only the best-matching (nearest) database sources to a given GALEX entry were preserved in cases where a single GALEX entry was a potential match to more than one MOCA database entry.

All sources without Gaia counterparts were also automatically cross-matched with a set of infrared or red-optical catalogs, listed in Table 5. Mis-matches can occasionally occur due to source confusion especially in crowded fields near the Galactic plane; these are identified based on color outliers and visual checks, and are manually corrected as they are encountered.

3.2. Companions and Co-Moving Stars

A table `moca_companions` is used to keep track of all `moca_oid` identifiers that are related to each other gravitationally. This includes co-moving or companions stars, substellar objects, or exoplanets that have a distinct MOCAdb entry. Typically, only those objects with a resolved spectroscopic or photometric spectral types, or separate entries in the Gaia, Pan-STARRS or WISE catalogs, have a separate entry in the MOCAdb to simplify the treatment of unresolved objects. Unlike in the SIMBAD database, no unique `moca_oid` identifiers are assigned to a system of objects. For example, the TW Hya association member TWA 13 AB has three distinct entries in Simbad: one for TWA 13 AB as a system (CD-34 7390), one for CD-34 7390 A, and one for CD-34 7390 B. In MOCAdb, only two entries correspond to this system: TWA 13 A (`moca_oid=7254`) and TWA 13 B (`moca_oid=7255`), with a hierarchical link from TWA 13 B to TWA 13 A in the `moca_companions` table. We assign the entry of any catalog (such as 2MASS) to the primary star when the companion is not

¹⁰ Available at <https://gaia.ari.uni-heidelberg.de/index.html>

¹¹ The nearest entries within $\approx 100 \text{ pc}$ were vetted using the `finder_charts` library available at https://github.com/jgagneastro/finder_charts.

¹² Available at <https://irsa.ipac.caltech.edu>.

¹³ Available at <https://gaia.ari.uni-heidelberg.de/tap.html>.

¹⁴ Available at <https://archive.stsci.edu/>.

resolved. This approach simplifies the treatment of binary stars, while still allowing to determine which stars are resolved or not based on the spatial resolution of individual catalog and projected angular separations between the components. More complex hierarchical cases are managed by establishing a link between any companion to the primary star of a given center of mass of a hierarchical link; for example, a hierarchical link points TWA 4 Bb to TWA 4 Ba, and another link points from TWA 4 Ba to TWA 4 Aa in `moca_companions`. A further advantage of the simple approach adopted here is that a new entry in the `moca_objects` table can be added for any newly identified companion, along with its relationship in the `moca_companions` table, without having to change the entry of the parent object.

3.3. Coordinates, Proper Motions and Parallaxes

All available coordinates were assembled from the various catalogs described in Section 3.1 and ported to the `data_equatorial_coordinates` table along with epochs and measurement errors, when available. The one row per `moca_oid` with the most useful reference epoch, with a known `measurement_epoch_yr` when possible, and including the proper motion (`pm_corrected=1`) and parallax motion (`plx_corrected=1`) when possible, is flagged with `adopt_as_reference=1`. This is the row that should be preferred when calculating projected coordinates at a future epoch, for example. Galactic and ecliptic coordinates are also available in two MySQL views (`calc_ecliptic_coordinates` and `calc_galactic_coordinates`), and are computed on-the-fly only for the reference equatorial coordinates.

The proper motions and parallaxes were compiled in the respective tables `data_proper_motions` and `data_parallaxes` along with their measurement errors and epochs. The `adopted` and `ignored` flags allow the MOCAdb maintenance libraries to either choose the single best measurement for a source when desired (`adopted=1`), or choose all good-quality measurements (`ignored=0`) when multi-epochs measurements are required¹⁵.

We have also included proper motions and parallaxes from a wide range of literature publications in the two respective tables, in addition to those obtained directly from the catalog tables.

3.4. Radial Velocities

Individual radial velocity measurements were compiled in the `data_radial_velocities` table from 916

distinct literature catalogs. 92% of the total measurements came from 9 catalogs (Gaia Collaboration et al. 2023; Trifonov et al. 2020; Gaia Collaboration et al. 2018; Jönsson et al. 2020; Soubiran et al. 2018; Kharchenko et al. 2007; Gontcharov 2006; Abolfathi et al. 2018; Steinmetz et al. 2020).

We avoided including any radial velocity measurements that are predictions based on kinematic models (e.g., Madsen et al. 2002; Malo et al. 2014; Bobylev & Bajkova 2007) or combinations of other sources in the literature. We included a column `n_measurements` to keep track of radial velocity measurements that arise from a combination of several raw measurements, such as is the case with Gaia DR3 radial velocities.

There were a few catalogs that did not provide radial velocities on an absolute frame-of-reference, but only relative radial velocities with the explicit goal of identifying exoplanet systems. These relative radial velocities were included in the `data_relative_radial_velocities` table for completeness, and were used to estimate the standard deviations of the radial velocity of individual sources in the `data_relative_radial_velocities_std` table.

3.5. Projected Rotational Velocities

Projected rotational velocities $v \sin i$ were collected in the MOCAdb table `data_vsini` from spectroscopic measurements in the literature. The Gaia DR3 release (Gaia Collaboration et al. 2023; Creevey et al. 2023) also provides two measurements that are related to projected rotational velocities, both of which have specific regimes where they are useful, and are subject to distinct biases. We describe in how we have included them in MOCAdb in the remainder of this section.

3.5.1. Projected Rotational Velocity Biases in Gaia DR3

Stars observed by Gaia with G_{RVS} magnitudes brighter than 16.2 (Katz et al. 2023) have their 846–870 nm Radial Velocity Spectrometer (RVS) spectra analyzed to determine their radial velocity. This is done by matching a Doppler-shifted synthetic spectrum (David et al. 2014; Sartoretti et al. 2018) broadened by the instrumental spectroscopic line spread function as well as an additional free line-broadening parameter `vbroad` that is modelled with a traditional rotation kernel. This parameter `gaiadr3.vbroad`¹⁶ is stored in the main Gaia DR3 source catalog, and it is named `vbroad` rather than $v \sin i$ to outline the fact that it

¹⁵ These tasks are recalculated every few minutes when required, using MySQL events.

¹⁶ See https://gea.esac.esa.int/archive/documentation/GDR3/Gaia_archive/chap_datamodel/sec_dm_main_source_catalogue/ssec_dm_gaia_source.html#gaiadr3.vbroad.

accounts not only for stellar rotation, but also other phenomena such as macro-turbulence or pulsations. It is worth noting, however, that this is also true of most other measurements and catalogs in the literature which are referred to as $v \sin i$, and hence Gaia DR3's v_{broad} should be directly comparable to those, after consideration of systematics and measurement errors. Our comparison of Gaia DR3's v_{broad} measurements to literature $v \sin i$ show reasonable agreement (see Figure 2(a)). (Frémat et al. 2023) performed a similar comparison with various $v \sin i$ catalogs and found that the `gaiadr3.vbroad` values tend to be over-estimated for $v \sin i < 10 \text{ km s}^{-1}$ and that the measurement quality degraded for stars with $T_{\text{eff}} > 7500 \text{ K}$ (spectral types earlier than approximately A8) and G_{RVS} magnitudes fainter than 10. We observe a similar trend, and find that applying a selection threshold of `gaiadr3.vbroad` $\geq 12 \text{ km s}^{-1}$ is sufficient to exclude these systematically over-estimated Gaia DR3 measurements. We also observe a standard deviation larger than what is expected if we only consider the reported errors in the Gaia DR3 main source catalog (`gaiadr3.vbroad_error`). We find that an extra error term must be added in quadrature in order for the deviations to be comparable to the expected errors: for stars with effective temperatures (`gaiadr3.rv_template_teff`) in the range 4,000–7,000 K, an additional 5 km s^{-1} error is sufficient, but for stars both cooler and hotter, we find that an additional error term of 14.5 km s^{-1} is required. Additionally, we observe a noticeable increase of outliers above the expected error bars (even when inflated) for values of `gaiadr3.vbroad` with a measurement error larger than 5 km s^{-1} (see Figure 3). For these reasons, we chose to only include the measurements with `gaiadr3.vbroad` $\geq 12 \text{ km s}^{-1}$ and `gaiadr3.vbroad_error` $\leq 5 \text{ km s}^{-1}$ in MOCAdb, and we added the extra error terms described above in quadrature.

In addition to the `gaiadr3.vbroad` measurement, another estimation of a star's $v \sin i$ is performed in the Gaia DR3 Apsis pipeline (Creevey et al. 2023), and reported in `astrophysical_parameters.vsini_esphs` (Fouesneau et al. 2023)¹⁷ for early-type stars with $T_{\text{eff}} > 7500 \text{ K}$. While these values are measured with a method similar to `gaiadr3.vbroad`, the measurements are performed by different pipeline which rely on a joint analysis of the BP/RP low-resolution spectra and the RVS spectra to determine the as-

trophysical parameters of early-type stars, therefore the resulting $v \sin i$ measurements should benefit from more carefully selected synthetic spectra that are specific to early-type stars and consistent with the low-resolution BP/RP spectra. A similar comparison of these `astrophysical_parameters.vsini_esphs` values with other projected rotational velocities cataloged in the literature show reasonable correlation for `astrophysical_parameters.vsini_esphs` values above 20 km s^{-1} (see Figure 2(b)), which we select are our inclusion threshold. Figure 3 shows that an extra error term of 26 km s^{-1} needs to be added in quadrature to the Gaia DR3 `astrophysical_parameters.vsini_esphs` values to obtain reasonable residuals, which we included when importing the measurements in MOCAdb.

3.6. Spectra

The MOCAdb currently contains 2943 non-duplicated spectra, mostly from the SpeX Prism Library¹⁸, the IRTF Spectral Library¹⁹ (Rayner et al. 2003), the Montreal Spectral Library²⁰ and the Ultracool RIZzo spectral library²¹. Each unique spectrum is described in a row of the `moca_spectra` table, with its header properties and a unique `moca_specid` identifier. The data associated with these spectra (wavelengths, spectral flux densities and measurement errors) are stored in the `data_spectra` table, which is linked through the `moca_specid` identifier. The spectra can be visualized and downloaded at <https://dataviz.mocadb.ca/spectra>, and were used to calculate secondary quantities described in Section 4.10.

3.7. Spectral Indices and Equivalent Widths

Measurements of spectral equivalent widths of the Li I $\lambda 6708 \text{ \AA}$ and $\text{H}\alpha \lambda 6563 \text{ \AA}$ lines are listed in the `data_equivalent_widths` table, and spectral indices ($\log R'_{\text{HK}}$ and Mount Wilson S -index, mostly from Zhang et al. 2020; Isaacson & Fischer 2010; White et al. 2007) are listed in the `data_spectral_indices` table. Measurements currently listed in both tables are compilations from the literature.

¹⁸ Available at <https://cass.ucsd.edu/~ajb/protect/penalty/z@browndwarfs/spexprism>.

¹⁹ Available at https://irtfweb.ifa.hawaii.edu/~spex/IRTF_Spectral_Library/.

²⁰ Available at <https://jgagneastro.com/the-montreal-spectral-library/>.

²¹ Available at <https://jgagneastro.com/the-ultracool-rizzo-spectral-library/>.

¹⁷ See https://gea.esac.esa.int/archive/documentation/GDR3/Gaia_archive/chap_datamodel/sec_dm_astrophysical_parameter_tables/ssec_dm_astrophysical_parameters.html#astrophysical_parameters-vsini_esphs.

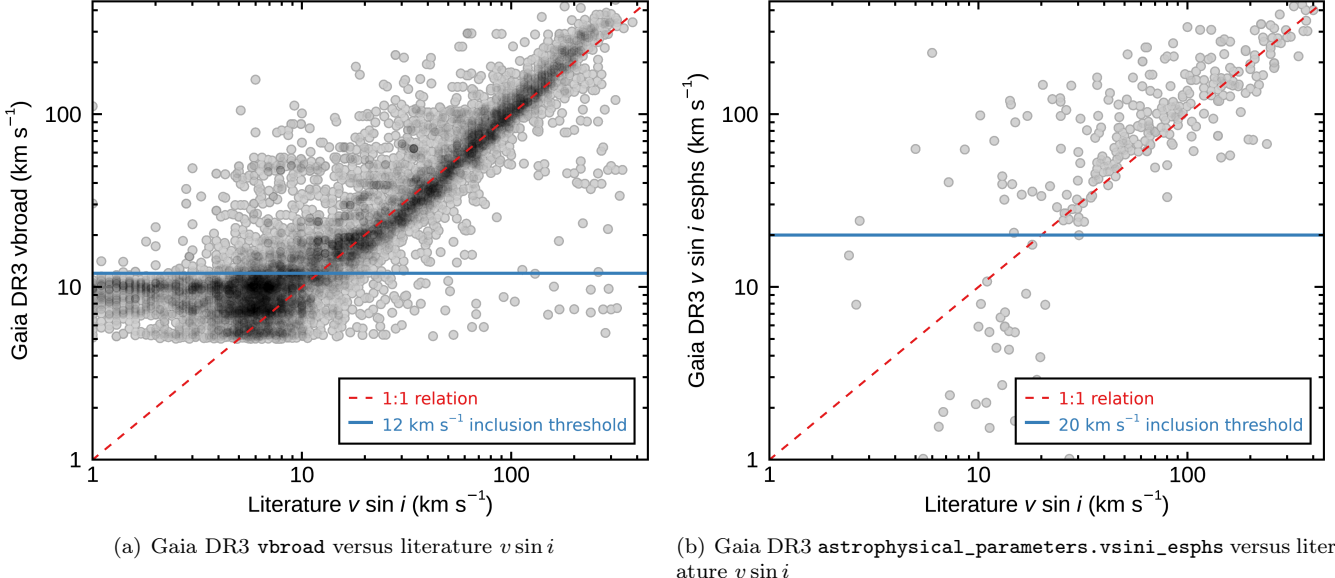


Figure 2. Gaia DR3 v_{broad} and $v \sin i$ measurements based on two distinct pipelines, compared with literature $v \sin i$ measurements. The Gaia DR3 v_{broad} measurements are representative of literature values above 12 km s^{-1} and the Gaia DR3 $v \sin i$ measurements are representative of literature values above 20 km s^{-1} . We have therefore chosen these respective thresholds for their inclusion in MOCAdb as a valid value for $v \sin i$. See Section 3.5.1 for more details.

4. CALCULATION OF DERIVED QUANTITIES

This section describes a number of parameters that are derived as part of the MOCAdb maintenance routines. In all MOCAdb calculations, the basic ingredients required for the calculation are combined into an MD5 hash that is stored in a column named `md5_uid`, which allows to only refresh the calculations when the data have changed for a specific object and quantity. Custom IDL and Python routines are regularly started to refresh all of the calculated quantities, along with the associated time stamps (`created_timestamp` or `modified_timestamp`) associated with the calculations²². These operations are also cataloged in the `moca_changelog` table.

4.1. Distances

We used the method of Bailer-Jones et al. (2021) to estimate the distances of every source in MOCAdb with a parallax measurement available in the `data_parallaxes` table. We elected to use the geometric prior of Bailer-Jones et al. (2021) in all cases, because a significant fraction of MOCAdb stars are young, which would complicate the use of photometry. A 10^4 -element Monte Carlo simulation is performed for every star to propagate the parallax measurement error onto the dis-

tance, and the 1 - to 3σ measurement errors are listed along with the best estimate in the `data_distances` table. A similar method was applied to all available parallaxes in MOCAdb, including the Hipparcos measurements and other literature sources.

The `data_distances` table can also accept photometric distance estimates from the literature, indicated with the flag `photometric_estimate=1`. For every `moca_oid` object in the `data_distances` table, the single best value is designated with the flag `adopted=1`. Trigonometric distances are systematically preferred over the photometric ones regardless of measurement errors; the Gaia DR3 values are preferred over Gaia DR2 distances, and otherwise distances with the smallest measurement errors are selected.

A MySQL view `calc_vtan` allows to query the tangential velocities (obtained by multiplying the distances with proper motions) of every object in MOCAdb, using their respective adopted values. These are computed on-the-fly when queried.

4.2. Galactic Coordinates

The XYZ Galactic coordinates of all objects with a distance in the `data_distances` table were calculated and are listed in the table `calc_xyz`. They are based on a 10^4 -element Monte Carlo simulation for error propagation, using the full probability distribution function of the distance estimates (which are in most cases based on the method of Bailer-Jones et al. (2021) as described in Section 4.1). We adopt the definition of XYZ axes

²² Specific calculation tasks are launched continuously on different hours and days of the week from an external computer, and simpler MySQL-only tasks, such as adopting the best calculation, are performed every few minutes with MySQL events

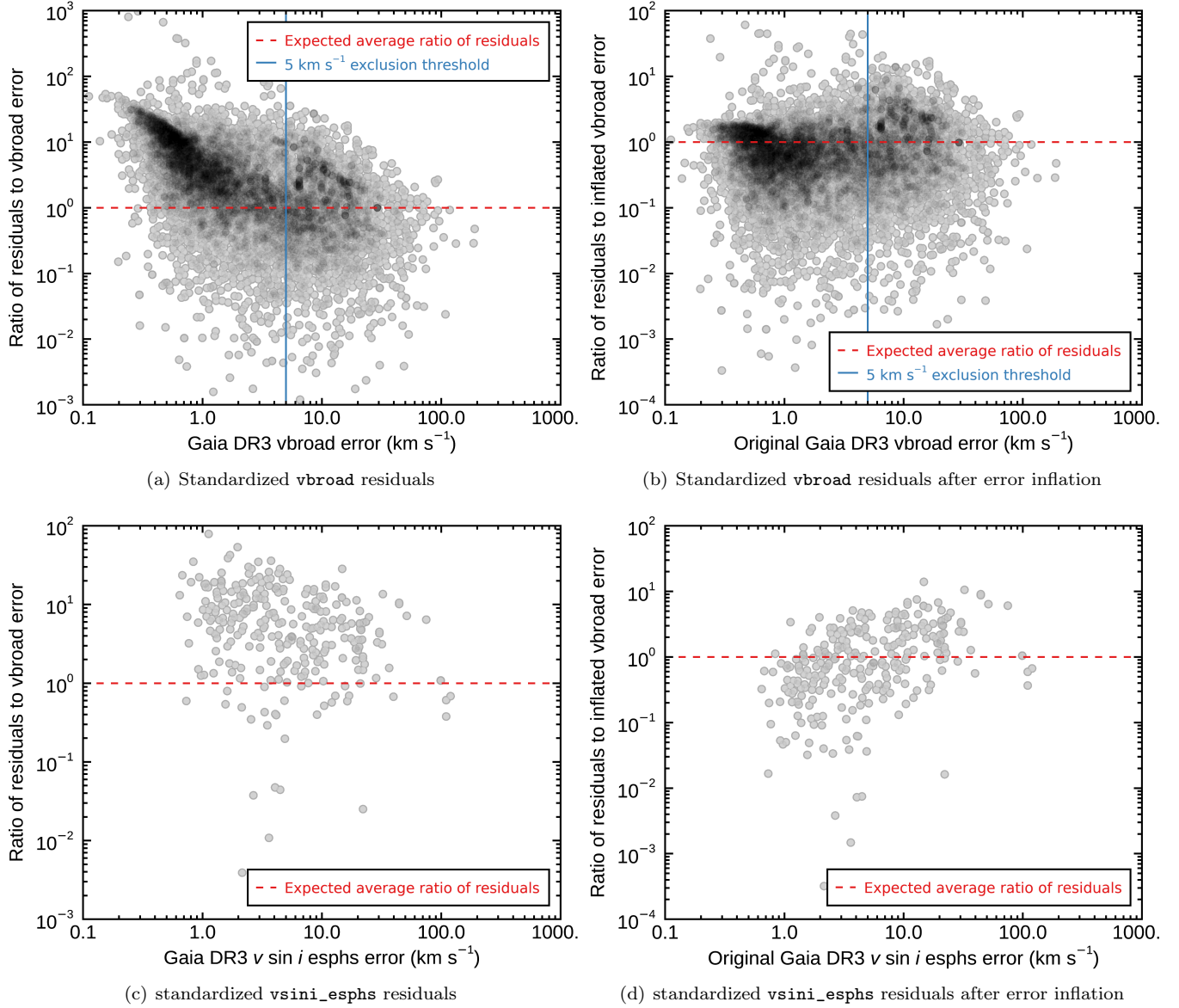


Figure 3. Upper panels: Gaia DR3 v broad errors compared with the error-normalized residuals for stars with a literature $v \sin i$ measurement (left). If the measurement errors of the Gaia DR3 v broad and the literature $v \sin i$ are realistic, normalized residuals should cluster around 1.0 (horizontal, red dashed line), which is not the case, indicating that an extra error term should be added in quadrature to the Gaia DR3 v broad errors. Once an extra error is added (5 km s^{-1} for stars with T_{eff} in the range 4,000–7,000 K, or 14.5 km s^{-1} for other stars), the normalized residuals (right) behave as expected. The selection threshold based on the raw Gaia DR3 v broad errors (5 km s^{-1}) for MOCAdb inclusion is also displayed with a vertical blue line. Bottom panels: idem but for the Gaia DR3 $v \sin i$ measurements determined by the Gaia DR3 Apsis pipeline, which warranted the inclusion of a 26 km s^{-1} error term in quadrature. See Section 3.5.1 for more details.

used in the IDL `astrolib` package, which forms a right-handed rectangular coordinates system centered on the Sun, with X pointing towards the Galactic Center. The complete map of XYZ coordinates for individual stars in MOCAdb is displayed in Figure 4.

4.3. Extinction

The method described by Gagné et al. (2020a) was used to estimate the extinction towards each source

in the database. A numerical integration of the 3D extinction map *STructuring by Inversion of the Local InterStellar Medium* (STILISM; Lallement et al. 2014; Capitanio et al. 2017; Lallement et al. 2018)²³ towards each star is performed, based on the best-available coordinates and parallax measurement (inverted using the

²³ Available at <https://stilism.obspm.fr>

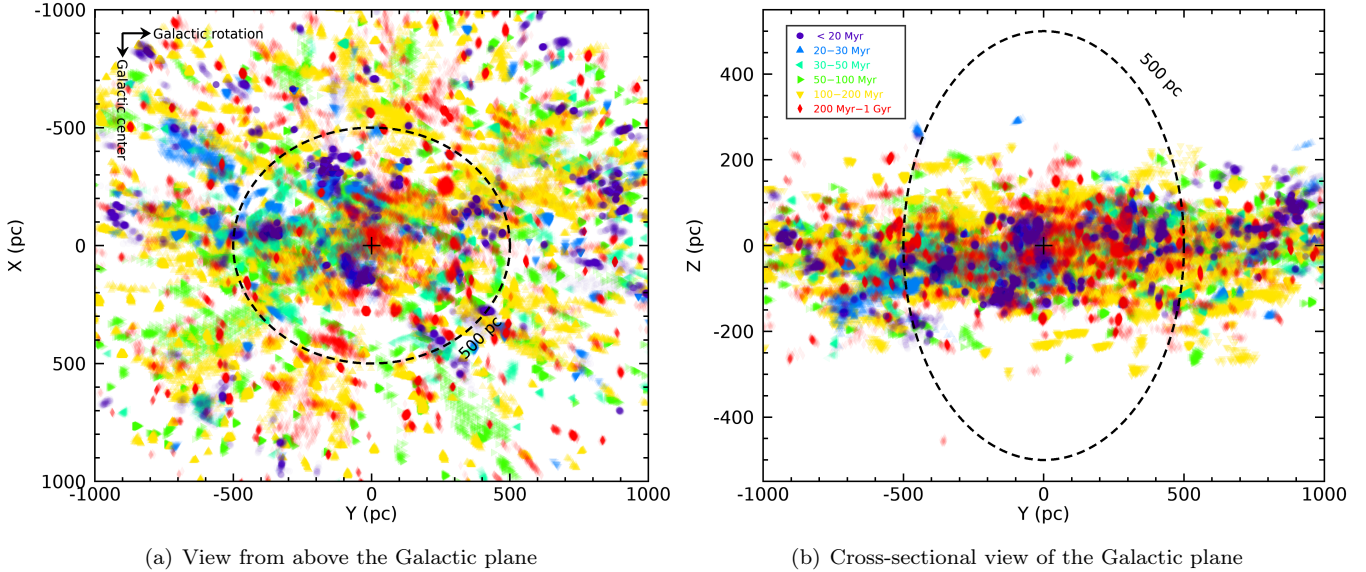


Figure 4. Galactic positions of individual stars in MOCAdb, color-coded by their association age. This figure shows how different age populations are not homogeneously distributed spatially, and how the nearby youngest stars are distributed along a plane that is slanted with respect to $Z = 0$. The MOCAdb census is mostly complete at distances up to 500 pc, marked within the dashed line.

method of Bailer-Jones et al. (2021) with a geometric prior). A Monte Carlo simulation, where 10^4 synthetic sets of equatorial coordinates and trigonometric distances are taken according to the best available measurements (the standard deviation of the Monte Carlo draws are set to the measurement errors). The corresponding XYZ Galactic coordinates are then calculated and used to integrate the STILISM map to obtain Monte Carlo realizations of interstellar extinction, along with the asymmetrical uncertainties provided by the STILISM map for each realization. The standard deviation of the Monte Carlo realizations was added in quadrature to the average asymmetrical STILISM uncertainties to obtain a final measurement error on the extinction, and the numerical integration of the STILISM map toward the most likely Monte Carlo distance was taken as the center of the extinction measurement.

4.4. Photometry

The individual photometric measurements of all surveys described in Section 3.1 were compiled in the `data_photometry` table, along with their epochs and measurement errors when available. The method of Gagné et al. (2020a) was used to correct the photometric reddening due to interstellar extinction on Gaia DR3 photometry. This method consists of numerically integrating the instrumental bandpass of the corresponding photometric band with a Fitzpatrick (1999) extinction curve anchored on the STILISM-based extinction measurements described in Section 4.3, weighed by the spec-

tral energy distribution of the corresponding spectral type in the Pickles library (Pickles 1998) corresponding to the spectral type of the star²⁴. Stars without known spectral types were corrected for extinction using the iterative method described by Gagné et al. (2020a). Each iteration of this method consists in estimating a spectral type based on the Gaia colors, using it to estimate extinction, using the corrected photometry to estimate a new spectral type, and repeating until the estimated spectral type converges²⁵. The `extinction_corrected` flag is set to 1 in the `data_photometry` table when the extinction was corrected successfully. The Gaia DR3 raw photometry that is not corrected for extinction is available in the `cat_gaiadr3` table directly, and we avoided also storing it in `data_photometry` table to improve the database efficiency.

4.5. Photometric Spectral Types

Photometric measurements and spectral types contained in the `data_photometry` and `data_spectral_types` tables were used to construct empirical sequences of spectral type to Gaia DR3 $G - G_{\text{RP}}$ colors, which we found were not significantly affected by age (see Figure 5), similarly to the spectral

²⁴ Consequently, extinction corrections were applied only for spectral types in the range O5–M6, and were not applied for giants, white dwarfs or substellar objects.

²⁵ Giants and white dwarfs were excluded from these calculations based on the position of the star in the Gaia DR3 color-magnitude diagram.

type–color sequences based on Gaia DR2 colors Gagné et al. (2020a).

We developed a method for fitting astrophysical sequences that relies on a Lagrangian approach similar to the radial velocity fitting method of (Allers et al. 2016). This approach is particularly useful for fitting spectral type–color or color–magnitude sequences, which typically contain many more objects at the red end due to the prevalence of M dwarfs, and simplifies determining the optimal number of fitting parameters. Standard polynomial fitting methods tend to over-fit the red end of such astrophysical sequences, and often require the fine-tuning of the polynomial order to obtain a reasonable fit.

In this Lagrangian approach, the free parameters are represented by anchor points with horizontal locations equally spaced in the astrophysical diagram, and with vertical locations adjusted to optimize the fit. A log-likelihood approach is used to determine the goodness-of-fit, assuming normally distributed measurement errors. The free model parameters that are optimized include the N anchor points, plus one parameter to represent the intrinsic standard deviation of the observed data around the sequence, which added in quadrature to the measurement errors when computing the log-likelihood. Optional parameters allow to consider alternate hypotheses in the log-likelihood calculation, consisting of:

- A penalty factor for high-order variations in the modelized sequence, which lowers the log-likelihood proportionally to the square of its second derivative;
- an outlier hypothesis, where the log-likelihood is computed as 10% of the regular log-likelihood plus a fixed value corresponding to a 3σ outlier; and
- a binary hypothesis (useful for color–magnitude diagrams), where the vertical location of the sequence is shifted by a 0.75 mag with an adjustable prior probability.

We found that the use of these alternate hypotheses allowed us to model a wide number of astrophysical sequences without needing to adjust any parameter except for the number of anchor points, which is typically in the range 20–30. Crucially, the resulting sequences visually fit the data equally well independently of the chosen number of anchors, with the caveat that too few anchor points tend to smooth over physical variations, and too many anchor points tend to over-fit high-order variations in the data, especially on the blue end where fewer stars are usually sampled.

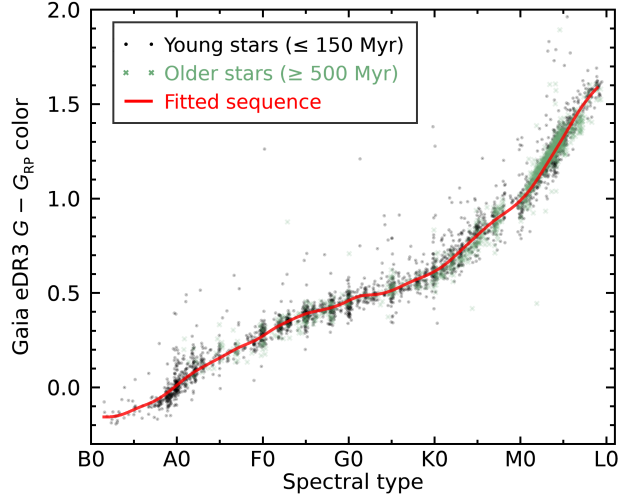


Figure 5. The best-fitting spectral type to Gaia DR3 sequence (red line) for stars younger than 150 Myr (black circles) and older than 500 Myr (green x symbols), as described in Section 5.4. We observe no significant systematic differences between younger and older stars in this particular parameter space, which allows us to assign color-based spectral type estimates independent of stellar ages.

A Markov chain Monte Carlo approach was used to sample the log-likelihood of this Lagrangian approach, using 10^4 Monte Carlo steps including a 3000-element burn-in phase. This method was applied to derive an underlying sequence to the spectral type–Gaia DR3 color data. The result is presented in Figure 6.

4.6. Fundamental Parameters

This section describes the determination of the fundamental parameters (ages, effective temperatures, masses, and radii) of stars and substellar objects in the MOCAdb database. The effective temperatures, masses, and radii are calculated with a focus on accuracy using empirical methods that are free of model assumptions when possible, at the cost of a significantly lower precision. We chose this approach in order to minimize biases and the impact of unresolved binaries on the determination of secondary quantities and allow reliable parameter estimates for a large number of objects with minimal human supervision. Robust but low-precision fundamental parameters are particularly useful to compute the initial mass function of a young association and to correct the impacts of gravitational redshift and convective blueshift on the heliocentric radial velocities of their members. We note that this approach is not optimal to constrain the properties of a star or its exoplanets with high precision. However, high-precision measurements calculated with other methods can still be included in MOCAdb for this purpose.

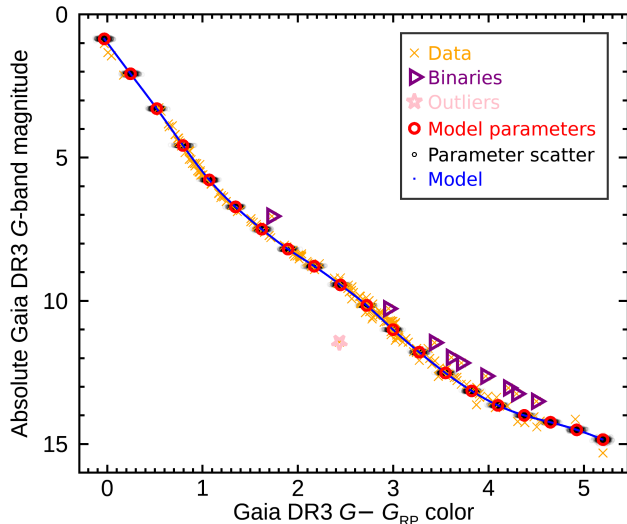


Figure 6. Example best-fitting sequence for members of the AB Dor moving group in a Gaia DR3 color-magnitude diagram, using the Lagrangian method described in Section 5.4. Model parameters are shown with red circles; their colors are fixed, and their absolute G -band magnitude are determined by the fitting algorithm, and are then used to construct the best-fitting sequence (blue line) with a spline. Individual stars that best matched the ‘young sequence’ Bayesian hypothesis are shown as orange x symbols, whereas those that matched the ‘binary sequence’ and ‘outlier’ hypotheses are shown with purple triangles and pink stars, respectively.

We did not attempt to determine the fundamental parameters of giant stars or white dwarfs as part of this work; however, literature measurements can be included in the relevant tables as needed in the future.

4.6.1. Literature Ages

A literature compilation of the ages of young associations is included in the `data_association_ages` table along with details of the age-dating method. We used the `association_ages.adopted` column to designate the most reliable age estimate for each association. These association ages are taken as a reference to determine the age as well as the other fundamental parameters of their members, as described in the remainder of this section.

4.6.2. Effective Temperatures

We used the spectral type– T_{eff} sequences of Pecaut & Mamajek (2013) extended with those of Filippazzo et al. (2015), both based on spectral energy distributions, to estimate the effective temperatures of all stars and substellar objects in MOCAdb. It is well known that pre-main sequence stars as well as brown dwarfs follow unique spectral type-to-effective temperature sequences. We have adopted the pre-main-sequence rela-

tions of Pecaut & Mamajek (2013) and Filippazzo et al. (2015) for stars and substellar objects that are likely members of associations 200 Myr or younger, and the main-sequence or field brown dwarf relations for all other objects (as shown in Figure 7). As a consequence, stars that have plausible membership to more than one association have multiple effective temperature calculations (one per pair of unique `moca_oid` and `moca_aid` identifiers).

The effective temperatures are calculated with a 10^4 -element Monte Carlo simulation. Synthetic values for spectral types are drawn randomly following the adopted spectral type measurement in the `data_spectral_types` table (the standard deviation is set to the measurement error, usually 0.5 subtypes). Each synthetic value is transformed to a T_{eff} value using the sequence of the appropriate age, and the medial absolute deviation of the resulting T_{eff} distribution in log space is taken as the measurement error that arises from the propagation of the spectral type error. Errors associated with the empirical spectral type– T_{eff} sequences were taken as the standard deviation of reference stars used to build these sequences around the expected T_{eff} values, from which we obtained uncertainties of 100 K for stars M5 and earlier, and respectively 113 K and 194 K for the later-type objects at ages above or below 200 Myr. These measurement errors were added in quadrature to the propagated spectral type measurement errors in order to obtain the final T_{eff} measurement error in the `data_teff` table of the MOCAdb. The Filippazzo et al. (2015) sequence covers spectral types up to T8; The T9 data was taken from an average of currently known T9 brown dwarfs²⁶, and the temperatures of Y dwarfs were taken from Leggett & Tremblin (2025). The resulting effective temperatures of individual stars and substellar objects in MOCAdb are shown as a function of age as a 2D histogram in Figure 8.

4.6.3. Masses

We used a similar approach as described in Section 4.6.2 based on empirical spectral type sequences to estimate the masses of all stars and substellar objects in the database. We used the spectral type to mass sequences of Pecaut & Mamajek (2013)²⁷ for main-sequence stars, and we compared them with available dynamical masses for stars with spectral types in the range A2–M5 from the literature, for stars of various

²⁶ <https://github.com/emamajek/SpectralType/blob/master/T9V.txt>

²⁷ Available at https://www.pas.rochester.edu/~emamajek/EEM_dwarf_UBVIJHK_colors_Teff.txt.

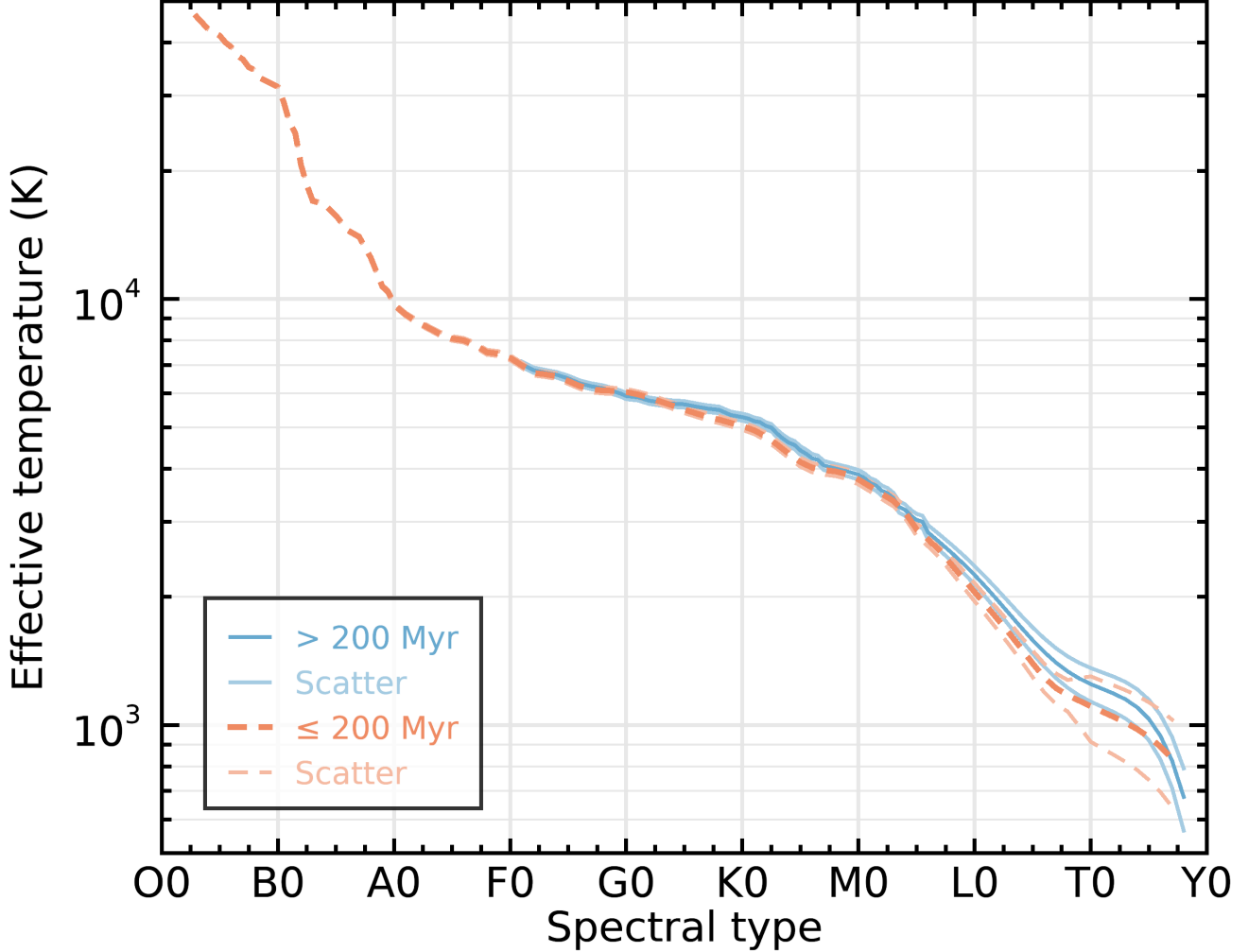


Figure 7. Spectral type– T_{eff} sequences of Pecaut & Mamajek (2013) for main-sequence stars (blue line) and pre-main-sequence stars (orange dashed line). Pale lines around each sequence delineate their respective error bars, determined by the standard deviation of individual stars around the sequence. There are small but statistically significant differences in the effective temperature to spectral type sequence of mid-G stars and later, plausibly related to the lower surface gravity of younger stars affecting the classification based on main-sequence templates. The extension to the substellar regime are from Filippazzo et al. (2015) and Leggett & Tremblin (2025).

ages (2–150 Myr and field stars)²⁸. In all cases where an updated Gaia DR3 parallax was available, we used it to rescale the dynamical mass and its measurement errors. This allowed us to estimate an uncertainty around the Pecaut & Mamajek (2013) sequence which did not need any modification to match these data from the standard deviation of measurements around the sequence in log space (0.11 dex). For the young sequences, we used members of young associations with a known age

to calculate a low-order polynomial deviation above the Pecaut & Mamajek (2013) sequence in log mass, shown in Figure 9. We have then extrapolated these two sequences (both for younger and older ages) between spectral types M5.5 and the expected masses from the Burrows et al. (2001) evolutionary sequences at spectral type M7 for each distinct age, and we have adopted the estimated masses from Burrows et al. (2001) for later spectral types. As the Burrows et al. (2001) evolutionary sequences provide effective temperatures rather than spectral types, we have used the empirical spectral type– T_{eff} sequences described in Section 4.6.2 to estimate the spectral type at each point on the Burrows et al. (2001) evolutionary tracks, using the sequence of

²⁸ See Hillenbrand & White (2004), Rodet et al. (2018), Janson et al. (2018), Azulay et al. (2017), Montet et al. (2015), Nielsen et al. (2016), Pegues et al. (2021), Braun et al. (2021) and Simon et al. (2019)

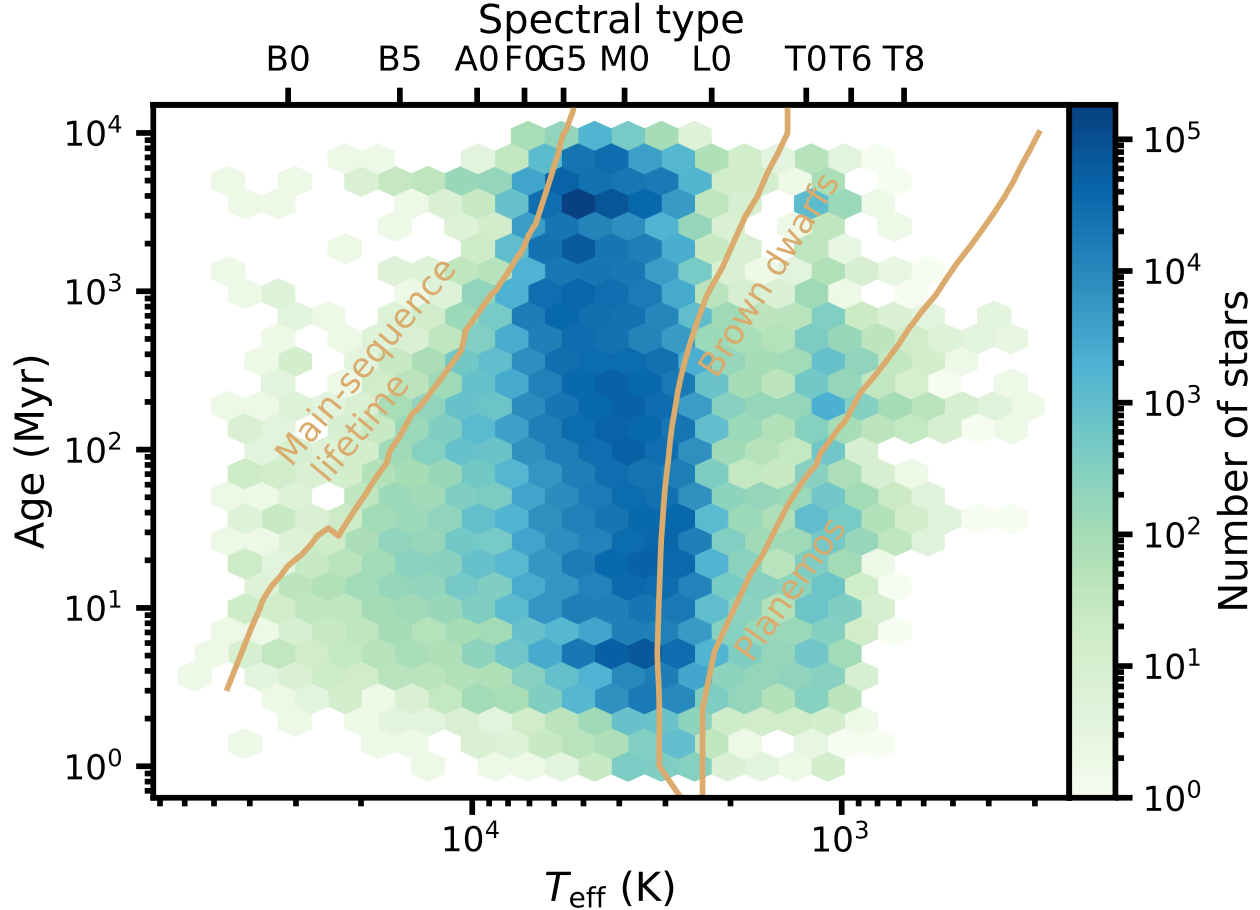


Figure 8. Distribution of ages as a function of T_{eff} and spectral types for individual stars in MOCAdb (hex bins). There is a relative dearth of hot stars at gradually older ages, which is a consequence of the limited lifetime of the most massive stars, indicated with the ‘Main-sequence lifetime’ orange line. The mass regimes of brown dwarfs and planemos, based on the Burrows et al. (2001) models, are also indicated.

the appropriate age. The resulting semi-empirical spectral type–mass sequences are shown in Figure 9. We have adopted conservative 20% measurement errors for objects later than M5.

4.6.4. Radii

We estimated the radii of each source and membership combination in the MOCAdb by constructing a spectral type–radii sequence with a similar method as described in Section 4.6.3. We started from the spectral type to radius sequences of Pecaut & Mamajek (2013)²⁹ for main-sequence stars, and we compared them with available radius estimates using the spectral energy distribution method of Masana et al. (2006) with the current best available literature parallaxes (mostly from Gaia DR3)

for field stars and members of young associations with known ages (6–45 Myr; Pecaut & Mamajek 2013). We estimated an uncertainty around the Pecaut & Mamajek (2013) sequence that is derived from the standard deviation of measurements around the sequence in log space (0.06 dex). For young sequences, we used members of young associations with a known age to calculate a low-order polynomial deviation above the Pecaut & Mamajek (2013) sequence in log radius, shown in Figure 10. We interpolated the resulting 5 sequences of distinct ages in logarithmic age to obtain sequences of intermediate ages. We then extrapolated these sequences between the M5.5 spectral types and the expected masses from the Burrows et al. (2001) evolutionary sequences at the M7 spectral type for each distinct age, and we adopted the estimates of Burrows et al. (2001) for later spectral types. We have again used the empirical spectral type– T_{eff} sequences described in Section 4.6.2 to estimate the

²⁹ Available at http://www.pas.rochester.edu/~emamajek/EEM_dwarf_UBVIJHK_colors_Teff.txt.

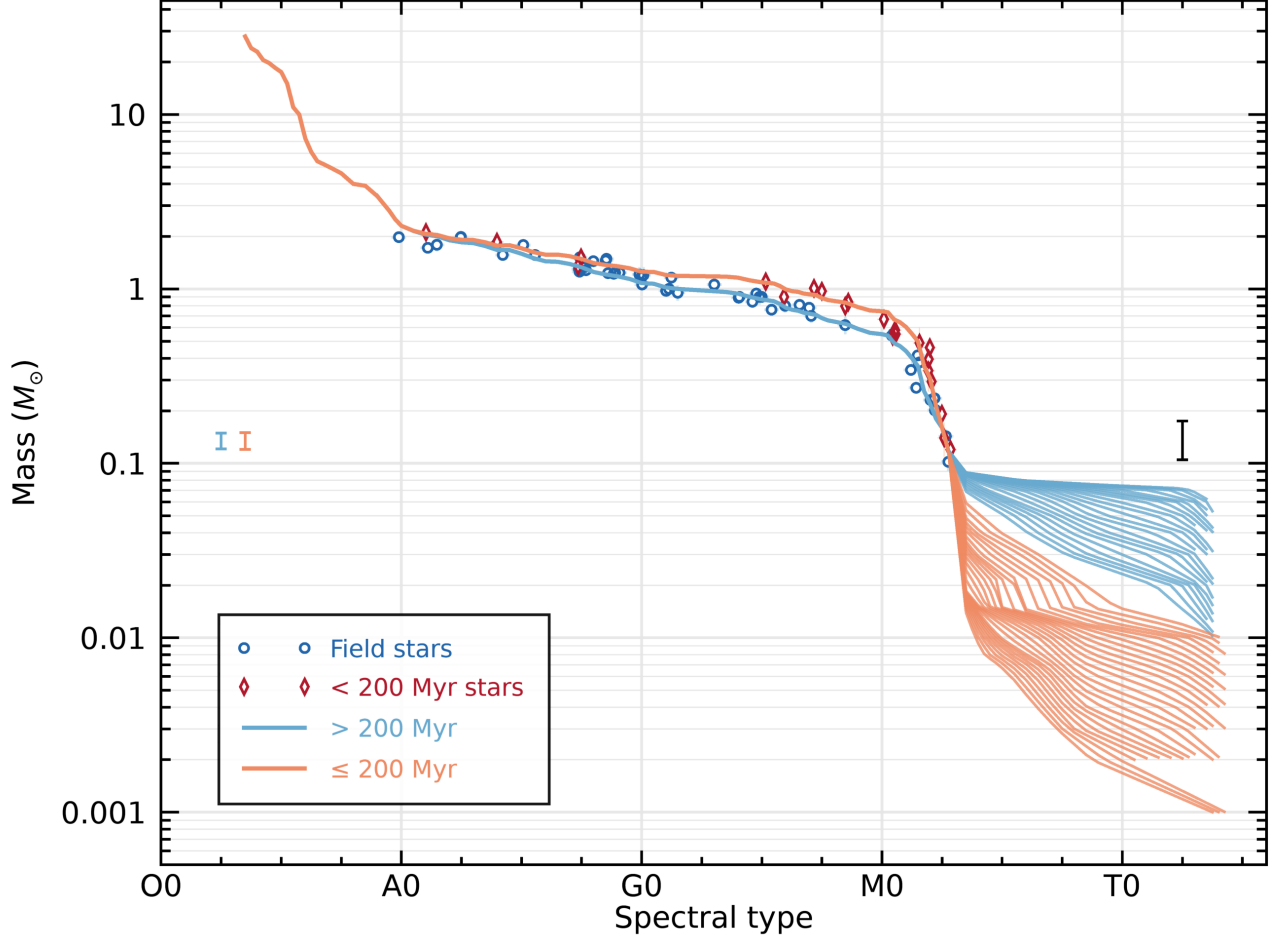


Figure 9. Mass to spectral type sequences based on Pecaut & Mamajek (2013) for main-sequence stars (blue lines) and extended to the substellar regime with Burrows et al. (1997) evolutionary models. Dynamical mass measurements updated with Gaia DR3 parallaxes are shown for main-sequence stars (blue circle) and young members of nearby moving groups (red diamonds) and were used to modify the Pecaut & Mamajek (2013) sequence for young stars (orange lines). The discontinuity at 200 Myr in the substellar tracks is due to our adoption of different spectral type to effective temperature sequences across this age boundary (see Figure 7). Typical log error bars based on the standard deviations of individual stars around their respective sequences are shown with blue and orange error bars. The black error bar represents the 25% uncertainty that we adopted for the substellar regime to encompass possible systematic errors in model tracks.

spectral type at each point on the Burrows et al. (2001) evolutionary tracks, using the sequence of the appropriate age. The resulting semi-empirical spectral type–mass sequences are shown in Figure 10. We adopted conservative 20% measurement errors for objects later than M5.

We used the same Monte Carlo method as described in Section 4.6.3 to propagate the spectral type and mass measurement errors to uncertainties on the radius estimates, which were added in quadrature to the uncertainties of the semi-empirical relations of Figure 10. The resulting radii and their measurement errors were included in the `data_radii` MOCAdb table.

4.7. Heliocentric Radial Velocities

In this section, we discuss the corrections of convective blueshift (Section 4.7.1) and gravitational redshift (Section 4.7.2) on radial velocity measurements, bias corrections for the Gaia DR3 radial velocities (Section 4.7.3), and how multiple individual radial velocity measurements are used to estimate the center-of-mass heliocentric radial velocity of each system (Section 4.7.4).

4.7.1. Estimation of Convective Blueshifts

Convection cells at the surface of a star can bias the measurement of radial velocity obtained by measuring the Doppler shift because the centers of convection cells are both hotter (thus brighter) and occupy more surface

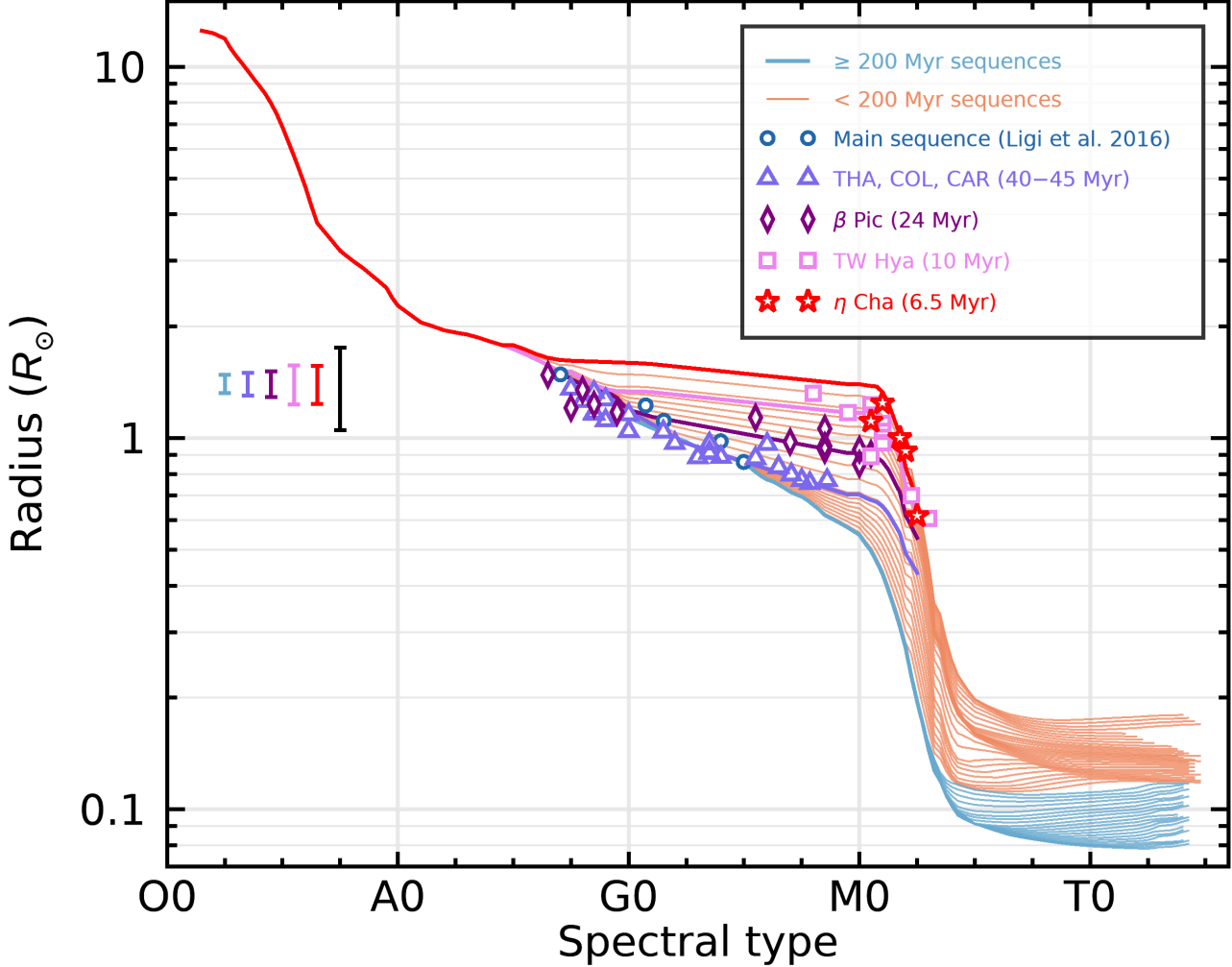


Figure 10. Radius to spectral type sequences based on Pecaut & Mamajek (2013) for main-sequence stars (blue line) extended to the substellar regime with Burrows et al. (1997) evolutionary models. Measurements for individual stars obtained with the spectral energy distribution method of Masana et al. (2006) updated with Gaia DR3 parallaxes are shown with different symbols depending on their membership in a nearby young association. These were used to adapt the Pecaut & Mamajek (2013) sequence to different ages, and intermediate ages were interpolated in log age. Typical log error bars are shown with their corresponding sequence ages, and the black error bar represents the 25% uncertainty that we adopted for the substellar regime to encompass possible systematic errors in model tracks.

area than the darker and narrower intergranular lanes. Because these convection cells contribute more light to the star's spectrum and they move towards the observer, they tend to shift the measured radial velocity by up to $\approx 0.4 \text{ km s}^{-1}$. The exact bias depends on the detailed properties of the star, and on the resolving power and line spread function of the instrument used to measure the radial velocity, but the accuracy of radial velocity measurements can be improved by deriving average convective blueshifts as a function of stellar type for a range of available instruments.

We estimated convective blueshift with an approach similar to that of Couture et al. (2023), based on a lit-

erature compilation of convective blueshifts as a function of spectral type (Gunn et al. 1988; Meunier et al. 2017; Allende Prieto et al. 2013; Dai et al. 2019; Liebing et al. 2021; Löhner-Böttcher et al. 2019; Leão et al. 2019; Baroch et al. 2020). We fit a broken second-order polynomial to the data of Meunier et al. (2017) in the range of spectral types F7–K4, which we extended with a linear extrapolation on either side, assuming a zero blueshift at spectral type F1 due to the expected radiative surface of hotter stars, and assuming a zero blueshift at spectral type M4 due to the constraint of (Baroch et al. 2020).

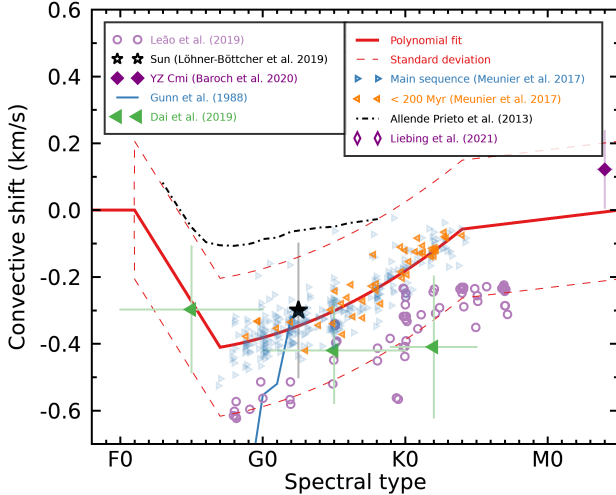


Figure 11. Estimates of convective blueshift as a function of spectral type from various literature studies. Our adopted estimate is shown with a thick, red line and a conservative conservative envelope is shown with a dashed red lines, which encompasses most of the studies and instruments. We do not apply a convective blueshift correction to stars F0 and earlier due to their lack of a convective envelope. See Section 4.7.1 for more details.

We adopted a conservative error estimate on the convective blueshift that is taken as the standard deviation of all data sets around the sequence (0.21 km s^{-1}), which was added in quadrature to the measurement errors of all corrected radial velocities. Achieving better precision in the spectral classes subject to convective blueshift will require an approach with a bias correction that is dedicated to every instrument design, configuration and radial velocity measurement algorithm. The measurement errors of the radial velocities of objects later than M5 were also inflated by the same amount given the lack of observational constraints on their convective blueshifts and the fact that they have a convective surface, but no error inflation was applied to the radial velocities of stars with spectral types F0 or earlier due to their lack of surface convection. The resulting sequence is compared to data from the literature in Figure 11. The convective blueshifts calculated for individual stars with a 10^4 -element Monte Carlo are listed in the table `calc_convective_blueshifts`.

4.7.2. Estimation of Gravitational Redshifts

The wavelength of light leaving the surface of a star is elongated as it escapes the gravitational well, as expected by the theory of general relativity. This affects the measurements of stellar heliocentric radial velocities by the Doppler method by shifting the measured radial velocities to the red, typically by $0.5\text{--}0.7 \text{ km s}^{-1}$ for main-sequence stars of spectral classes AFGK (e.g.,

see Pasquini et al. 2011; Couture et al. 2023), and more for earlier-type stars. We used the empirical mass and radius sequences as a function of spectral types (see Sections 4.6.3 and 4.6.4) to calculate the impact of gravitational redshift, and propagated the measurement errors using a 10^4 -element Monte Carlo. The resulting sequences are displayed in Figure 12(a), and the combined impacts of gravitational redshift and convective blueshift are shown in Figure 12.

The gravitational redshifts calculated for individual stars with a 10^4 -element Monte Carlo are listed in the table `calc_gravitational_redshifts`. Because the mass and radius estimates of stars are age-dependent, so are the corrections to the impact of gravitational redshift on their radial velocities. For this reason, gravitational redshift corrections are calculated for every membership hypothesis discussed in MOCAdb, meaning that one measurement is listed for each star (identified with a `moca_oid` identifier) and relevant young association (identified with a `moca_aid` identifier) combination. Those that correspond to the current most likely membership are indicated with the `adopted` flag.

We note that the gravitational redshifts of white dwarfs are much more important than those of main-sequence stars, and those of giant stars are conversely much less important. We have not attempted to calculate them for either white dwarfs or giants in the MOCAdb. In the case of substellar objects, the gravitational redshift is strongly dependent on the object’s age because these objects cool down over time. Consequently, a young object of a fixed spectral type (and thus temperature) has a much smaller mass, leading to a smaller surface gravity and gravitational redshift.

4.7.3. Radial velocity biases in Gaia DR3

This section describes radial velocity biases corrected at the step where MOCAdb pulls existing measurements from the table `cat_gaiadr3` to insert them into `data_radial_velocities` (radial velocity values in the table `cat_gaiadr3` are not corrected).

We corrected the hot-star radial Gaia DR3 velocity biases described by Blomme et al. (2023). This specific bias results in a systematic blueshift of the radial velocities measured for stars with T_{eff} in the range 8500–14500 K, and is caused by the proximity of the calcium infrared triplet³⁰, to hydrogen Paschen lines in hot stars. The following quantity was therefore subtracted from the existing Gaia DR3 radial velocities:

³⁰ used by the Gaia DR3 Radial Velocity Spectrometer (RVS) to calculate radial velocities (Cropp et al. 2018).

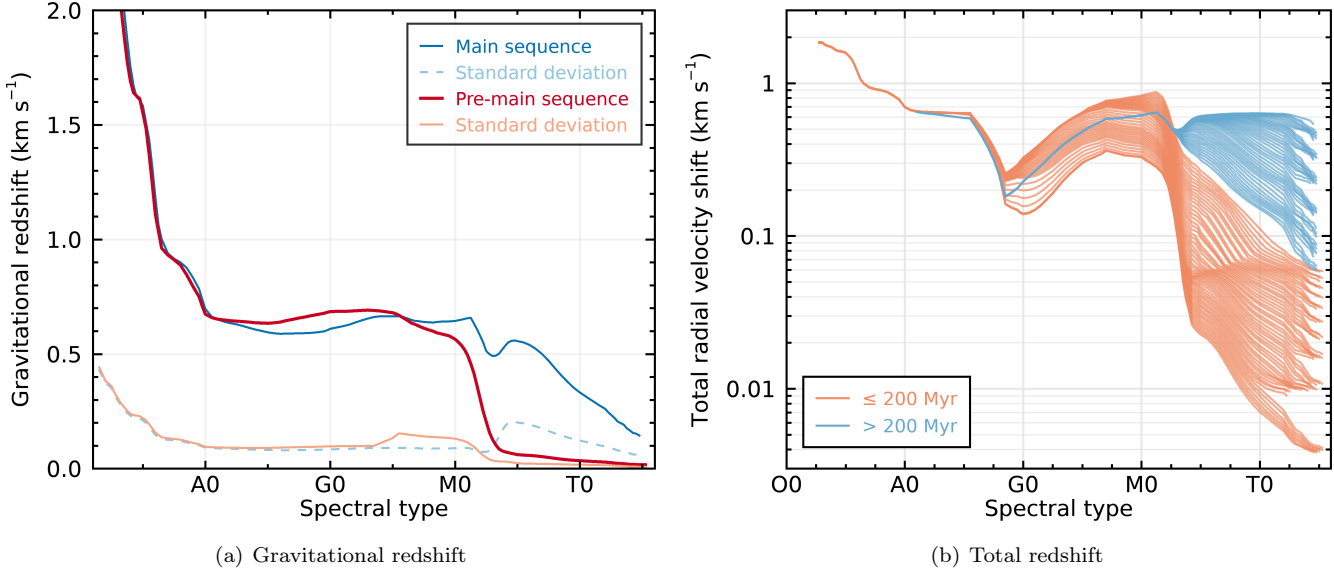


Figure 12. Left panel: The gravitational redshift adopted in this study for young (red) or main-sequence (blue) stars, derived from empirical spectral type to mass and radii relations. The associated uncertainties are shown with dashed lines. Right panel: The combined total velocity shift (convective blueshift + gravitational redshift) adopted in this work, shown in logarithmic shift for clarity. The total shift sequences split across ages for stars of spectral classes F or later because of the age dependence of their radii (shown in Figure 10).

$$7.98 \text{ km s}^{-1} - (1.135 \text{ km s}^{-1} \text{ mag}^{-1}) \cdot \text{grvs_mag}, \quad (1)$$

only for stars with the Gaia DR3 column `rv_template_teff` in the range 8500–14500 K and `grvs_mag` in the range 6–12 mag, as prescribed by Blomme et al. (2023), where `grvs_mag` is the Gaia DR3 G_{RVS} magnitude measured by the Radial Velocity Spectrometer (Cropper et al. 2018). These biases range from $\approx +1 \text{ km s}^{-1}$ to $\approx -8 \text{ km s}^{-1}$.

We also applied the bias correction of Katz et al. (2023) for cool and faint stars in Gaia DR3 that is caused by RVS detector traps that delay the release of electrons as the science target moves across the CCD in the spectral direction. This causes a slight redshift in the radial velocities measured for faint stars, which can be corrected by subtracting the following quantity to the Gaia DR3 radial velocities:

$$(0.0275 \text{ km s}^{-1} \text{ mag}^{-2}) \cdot \text{grvs_mag}^2 \quad (2)$$

$$- (0.55863 \text{ km s}^{-1} \text{ mag}^{-1}) \cdot \text{grvs_mag} \quad (3)$$

$$+ 2.81129, \quad (4)$$

This correction is applied to stars with `rv_template_teff` below 8500 K and `grvs_mag` fainter than 11 mag, as prescribed by Katz et al. (2023). These biases range from zero to $\approx +0.4 \text{ km s}^{-1}$.

Curtis (priv. comm.) identified yet another bias in the Gaia DR3 radial velocities of A-type stars³¹ by investigating the deviations in the Gaia DR3 radial velocities of Pleiades members (corrected for the two biases mentioned above) with respect to the median space velocities UVW of the cluster. This bias was observed to be independent of Gaia $G_{\text{BP}} - G_{\text{RP}}$ colors and is rather dependent on the T_{eff} of the chosen radial velocity template in Gaia DR3.

Figure 13 shows the resulting trend in the Gaia DR3 radial velocities³² minus the BANYAN Σ radial velocity prediction³³ using MOCAdb members of all nearby associations within 200 pc of the Sun with ages 1 Gyr or younger (excluding Theia groups, open cluster coronae or any group with a standard deviation above 1.5 km s⁻¹ in either dimension of its Galactic space velocity). We observe a trend similar to that reported in the Pleiades, where A-type stars of effective temperatures around 8500 K appear artificially blueshifted and require an additive $\approx 3.7 \text{ km s}^{-1}$ correction to be applied. We also ob-

³¹ See <https://aas242-aas.ipostersessions.com/?s=0E-AC-3F-05-83-84-86-EA-54-A8-43-E1-57-13-A7-E1>.

³² Corrected for the two biases mentioned above, as well as gravitational redshift and convective blueshift.

³³ We used the BANYAN Σ radial velocity prediction using all other observables but the radial velocity. This corresponds to the radial velocity that minimizes the distance between a star's Galactic space velocities UVW and those of the corresponding BANYAN Σ model of the association.

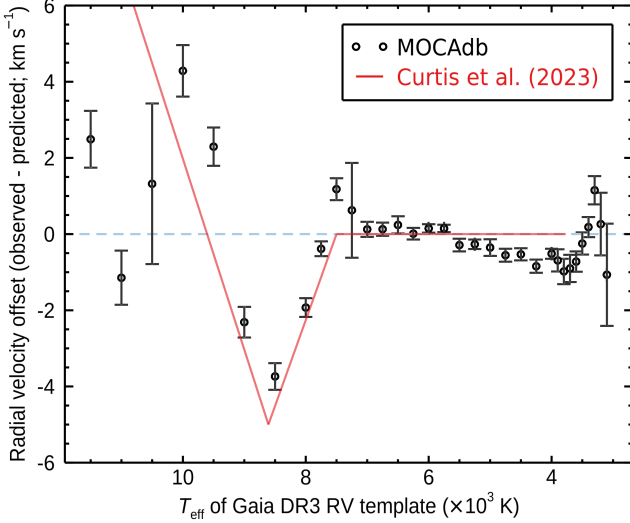


Figure 13. Average radial velocity offset between Gaia DR3 measurements and predictions based on cluster membership using BANYAN Σ , grouped by the effective temperature of the Gaia DR3 radial velocity template (black circles). The error bars represent measurement errors on the average; effective temperatures at both extremes have larger errors because of the smaller number of available cluster members. The blue dashed line represents zero offset, and the red line represents the Gaia DR3 radial velocity bias observed by Jason Curtis with the Pleiades members, consistent with our observed trend.

serve a more subtle blueshift of up to $\approx 1 \text{ km s}^{-1}$ for K dwarfs, which could be due to an insufficient correction of gravitational blueshift, specifically for the Gaia instrumental setup and this range of spectral types, rather than a systematic problem with the Gaia radial velocity templates. The underlying reason for this bias warrants future investigation and could be an age-dependent effect given that young low-mass stars tend to display enhanced magnetic activity.

The radial velocity bias shown in Figure 13 does not disappear if the biases of Blomme et al. (2023) and/or Katz et al. (2023) are left uncorrected; the three biases are independent of each other and must all be corrected, in the order described here.

4.7.4. Combined Center-of-Mass Radial Velocities

All radial velocity measurements from the `data_radial_velocities` table were combined in a `calc_radial_velocities_combined` with the explicit goal of approximating the center-of-mass radial velocity of unresolved multiple systems. In order to achieve this, we have drawn 10^4 synthetic radial velocity measurements for each individual literature radial velocity measurement (with a standard deviation set to the measurement error, for which we adopted a floor of

0.01 km s^{-1}), scaled by the `n_measurements` column to weigh combined radial velocities appropriately. Radial velocities taken within the same Julian day were combined with a weighted average before this Monte Carlo step, and were counted as a single measurement, to avoid over-representing single-epoch values from intensive high-accuracy radial velocity monitoring campaigns, which may otherwise over-sample a short phase of the radial velocity curve for multiple stars. We have adopted the weighted averages and weighted standard deviations (divided by the square root of the number of distinct epochs) of the resulting set of synthetic radial velocities for each given source as our estimated combined radial velocity and its measurement error. This method is similar to the approach adopted by Miret-Roig et al. (2020), who also used a Monte Carlo simulation to estimate the center-of-mass radial velocities of unresolved multiple systems.

We have mutually excluded radial velocities from some radial velocity catalogs, listed in the MOCAdb table `mechanics_combinatoric_logic`. One such example is Gontcharov (2006) and Kharchenko et al. (2007): when individual measurements were available from both compilations, we only used the values from Kharchenko et al. (2007) because both catalogs were constructed in part from the same sources. Another example is Gaia DR3 radial velocities, which supersede those listed in Gaia DR2.

Radial velocities corrected for the combined effects of gravitational redshift and convective blueshift are listed in the `calc_radial_velocities_corrected` table.

We note that these combined radial velocities can be used to calculate approximate UVW space velocities, but the combined effects of gravitational redshift and convective blueshift (described further in sections 4.7.2 and 4.7.1) can have systematic impacts much larger than the measurement errors quoted in the `calc_radial_velocities_combined` table. If these measurements were to be taken at face value for such calculations, we would recommend subtracting an average 0.6 km s^{-1} from the combined radial velocities, and adding 0.6 km s^{-1} in quadrature to the measurement errors (see e.g., Couture et al. 2023), to account for the two effects.

4.8. Galactic Space Velocities

The *UVW* Galactic space velocities are calculated for every MOCAdb object with available distance, proper motion, and radial velocity measurements in the respective MOCAdb tables `data_distances`, `data_proper_motions` and `data_radial_velocities_combined`, and are listed in the table `calc_uvw_raw`. They are based on a 10^4 -element Monte Carlo simulation for error propagation, using the full probability distribution function of the distance estimates (which are in most cases based on the method of Bailer-Jones et al. (2021) as described in Section 4.1). We adopt the definition of *UVW* axes used in the `gal_uvw` routine of the IDL `astrolib` package, which forms a right-handed rectangular coordinates system centered on the Sun’s velocity, with U pointing towards the Galactic Center.

Radial velocities are subject to age-dependent biases caused by gravitational redshift and convective blueshift, as described in Section 4.7. As a consequence, so are the Galactic space velocities. We have thus calculated *UVW* velocities using the corrected radial velocities from the `data_radial_velocities_corrected` table, with a similar Monte Carlo method. Because these calculations are age dependent, a value is listed not only for every unique `moca_oid` object, but also for every plausible `moca_aid` association. The calculation which corresponds to the most likely host association is flagged with `adopted= 1`. The resulting Galactic space velocities of individual stars in MOCAdb are shown in the *UV* plane in Figure 14.

4.9. Spectral Types

All available spectral types are cataloged in the table `data_spectral_types`, along with a quality flag (mostly obtained from Simbad), and an associated `spectral_type_number` for convenience (0 for M0, 10 for L0, -10 for K0 and so on). The best-available spectral types (those with the highest quality flags and the smallest measurement errors) are flagged with `adopted= 1`, and columns such as `luminosity_class`, `gravity_class` and `suffix` allow to store detailed peculiarities about different types of objects. The binary columns `wd_like` and `giant_like` allow to quickly identify white dwarfs and giants based on automated pattern matching, and the substellar-specific columns `lowg_like`, `subdwarf_like` and `field_like` allow to quickly flag peculiar objects with low surface gravity or unusually red colors (typically young substellar objects); those with a high surface gravity or unusually blue colors (typically older, low-metallicity subdwarfs); or those

that do not show any spectroscopic peculiarity, respectively.

4.10. Spectra

Stellar and substellar spectra from the Montreal Spectral Library³⁴, the SpeX Prism Library (Burgasser 2014) and the IRTF spectral Library (Rayner et al. 2009), and the SIMPLE archive Cruz et al. (2025)³⁵ were included in the MOCAdb. The table `moca_spectra_packages` lists individual packages of spectra that share similar properties; the table `moca_spectra` lists individual spectra along with their header properties, and the table `data_spectra` lists the wavelengths and spectral flux densities of all spectra stored in the database.

4.11. Equatorial Rotational Velocity Predictions

A prediction of equatorial velocity can be produced for all objects in the MOCAdb that benefit from both a radius estimate in the `data_radii` table and the adopted rotation period in the `data_rotation_periods` table. These estimations can be useful for example to exclude fast rotators from radial velocity-based exoplanet searches. The MOCAdb equatorial radial velocity predictions are calculated by generating a 10^4 -element Monte Carlo simulation, where the calculated radius corresponding to each membership hypothesis is randomly sampled in log space, and the rotation periods are also randomly sampled in log space. The corresponding equatorial rotational velocity prediction v_{pred} is then obtained for every Monte Carlo element with:

$$v_{\text{pred}} = 50.607 \frac{\text{km s}^{-1} \text{ days}}{R_{\text{Sun}}} \frac{R}{P_{\text{rot}}} \quad (5)$$

A Cumulative Distribution Function (CDF) is then built for every Monte Carlo value. The CDF median is adopted as the best prediction, and asymmetrical error bars covering 68% of the distribution based on the CDF are adopted.

We did not calculate equatorial rotational velocity predictions for objects that already have a measured projected rotational velocity in the `data_vsini` table. These cases allow to pose constraints on the projected inclination instead, discussed in Section 4.12.

4.12. Projected Inclinations

It is possible to estimate a projected inclination for the objects that benefit from a radius estimate

³⁴ Available at <https://jgagneastro.com/the-montreal-spectral-library/>.

³⁵ A persistent and versioned copy of the SIMPLE archive is available on Zenodo at doi:10.5281/zenodo.13937301, and the current version is available at <https://simple-bd-archive.org>.

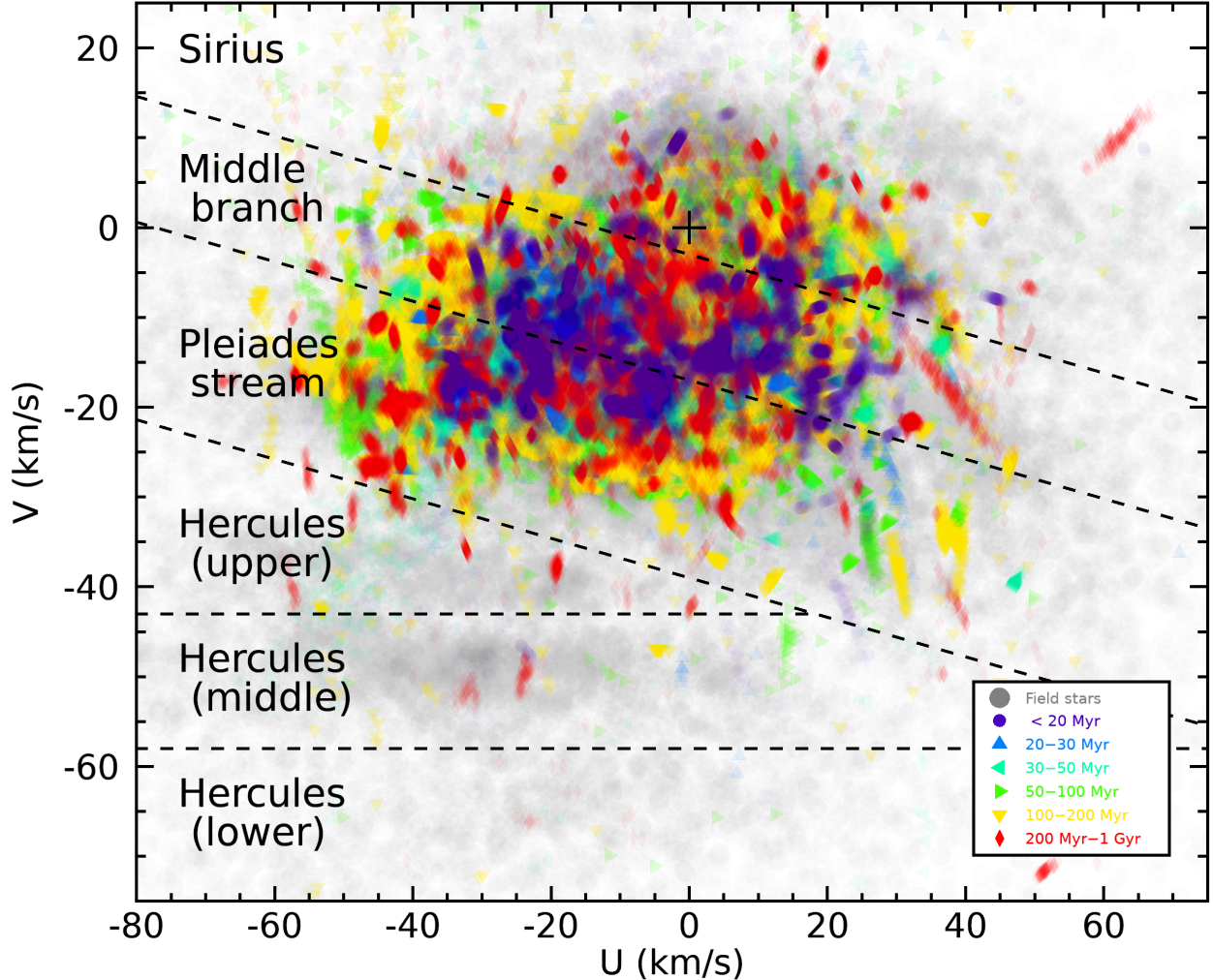


Figure 14. Median UV Galactic space velocities of individual stars in MOCAdb, color-coded by their association age, compared with nearby Gaia DR3 stars (black circles) and the regions delimited by Eggen (1958) and Eggen (1971).

in the `data_radii` table, a rotation period in the `data_rotation_periods` table and a projected rotational velocity $v \sin i$ measurement in the `data_vsini` table. This is done with a 10^4 -element Monte Carlo similar to that described in Section 4.11, where the inputs are sampled in log space, and the inclination is calculated with the following equation:

$$\sin i = \frac{v \sin i}{50.607 \text{ km s}^{-1} \text{ days} R_{\text{Sun}}^{-1}} \frac{P_{\text{rot}}}{R} \quad (6)$$

In this case, we have also included a $P(i) = \sin i$ prior appropriate for the projections of randomly distributed 3D inclinations.

5. DISCUSSION

5.1. Establishing a Hierarchical Structure of Nearby Associations

Some associations have been historically described using different names, which can sometimes refer to an ensemble or substructures (e.g., the Scorpius Centaurus OB association includes the smaller Lower Centaurus Crux, Upper Scorpius and Upper Centaurus Lupus associations among others), or refer to different parts of a larger group that had not yet been fully explored. For example, the Local Association Subgroup B4 of [Asiaian et al. \(1999\)](#), with the database keyword `LAB4`, was later included with a spatially larger set of stars that now forms the AB Doradus moving group ([Zuckerman et al. 2004](#); keyword `ABDMG`). As a consequence, the associations listed in the MOCAdb can overlap with each other and bear a hierarchical parent and child relationship.

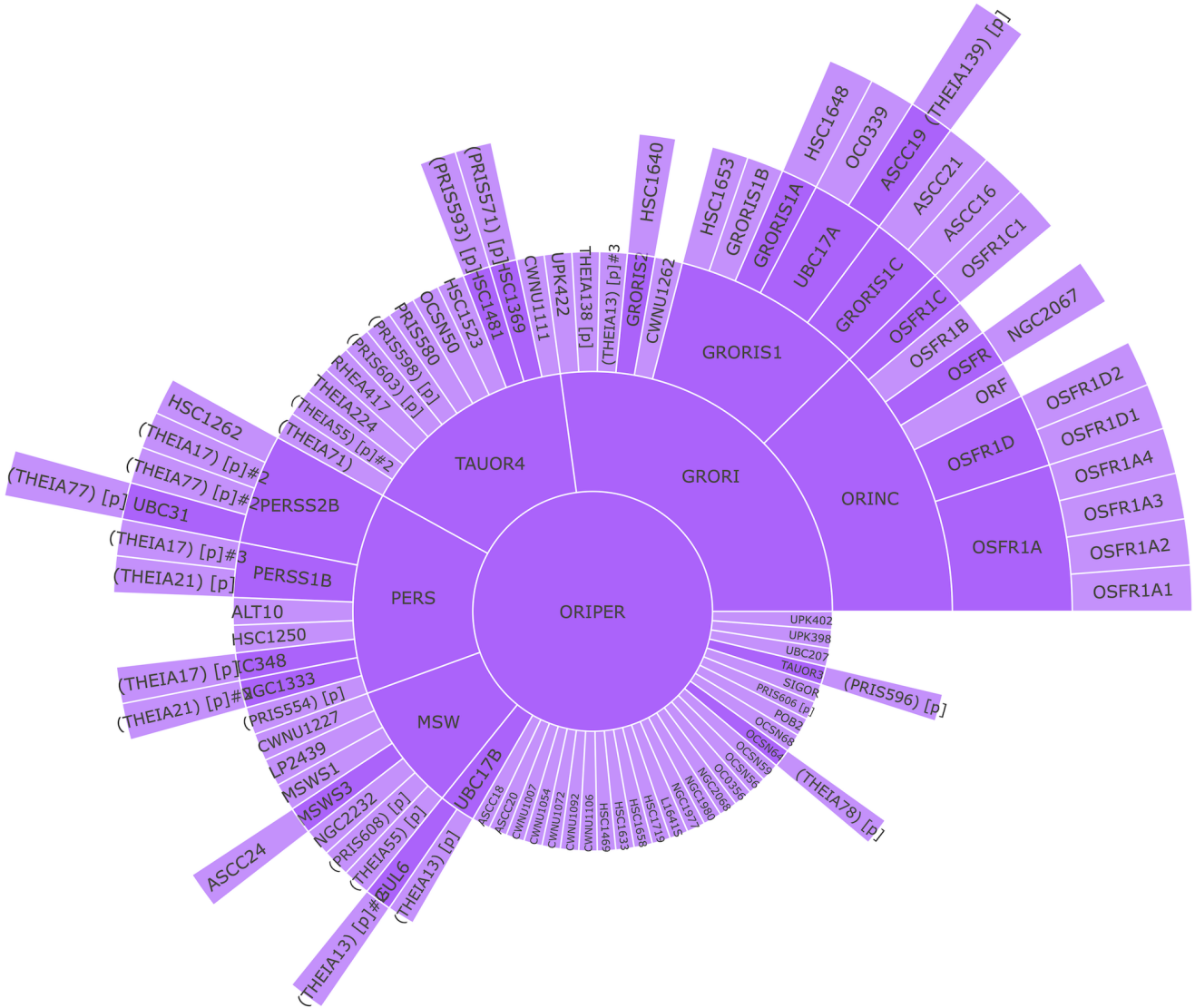


Figure 15. A visualization of the Orion-Perseus branch in the hierarchical structure of young associations included in MOCAdb. The `moca_aid` association codes with a [p] suffix indicate that only a part of that specific definition is related to the parent association. Associations with the flag `moca_associations.suboptimal_grouping` are indicated between parentheses, which means that they are not used in MOCAdb as an optimal way of delimiting stellar populations (i.e., either the group is split differently using another definition, or it is not recognized as real).

In the previous example, LAB4 is registered as a child of ABDMG in the database. Cases where a young association is essentially an exact match to another, better characterized association (e.g., Group 1 of [Oh et al. 2017](#) corresponds to the well-known α Per open cluster, see e.g. [Heckmann & Lübeck 1958](#)) are flagged in the `data_association_relationships` table, with the flag `complete_parent_overlap=1`.

There are other cases where groups of stars defined in recent publications through automated clustering methods have merged several known structures that are not coeval. For example, Theia 55 of Kounkel &

Covey (2019) includes a large number of members of the NGC 2232 open cluster (≈ 18 Myr; CD20), the LP 2439 open cluster (27 ± 0.7 Myr; Kerr et al. 2021), the Greater Taurus, Taurus-Orion and Monoceros Southwest regions of Kerr et al. (2021). Although this may indicate that these regions are related to each other in some way, there are many scenarios where grouping these stars together is not optimal. We have therefore preserved groupings such as LAB4 or Theia 55 that are either obsolete, collections of non-coeval associations, or groupings with high contamination, but have assigned them a flag `suboptimal_grouping= 1` in the database. This

will make it possible to retrieve their lists of members, but they will not automatically be investigated further. The relationships between such associations are also listed in the table `data_association_relationships` with a flag `partial_subgroup_overlap` (e.g., `moca_aid=THEIA55` is linked to `parent_aid=NGC2232` with `partial_subgroup_overlap=1`).

Several known young associations also have a hierarchical structure, whether because star-forming regions contain multiple overdensities, open clusters, or because open clusters and their tidal tails or ‘corona’ can be grouped as a larger system (Meingast & Alves 2019; Meingast et al. 2021; Röser & Schilbach 2019; Tang et al. 2019). These cases are also marked in the `data_association_relationships` table, with `complete_parent_overlap=0` and `partial_subgroup_overlap=0`. Several of these structures were also identified directly in the MOCAdb database, based on 3-dimensional visualizations and overlaps in the lists of members.

In order to separate the lists of stars that belong to the core of an open cluster or its corona, we have created separate entries for such open clusters with known coronae, with the original name of the association (e.g., Hyades with the database keyword `HYA`) referring to the core of the cluster, the corona being explicitly named (e.g., Hyades corona with a `C` preceding the database keyword: `CHYA`) and the system referring to all stars from both the core and corona (e.g., Hyades System with an `S` preceding the database keyword: `SHYA`). In these cases, both the core and corona of the open cluster are registered as children of the full open cluster system.

The resulting hierarchical structure of a few complexes of young associations is shown in Figure 15 and can be dynamically explored in <https://mocadb.ca>.

5.2. Compilation of Propagated Membership Lists

Once all memberships were cataloged, we combined all membership claims while accounting for hierarchical relationships between associations into the table `mechanics_memberships_propagated`. Any claim of membership which refers to a stellar association (e.g., Upper Scorpius, or keyword `USCO`) with a non-null parent association (e.g., Scorpius-Centaurus or keyword `SCOCEN`) and without the `data_association_relationships.partial_subgroup_overlap= 1` flag are therefore repeated as a membership claim in both of the child (`USCO`) and parent (`SCOCEN`) association in the `mechanics_memberships_propagated` table. This allows a user to obtain the full set of membership claims in the literature at either hierarchical grouping level with a single filter-

ing step of the `mechanics_memberships_propagated` table. All associations with a zero-valued `is_real` flag are ignored in this step and excluded from the `mechanics_memberships_propagated` table.

Although the tables `data_memberships` and `mechanics_memberships_propagated` contain an exhaustive list of membership claims in the literature, they will result in various levels of contamination, depending on the association, if they are used to construct a sample of members. A table that lists all currently accepted membership rejections is therefore included in the database table `mechanics Automatically_rejected_memberships` to provide an easily managed mechanism for reducing the sample contamination. This table can link a specific star in the `moca_objects` table to a young association that it is not a member of, or more generally specify a range of acceptable ages for the star with the `minimum_age_myr` and `maximum_age_myr` columns, and further details such as comments, a method and a literature reference.

We used external libraries to compile the lists of memberships from the `mechanics_memberships_propagated` table, and exclude those which constraints listed in `data_rejected_memberships` make the proposed membership claim unlikely. The membership claims are grouped by the unique star and association, and the membership confidence level and literature references are concatenated into a new table `mechanics_memberships_vetted`. Additionally, the table `data_rejected_memberships` allows to automatically reject members of a group based on fixed parameters such as a specific range in its *UVW* velocity components; those are usually only useful to reject extreme outliers in a list of members. The resulting stars that are rejected based on these parameters are listed in `mechanics Automatically_rejected_memberships`, and their status is also reflected in `mechanics_memberships_vetted`.

5.3. Construction of Kinematic Models

We used the lists of members compiled here to update the spatial and kinematic models of the BANYAN Σ tool (Gagné et al. 2018e) for 8125 associations that we consider potentially coeval and non duplicated (i.e., those with the flag `moca_associations.in_banyan= 1`).

BANYAN Σ is a Bayesian model selection tool that allows users to determine whether a star is more likely to belong to a known population of stars based on 6D multivariate Gaussian models in *XYZ* Galactic coordinates and *UVW* space velocities for stars that belong in known associations and a 10-components multivariate Gaussian model of field stars in the Solar neighborhood.

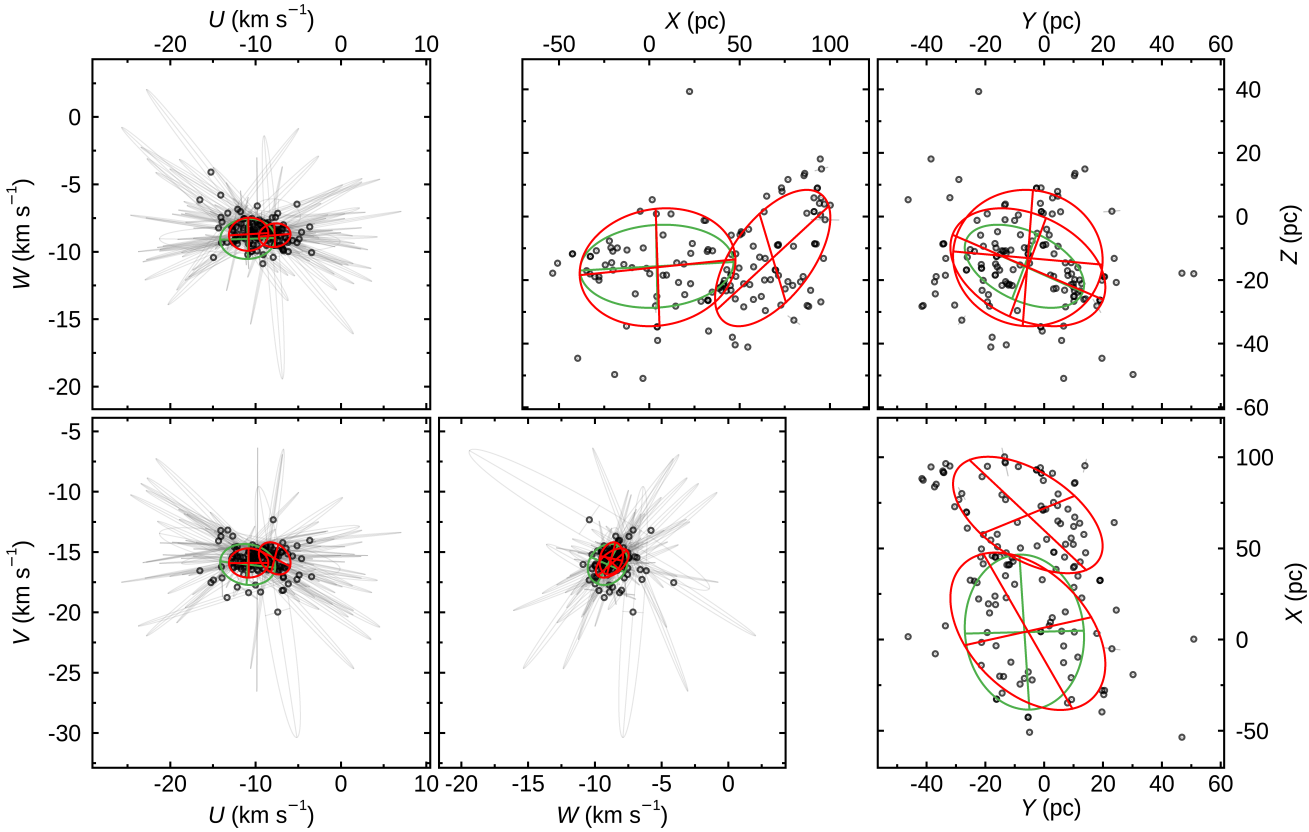


Figure 16. Projections of the multivariate Gaussian models determined with the extreme deconvolution algorithm for members of the β Pic moving group in XYZ Galactic positions and UVW space velocities (red ellipses). Projected semi-major axes are shown with red lines, and the previous model of Gagné et al. (2018e) based on Gaia DR1 and a simpler model construction method are shown in green. Individual stars are shown with black circles, and their error bar ellipses are shown in gray, with the correct orientations accounting for the fact that the largest error contributions (radial velocities or parallaxes) are oriented differently in 6D space for stars in different directions in the sky. Stars that were automatically flagged as outliers and not included in our the model construction are displayed in pink in the complete figure set (no such outliers were detected in the case of the β Pic moving group, shown above). The extreme deconvolution algorithm properly accounts for the orientation of the error bar ellipses of the individual stars, which would otherwise artificially inflate the models and affect its ratios of semi-major axes. The complete figure set (491 images) is available in the online journal.

When required, BANYAN Σ uses analytical solutions to marginalization integrals over missing heliocentric radial velocities and/or parallaxes, allowing it to identify likely candidate members even if only sky coordinates and proper motions are available. With the advent of the latest Gaia data releases, complete $XYZUVW$ coordinates can be calculated for a larger number of stars, which makes it possible to use other clustering metrics such as HDBSCAN (McInnes & Healy 2017) that are not model dependent and do not assume Gaussian distributions for young coeval associations, however, a number of white dwarfs, lower-mass stars or distant stars will still be missing heliocentric radial velocity measurements for the foreseeable future, and will still benefit from a Bayesian analysis that marginalizes over this dimension. Brown dwarfs and isolated planetary-mass objects will still benefit even more from such an approach, given that

there is currently no future plan to measure their parallaxes or heliocentric radial velocities on a large scale.

The spatial and velocity distributions of the unique young associations compiled in MOCAdb were built using a Gaussian mixture model in 6D $XYZUVW$ space. For each association, a list of all members were first selected from the table `mechanics_memberships_propagated`, excluding the low-probability members (`mechanics_memberships_propagated.moca_mtid='LM'`) or rejected members (`mechanics_memberships_propagated.moca_mtid='R'`), and known companions (using the `moca_companions` table). The best-available kinematic observables (coordinates, proper motions, parallax, radial velocity) and spectral types were then compiled for each member. In the cases where a Gaia DR3 parallax was adopted as the best-available parallax measure-

ment, we automatically selected the proper motion and sky coordinates from the same catalog, and also compiled all the covariances between sky coordinates, proper motions, and parallaxes. In the cases where the only available kinematic measurements came from a range of different catalogs, we assumed zero covariances between the different observables. The [Bailer-Jones et al. \(2021\)](#) geometric priors (described in Section 4.1) were also included when converting the parallaxes of individual stars into distances during the spatial-kinematic models construction because the spatial-kinematic models of the most distant open clusters are subject to this bias in a non-negligible way. The information content of the prior is overwhelmed by the collective information of the parallax measurements of individual stars in most cases, however. Instead of relying on the average distance and asymmetric error bars stored in the `data_distances` table, we used the complete reconstructed distance probability distribution function.

The radial velocities obtained from a combination of all available literature measurements were used and corrected for the convective blueshift and gravitational redshift, using the best available spectral type and assuming the age of the specific association for which the model was being constructed.

The 6D $XYZUVW$ distribution of each member was then reconstructed using a 10^4 -element Monte Carlo using the appropriate covariances. In order to reflect the parallax covariances onto the distances based on the [Bailer-Jones et al. \(2021\)](#) prior, we first generated a Gaussian distance distribution from one slice of the 5-dimensional Gaussian based on all available covariances. We then determined the position of each synthetic star with respect to this Gaussian distance cumulative distribution function, and interpolated it on the desired cumulative distribution function which accounts for the proper parallax inversion and prior. Once we have obtained the appropriate set of Monte Carlo simulations, we used them to calculate the Galactic XYZ coordinates and the UVW space velocities with the method described in Sections 4.2 and 4.8.

We determined the 6-dimensional median position of every star in a uniformized space with consistent units $[X, Y, Z, cU, cV, cW]$ by multiplying all UVW values by a factor of $c = 12 \text{ pc km}^{-1} \text{ s}$, a value chosen to penalize UVW outliers significantly. We then computed the 6D Euclidian distance between each star and the median $XYZUVW$ position and rejected any star that is located at more than 5 median absolute deviations from the median from the model construction. This step is intended to remove only the most significant outliers that

may otherwise affect automated outlier rejection algorithms.

In a second outlier rejection step, we used the Extended Isolation Forests (`eif`) Python package of [Hariri et al. \(2018\)](#) with the 6D spatial-position vectors of every star and rejected any star with an outlier score above 0.55, which we found was efficient in only rejecting stars which visually appear outside of the typical distributions.

Once a clean set of non-outlier stars was assembled, a covariance matrix was built for each star from the full Monte Carlo distribution of its $XYZUVW$ values, using medians and comedians ([Falk 1997](#)) instead of averages and covariances to avoid a disproportionate impact that wide-tailed distributions may otherwise have on the covariances. We have then applied the extreme deconvolution technique of [Bovy et al. \(2011\)](#) to estimate the underlying density distribution of members, iterating with one to 20 individual Gaussian components. Stars without a radial velocity measurement were included in the model construction by assigning them optimal radial velocities that place them at the center of the median UVW distribution of each group, with a very wide measurement error (30 km s^{-1}), as prescribed by [Bovy et al. \(2011\)](#) for missing values. In rare cases where no member of a given association has a measured radial velocity, we forced the use of a single Gaussian model component and replicated each star twice, once with a radial velocity of 30 km s^{-1} , and once with a value of -30 km s^{-1} , to artificially extend the Gaussian model in the direction where the projected true velocity of the association is unknown.

We used an increasing number of Gaussian mixture components until the corrected Akaike Information Criterion (AICc; see [Burnham & Anderson 1998](#)) started increasing, an indication that the addition of extra components is not justified by the data. We elected to use the AICc rather than the standard Akaike Information Criterion (AIC) or the Bayesian Information Criterion (BIC) because our goal is to use as many mixture components as required to improve the mapping of a specific young association, in a context where the computational cost of additional components on calculating membership probabilities is small (a consequence of BANYAN Σ using analytical solutions to the marginalization priors). Therefore, we required a metric that does not strongly penalize the addition of mixture components (such as the BIC), but we required a metric that does not allow for an arbitrarily large number of components in the situation where many stars are part of a unimodal distribution. The AIC metric would allow a large number of mixture components in this scenario because it includes

no penalty for the number of stars. Because the AICc includes a corrective term involving the number of stars, we chose it as the preferred metric as it achieves our goal of using as many mixture components as justified in order to improve the mapping of stars (i.e., the average log-likelihood over all stars) without adding components that are not justified by the data with statistical significance.

There are scenarios where a relatively small number of stars presents a statistically complex spatial shape, but not necessarily in the spatial-kinematic or the purely kinematic subsets of the complete 6D space. In order to properly model these scenarios, we employed four categories of model complexities with a varying number of Gaussian mixture components (1–20 components for each category), to pick the single model with the smallest AICc: (1) The models with full 6D covariance matrices (27 free parameters per GMM component, plus $N - 1$ mixture weights for N Gaussian components); (2) without spatial-kinematic covariances (18 free parameters per component excluding the mixture weights); (3) without spatial-kinematic or purely kinematic covariances (15 free parameters per component excluding the mixture weights); and (4) without any covariance term (12 free parameters per component excluding the mixture weights).

We required that the effective number of fitted stars, multiplied by the number of dimensions for every individual star (up to 6 for complete measurements of the Galactic coordinates and space velocities), were at least as large as the number of parameters in the Gaussian Mixture Model. Any model category or number of Gaussian mixture components that did not satisfy this requirement were ignored in our final model selection.

In the cases of associations with 5 stars or less, a more stringent minimum eigenvalue of 15 pc or 1.5 km s^{-1} was imposed on the components of the Gaussian model to avoid artificially small distributions. Associations with a single cataloged member were modeled with a single spherically symmetric Gaussian component with a characteristic width of 15 pc and 1.5 km s^{-1} to represent the unknown true spatial extent of the association.

This overall process of model construction described above is similar in principle to the model construction used in the original BANYAN Σ tool (Gagné et al. 2018e), with the following improvements: (1) The outlier rejection steps are much more robust and we found did not need any form of human supervision (although every model was visually inspected); (2) multiple Gaussian components are allowed to fit the data to obtain a better representation of the associations with non-Gaussian distributions; and (3) the underlying measure-

ment errors and covariances are treated more appropriately by using the extreme deconvolution method. This led to models with a smaller UVW dispersion on average compared with the previous method, and to more spherical distributions in many cases where biases would otherwise be introduced because of large parallax or radial velocity errors (e.g., distant associations would otherwise be elongated toward the observer).

The resulting fit to the members of the β Pictoris moving group is shown in Figure 16, and the models of all other associations are included as an online-only figure set. Individual members are shown with black circles and their 6D measurement errors are represented by projected gray ellipsoids with their principal axes, and members that were automatically flagged as outliers are marked with purple circles instead. Projections of the single Gaussian cluster that was fitted by `xdeconv` are shown in red with its projected principal axes, and the previous multivariate Gaussian model of Gagné et al. (2018e), which relies on a simpler algorithm that does not account for the proper orientations of measurement errors in $XYZUVW$ space, is shown with a green circle. In most cases where a previous BANYAN Σ model was available, the updated version is both much narrower in UVW space, and the instances of models elongated along the line of sight in either XYZ or UVW space are drastically reduced. The complete set of average association distances and ages are shown in Figure 17, along with a 2D histogram of the individual stars in MOCAdb.

The results from BANYAN Σ applied on every star in MOCAdb (such as the membership probability, and $XYZUVW$ separation from the core of the best model, the optimal distance and radial velocity) are available in the table `calc_banyan_sigma`. We provide calculations for every combination of available input observables to help diagnostics (the possibilities are: proper motion only, proper motion and radial velocity, proper motion and distance, or all of the above), and the one with the most available observables are set to `max_observables= 1`. The calculations can be performed on more than one set of BANYAN Σ models (`moca_bsmdid= 23` for this work). The unique BANYAN Σ model versions are detailed in the table `moca_banyan_sigma_models`; a single one is adopted with the `adopted= 1` flag. The view `calc_banyan_sigma_best` allows to view only the BANYAN Σ results yielded by the adopted models and the full set of available observables, for a given star. The table `calc_banyan_sigma_details` allows to view all detailed calculated quantities (such as the optimal distance and radial velocity) for every plausible association. These detailed outputs should

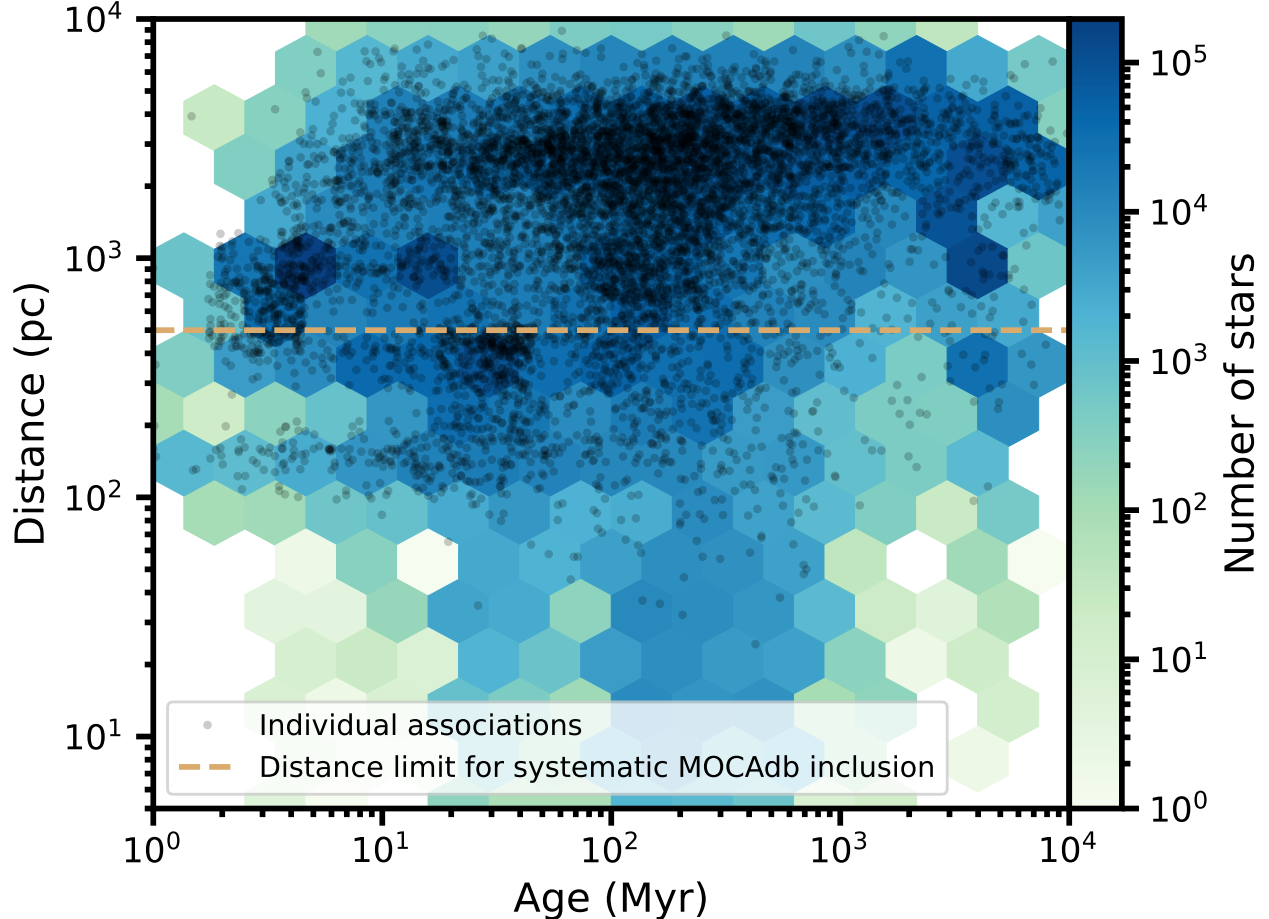


Figure 17. Distribution of distances and ages for individual stars in MOCADB (hex bins) compared with per-association averages (black circles). Although we included only associations with median distances within 500 pc of the Sun (horizontal orange, dashed line), some of their members are located further away. There is a well-documented lack of stars younger than ≈ 10 Myr in the immediate Solar neighborhood ($\lesssim 100$ pc).

be matched to the `calc_banyan_sigma` table using `calc_banyan_sigma_details.cbds_id=calc_banyan_sigma_id`.

5.4. Empirical Color-Magnitude Diagram Sequences

We used the Lagrangian method described in Section 4.5 to model the Gaia DR3 color-magnitude diagram of nearby reference young associations with approximately solar metallicity, accounting for interstellar extinction. The resulting sequences, grouped by age, are shown in Figure 18. These sequences provide empirical isochrones to compare the Gaia DR3 photometry of solar-metallicity stellar populations, allowing users to determine approximate ages without model assumptions.

5.5. Identification of New Candidate Members with Gaia DR3 and Hipparcos

We used the updated BANYAN Σ models constructed in Section 5.3 to identify potentially missing candidate

members of all likely coeval associations cataloged in the `sigmadatabase` using a subset of all Gaia DR3 entries within 500 pc of the Sun. In order to reduce the rate contamination that can be especially significant near the Galactic plane, we have only included Gaia DR3 entries with a parallax measurement error below 0.4 mas.

All stars with a membership Bayesian probability above 70% as determined by BANYAN Σ that also have a most favorable UVW position that is within 3 km s^{-1} of the potentially related association are included in MOCADB for a full compilation of their literature kinematics and future membership assessment, but only those with a membership probability above 90% are considered as robust new candidate members. The constraint UVW informs us about the best-case scenario separation between a star and the center of its potential host association in UVW space, and is useful for excluding stars with unusual kinematics that do not fit

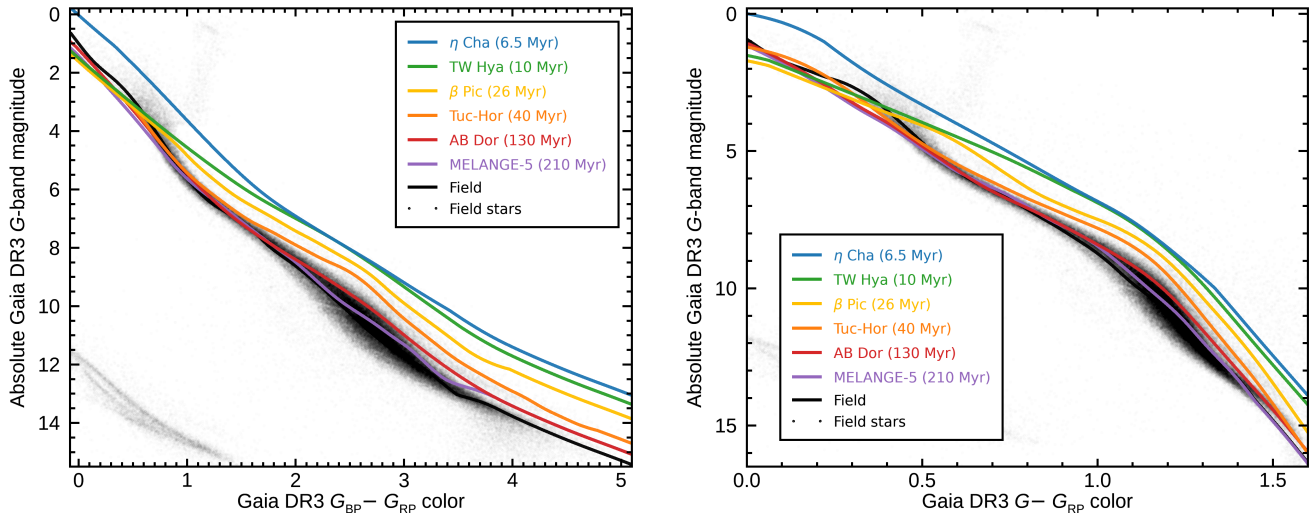


Figure 18. Gaia DR3 color-magnitude diagram of nearby reference populations of distinct ages, compared with the best-fitting sequence constructed using the Lagrangian method described in Section 5.4. The reference populations are as follows: η Cha association, 6.5 Myr (Murphy et al. 2013); TW Hya association, 10 Myr (Bell et al. 2015); β Pic moving group, 26 Myr (Malo et al. 2014); Tuc-Hor association, 40 Myr (Kraus et al. 2014); AB Dor moving group, 130 Myr (Gagné et al. 2018c); MELANGE-5 association, 210 Myr (Thao et al. 2024).

any Bayesian hypothesis considered by BANYAN Σ , including its model of nearby field stars.

Any potential candidate member with an existing entry in the `data_memberships` database table has already been assessed in the existing literature, and was therefore ignored. The resulting candidate members were further vetted in a M_G versus $G - G_{RP}$ Gaia DR3 color-magnitude diagram, and were rejected if they are at least 0.25 mag fainter than the empirical sequence of the appropriate age (see Section 5.4 and Figure 18). Candidates that were flagged as likely interlopers based on this color-magnitude diagram cut were included in the `data_memberships` table as rejected candidates (`moca_mtid='R'`), to inform future searches for candidate members that may recover them.

Some of the brightest stars with parallax measurements in the Hipparcos mission Perryman et al. (1997) are either too bright for Gaia to measure their kinematics, or bright enough that the Gaia accuracy is decreased compared with the Hipparcos analysis of van Leeuwen (2007). Because of this, we have also used the complete Hipparcos compilation to identify some potentially missing brighter members of nearby young associations, using the same method and selection criteria.

In addition to the Gaia and Hipparcos samples, we included in our BANYAN Σ every object that were included in MOCAdb, which allowed us to identify a few other candidate members beyond 500 pc of the Sun. Those mainly come from literature claims of non-memberships in a specific open cluster or association,

which were included as non-members (`moca_mtid='R'`) and which we categorized as a candidate member of another association. Additional sources come from catalog compilations of rotation periods or equivalent width measurements that were not previously identified as members of a young association. The candidate members resulting from this analysis are shown in Figures 19, 20 and 21.

The 11535 resulting new candidate members are listed in Table 2 and were included in the `data_memberships` database table.

It is notable that the B2.5V star Nunki (Sig Sgr) appears to be a candidate member in the 26 ± 3 Myr-old β PMG (Zuckerman et al. 2001; Malo et al. 2014) with a 74% membership probability in BANYAN Σ (at a UVW separation of 4.3 km s^{-1} from the center of the β PMG kinematic model). This massive star had not been previously identified as a candidate member in β PMG, possibly because it is somewhat of a kinematic outlier and for its lack of Gaia astrometry, which is a consequence of its brightness (its Hipparcos magnitude is 2.0 mag). This would be the most massive member of the β PMG, to which β Pictoris itself (an A6V star) is second. A B2.5V star such as Nunki is expected to leave the main sequence ≈ 60 Myr after formation, and it is therefore plausible that it may be young enough to be a member of β PMG.

Nunki has long been known as a candidate equal-mass binary based on interferometry (Hanbury Brown et al. 1974; Bedding et al. 1994), but it was more recently

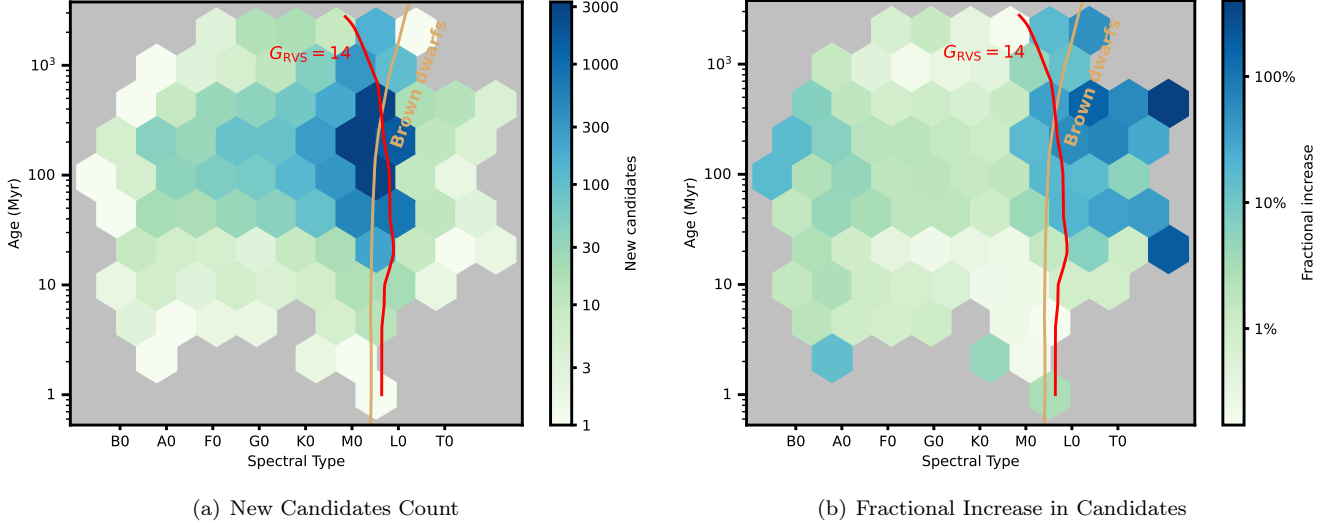


Figure 19. Spectral types and ages of the newly identified candidate members in this work. The left panel shows the absolute number of new candidates, and the right panel shows the fractional increase versus previous literature membership lists. Most of the newly identified candidates are early M dwarfs with ages in the 30–500 Myr range, but the largest fractional increases are observed for later-type objects in the substellar regime or for BA stars, in part due to their lack of radial velocity measurements in Gaia DR3, which BANYAN Σ does not require to make a probabilistic membership assessment. The red line outlines the spectral types past which the Gaia DR3 radial velocities are unavailable, which correspond to an apparent G_{RVS} -band magnitude of 14 mag. We have assumed the distances of the nearest young association to the Sun at every age bin to calculate this delimiting apparent G_{RVS} .

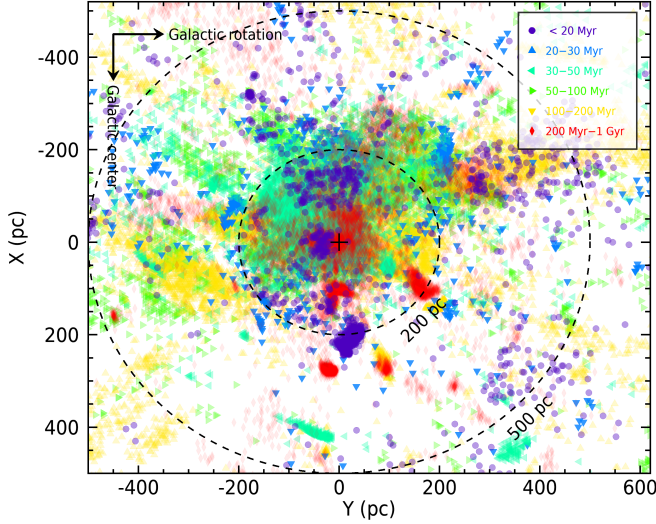


Figure 20. Galactic space coordinates of newly identified candidate members of young moving groups. Most newly identified candidates are located within 500 pc of the Sun because they originate from the dedicated Gaia DR3 + Hipparcos search within that radius. See Section 5.5 for more details.

resolved as a near equal-mass $\approx 6.5 M_{\odot}$ $0.^{\prime\prime}6$ binary star with VLT/GRAVITY (Eisenhauer et al. 2009), along with an estimated system age of 30 Myr (Waisberg et al. 2025).

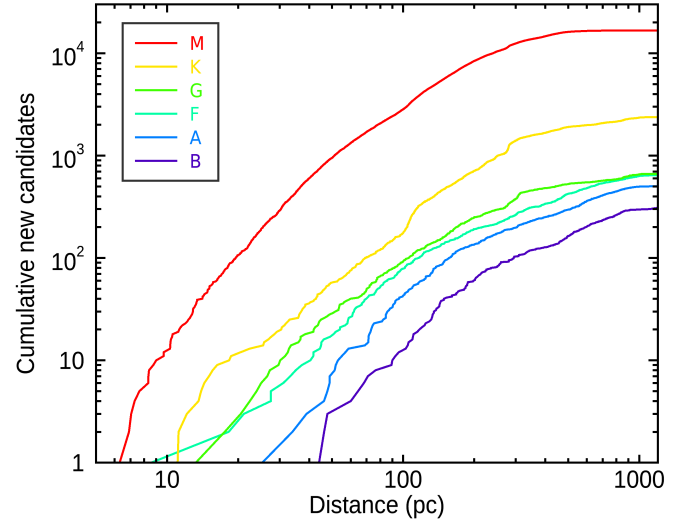


Figure 21. Distance cumulative distribution functions for all new candidate members reported here, by spectral class, and that most other types of stars were identified at distances further than 100 pc. Follow-up work such as direct-imaging campaigns that target nearby young M dwarfs will therefore benefit from this refreshed sample of nearby, young M dwarfs. This figure illustrates that most of the newly identified members are M dwarfs. See Section 5.5 for more details.

5.6. Combined Age Diagnostic Sequences

In Figures 22, 23 and 24, we provide a preview of several age-dependent diagnostic measurements in the

MOCA database. These data sets will provide valuable comparison sequences as well as training sets to build future age-dating tools that will allow inverting either a single age-dependent diagnostic measurement or a combination of them into an age estimation for a single star.

We also provide additional age probability density functions for several MOCAdb associations and their individual stellar members based on publicly available Bayesian age-dating Python algorithms:

- **ChronoFlow** is an empirical gyrochronology model constructed in Gaia DR3 color versus rotation period space based on normalizing flows (Van-Lane et al. 2025);
- **EAGLES v2** estimates ages using an artificial neural network trained on reference lithium equivalent width sequences (Jeffries & Jackson 2023; Weaver et al. 2024);
- **BAFFLES** estimates ages based on empirical sequences in R'_{HK} activity indices versus $B - V$ color for stars with spectral types as late as early M dwarfs (for those with available $B - V$ colors) (Stanford-Moore et al. 2020);
- The Engle & Guinan (2023) relations similarly allow to determine Bayesian age posteriors based on empirical sequences of R'_{HK} activity versus age, for spectral types M0–M2 and M2.5–M6.5, in cases where $B - V$ colors are not available;
- **EVA** uses an empirical relationship between the excess Gaia DR3 photometric error and young association ages established by Barber & Mann (2023). The excess photometric error was established by Guidry et al. (2021) as a proxy for variability, which explains its correlation with age.

In most cases, age probability density functions were constructed for each individual star and age-dating method. The only exception is EVA, where the age calibration is based on the 90th centile of an association’s excess error distribution, meaning that only a single combined probability density function is generated for each young association.

The ages obtained from these methods are stored in the respective tables `data_object_ages`, `calc_object_age_pdfs`, `data_association_ages` and `calc_association_age_pdfs`. A more extensive characterization, including additional age-dating methods, will be presented in future work.

5.7. Exoplanets

The latest version of the NASA Exoplanet Archive was imported in the MOCAdb in order to identify exoplanet companions to members or candidate members of age-calibrated associations, shown in Figure 25. This figure outlines the recently growing, albeit still sparse, set of known exoplanets with well-calibrated ages determined from membership in a young association.

We identify a current total of 134 confirmed exoplanet systems that may be members of age-calibrated associations, in addition to 121 TESS (Ricker et al. 2015) exoplanet candidates that are not yet confirmed. Among these, 46 confirmed exoplanets and 53 TESS exoplanet candidates appear to be identified as candidate members of a young association for the first time here. The set of age-calibrated confirmed exoplanets and exoplanet candidates are listed in Tables 6 and 7, respectively. Focused searches for exoplanets around members of young associations (e.g., Newton et al. 2019; Wood et al. 2023; Thao et al. 2024; Distler et al. 2025) will enable population-level studies of how exoplanet properties evolve over time in the near future.

5.8. Brown Dwarfs and Isolated Planetary-Mass Objects

The MOCA database allows us to conveniently refresh the list of potential isolated planetary-mass objects that currently stand the membership test based on updated BANYAN Σ models.

In 19 cases where reliable substellar proper motions were not available, we used individual detections in the near-infrared and red-optical catalogs available in MOCAdb to calculate proper motions (Skrutskie et al. 2006; Wright et al. 2010; Marocco et al. 2021; Nidever et al. 2021; Chambers et al. 2016; Dye et al. 2018; McMahon et al. 2013; Lawrence & Warren 2005; Meisner et al. 2023). These cases are listed in Table 8.

It was recently demonstrated that the impact of clouds is non-negligible on the cooling tracks of the coolest-mass substellar objects (Morley et al. 2024), causing a flattening, overlap and even crossings of isomasses near the planetary-mass boundary ($13 M_{Jup}$) in a temperature–age diagram (see Figure 26). Because of this, estimating the masses of isolated planetary-mass objects is not straightforward. While the Burrows et al. (2001) evolutionary tracks used in Section 4.6.3 are appropriate for estimating the small impact of gravitational redshift on the heliocentric radial velocities of substellar objects, a more careful analysis is required to estimate which substellar objects have masses comparable to gas giant exoplanets.

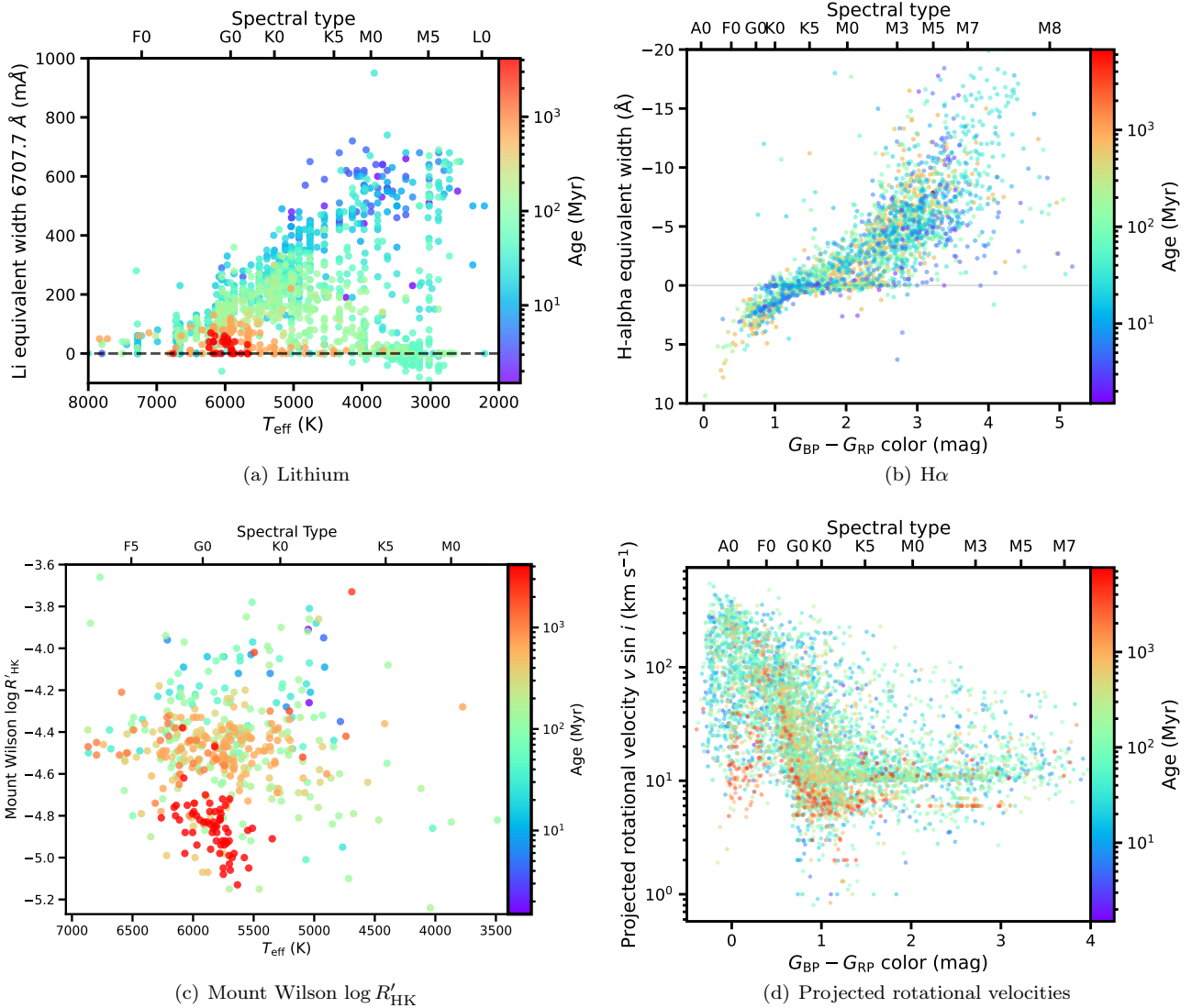


Figure 22. Various age-dependent measurable available in MOCAdb as a function of stellar ages based on membership. These data sets will be useful as comparison sequences to determine the ages of non-members. See Section 5.6 for more details.

We used a method based on the tracks of (Morley et al. 2024) extended onto the empirical tracks of Section 4.6.3 by log-interpolation to achieve this. We converted the best-available spectral type of each object M6 or later in MOCAdb to an effective temperature with a 10⁴-element Monte Carlo and the T_{eff} –spectral type sequence described in Section 4.6.2³⁶, and combined it with random draws from an asymmetrical log-normal distribution for the age (using asymmetrical age measurement errors when they are available). These random realizations in (T_{eff} , age) space are then used to

construct a two-dimensional kernel density estimate using Python’s `scipy.stats.gaussian_kde` (Scott 1992), along which every isomass track is integrated to produce a probability for that specific mass. This was repeated for every isomass track to determine a mass probability density function, which is then translated to an estimate and asymmetric error bars by sampling the 15.9%, 50%, and 84.1% centiles of the cumulative distribution function.

It is interesting to note that we revise the estimated mass of the Carina-Near member SIMP J013656.5+093347.3 upwards at $17_{-5}^{+7} M_{\text{Jup}}$ (a $\approx 20\%$ increase), and revise the mass of the younger TW Hya association member 2MASS J12074836-3900043 (TWA 40) down to $14_{-2}^{+3} M_{\text{Jup}}$ (a 7% decrease), illustrating the role that clouds play in pushing the

³⁶ The probability density function representing the spectral type measurement is assumed to be Gaussian, but the resulting T_{eff} is not assumed to be.

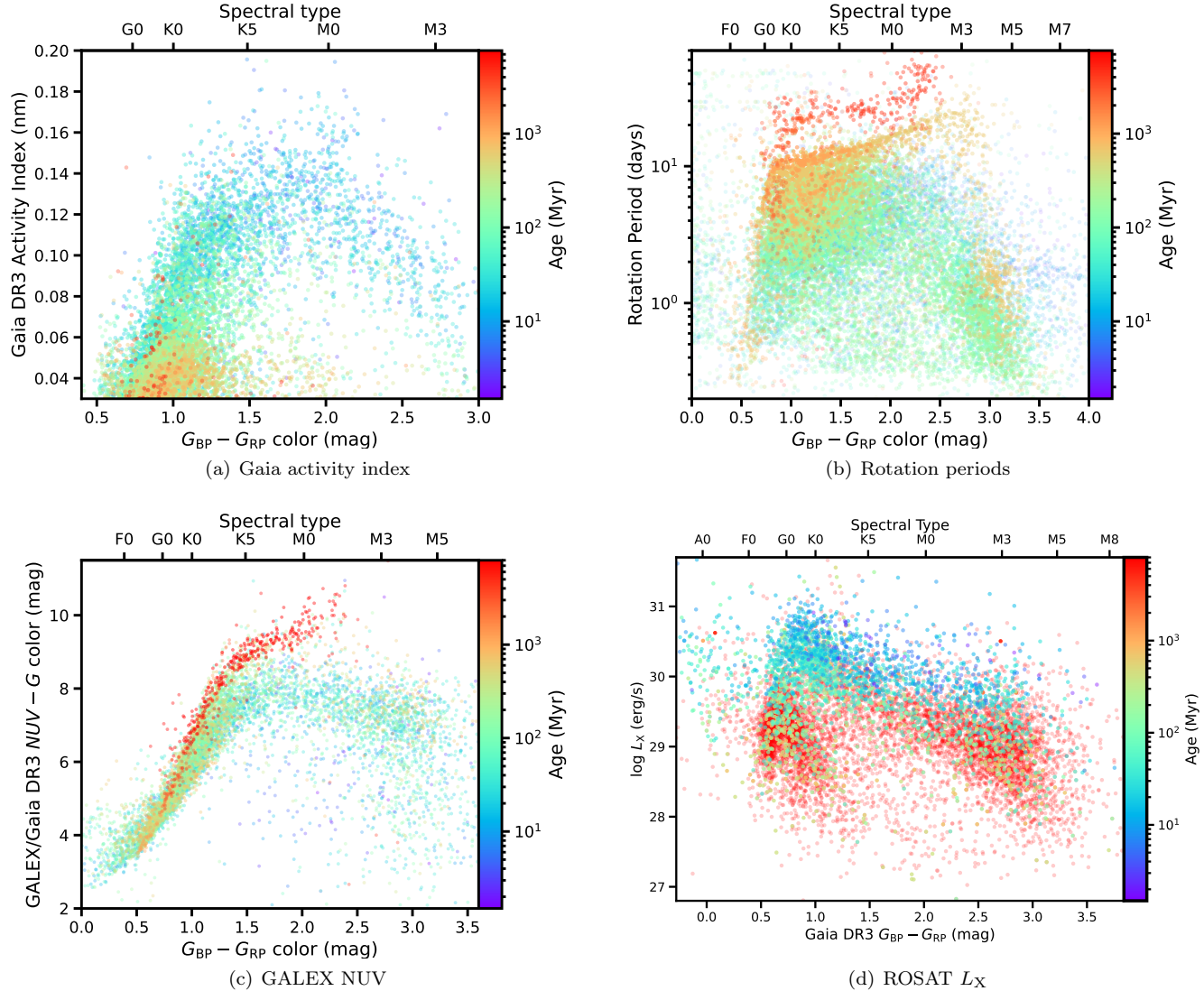


Figure 23. Various age-dependent measurable properties available in MOCAdb as a function of stellar ages based on membership. A transparency that favors high-density regions in $(x,y,\log \text{age})$ space was used to improve visibility. These data sets will be useful as comparison sequences to determine the ages of non-members. See Section 5.6 for more details.

masses of older planetary-mass candidates in particular to higher values. Furthermore, Gagné et al. (2015) discussed an intriguing pile-up of objects with estimated masses around $13 M_{\text{Jup}}$ in the young association Tucana-Horologium, composed of a dozen objects with early-L spectral types. Although most of them still survive as likely members of this population, their masses are revised upward in the range $20\text{--}30 M_{\text{Jup}}$, which means that the previously observed piling-up at $13 M_{\text{Jup}}$ was likely an artifact of earlier cooling tracks that underestimated the masses of low-mass brown dwarfs at ≈ 40 Myr.

We provide in Table 8 a compilation of all currently known substellar objects that may belong to a nearby young association, based on updated BANYAN Σ membership probabilities, along with their estimated masses.

Membership probabilities include radial velocities when they are available, trigonometric distances when available, and otherwise photometric distances (the absolute K -band magnitude versus $W1 - W2$ color sequence is used when possible, otherwise the absolute $W2$ -band magnitude versus $W1 - W2$ sequence is used).

We catalog a total of 1620 potentially young substellar objects, 455 of those with spectral types L0 or later. About 196 of the L0 and later-type young substellar objects are newly identified, mostly in recently discovered or poorly studied nearby young associations. It is noteworthy that a number of young brown dwarfs appear to match the recently discovered tidal tails of Coma Ber and the Hyades, and the corona of IC 2391. We find 101 objects whose central mass estimates fall in

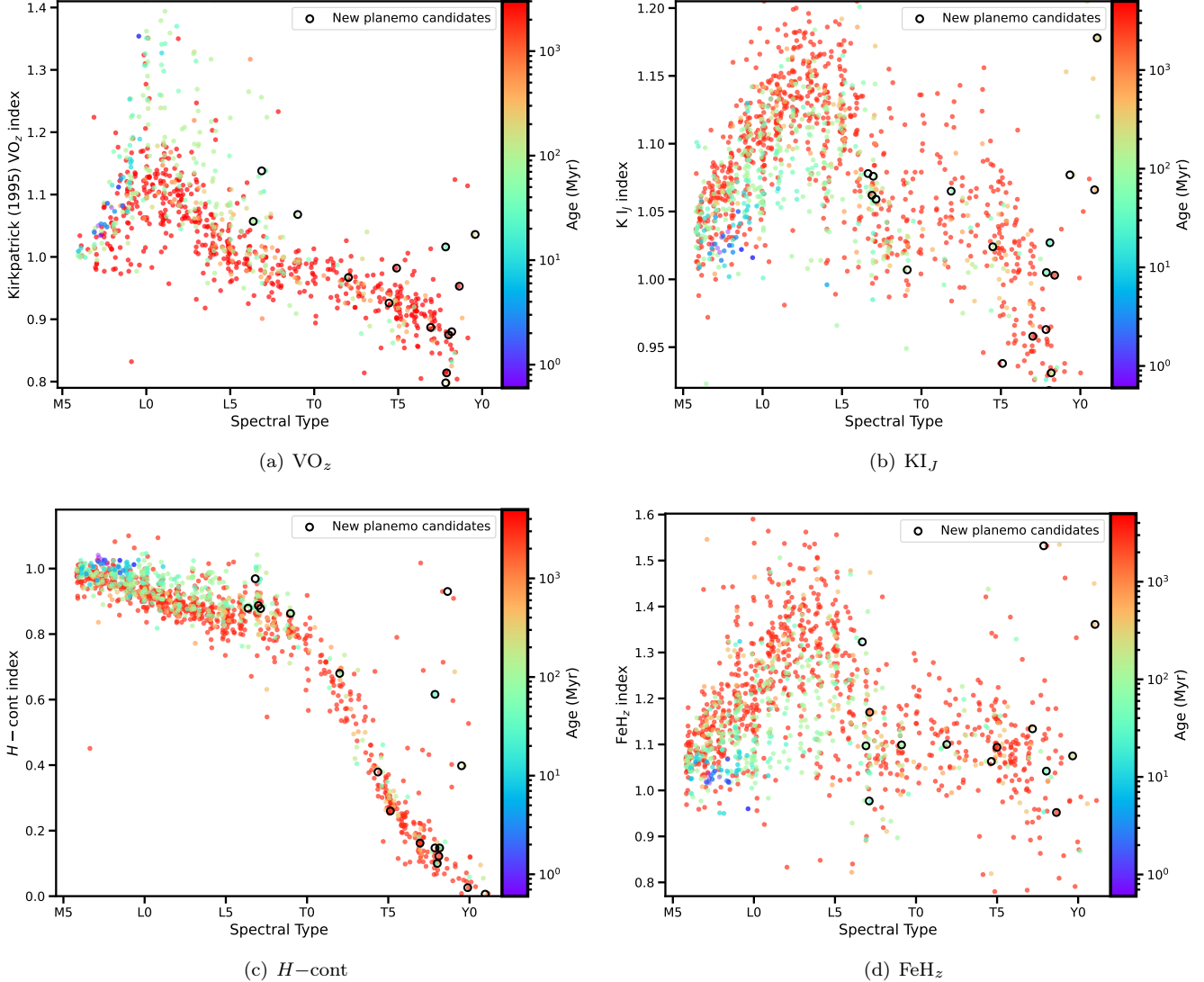


Figure 24. Various surface gravity-dependent spectral indices (see e.g. Allers & Liu 2013) computed in MOCAdb from the publicly available near-infrared spectra of substellar objects in MOCAdb as a function of stellar ages based on membership. For substellar objects without a known membership, we assumed an age of 3 Gyr or 200 Myr when a spectroscopic sign of low-gravity is noted in the literature, for display purposes. See Section 5.6 for more details.

the planetary-mass regime, 53 of which are newly recognized here.

We provide a list of 64 previously suggested isolated planetary-mass candidates which memberships appear to be rejected by BANYAN σ in Table 9. We caution that this could be subject to change if the measurement inputs are refined or if the BANYAN Σ models do not capture the full details of the spatial shapes of the respective associations.

It is important to note that the census of isolated planetary-mass objects presented here ignores some of the coldest Y dwarfs that do not benefit from a precise age estimation, as we focused here on age-calibrated objects. A number of Y dwarfs are so cold that, even at

the age of the Universe, have estimated masses below $13 M_{Jup}$ (see e.g., Luhman 2014; Leggett & Tremblin 2025).

Some of the newly identified candidate planetary-mass objects are of particular note. For example, the ≈ 19.5 candidate brown dwarf CWISEP J053644.82–305539.3 identified by Kirkpatrick et al. (2011) benefits from a parallax and proper motion (but no spectrum), and could potentially be a $\approx 2 M_{Jup}$ isolated planetary-mass object in the β Pic moving group, if corroborated with a spectral analysis and radial velocity measurement.

The Y0 CWISE J201146.50–481259.8 from Meisner et al. (2020) is similarly interesting, and may be a $\approx 4 M_{Jup}$ member of the ≈ 210 Myr-old MELANGE-5

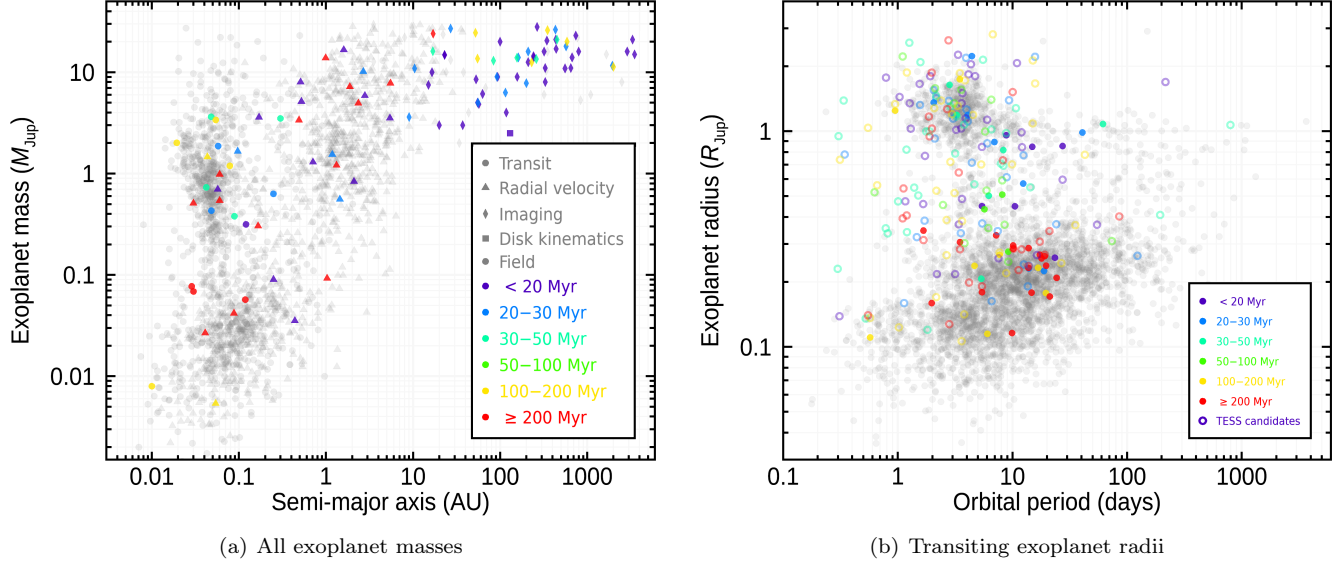


Figure 25. Population properties of confirmed exoplanet systems listed in the NASA Exoplanet Archive (left panel and filled symbols in right panel) and the current TESS candidate exoplanets (empty circles in right panel). Systems that are members of a young association are indicated with a color and symbol that corresponds to the host association’s age. See Section 5.7 for more details.

association of Thao et al. (2024). Our updated census of isolated planetary-mass objects includes a few more candidates with very low masses below $\approx 6 M_{\text{Jup}}$ that warrant further characterization, as very few isolated objects are currently known with such low masses.

The T1.5 PSO J159.2399–26.3885 (Best et al. 2015) is also of particular interest as it is flagged here as a $\approx 5 M_{\text{Jup}}$ candidate member of the ≈ 10 Myr TW Hya association (Bell et al. 2015). (Best et al. 2015) note that this object satisfies four of the six Burgasser et al. (2010) spectroscopic binary classification criteria, making it a strong candidate substellar unresolved binary of unequal T_{eff} , but they did not note anything else that may make it an immediately compelling low-gravity object. If confirmed, this would be one of the youngest known early-T objects, and it would make it a valuable benchmark to better understand the L/T transition at young ages.

6. THE MOCADB WEBSITE

Most of the database content can be consulted at the <https://mocadb.ca> website with a simple user interface and a series of Python dash applications, allowing users to access distinct aspects of the database:

- **Database Reports** on a single star or young association, listing a compilation of data relevant to this specific object;
- **The MOCAdb Explorer** allows users to display members of several young associations

across different graphics (color-magnitude diagrams, spatial-kinematic positions, Lithium and rotation periods);

- **The Spatial-Kinematic Explorer** allows users to any three combinations of the $XYZUVW$ axes for members of specific associations with the relevant BANYAN Σ models;
- **The Substellar Photometry Explorer** allows users to view any combinations of spectral types, colors, absolute magnitudes, spectral indices or equivalent widths for substellar objects;
- **The Spectral Explorer** allows users to quickly view a spectrum stored in MOCAdb;
- **The Spectral Typing Tool** allows users to assign spectral types to substellar objects which spectra are stored in MOCAdb;
- **The Astrometric Explorer** allows users to view the astrometry of any object versus epoch and perform a quick fit of its proper motion and/or parallax;
- **Age PDF Explorers** allow users to view the individual age probability density functions for a given star or association, for each calculation method, with an optimal combined PDF across all methods;

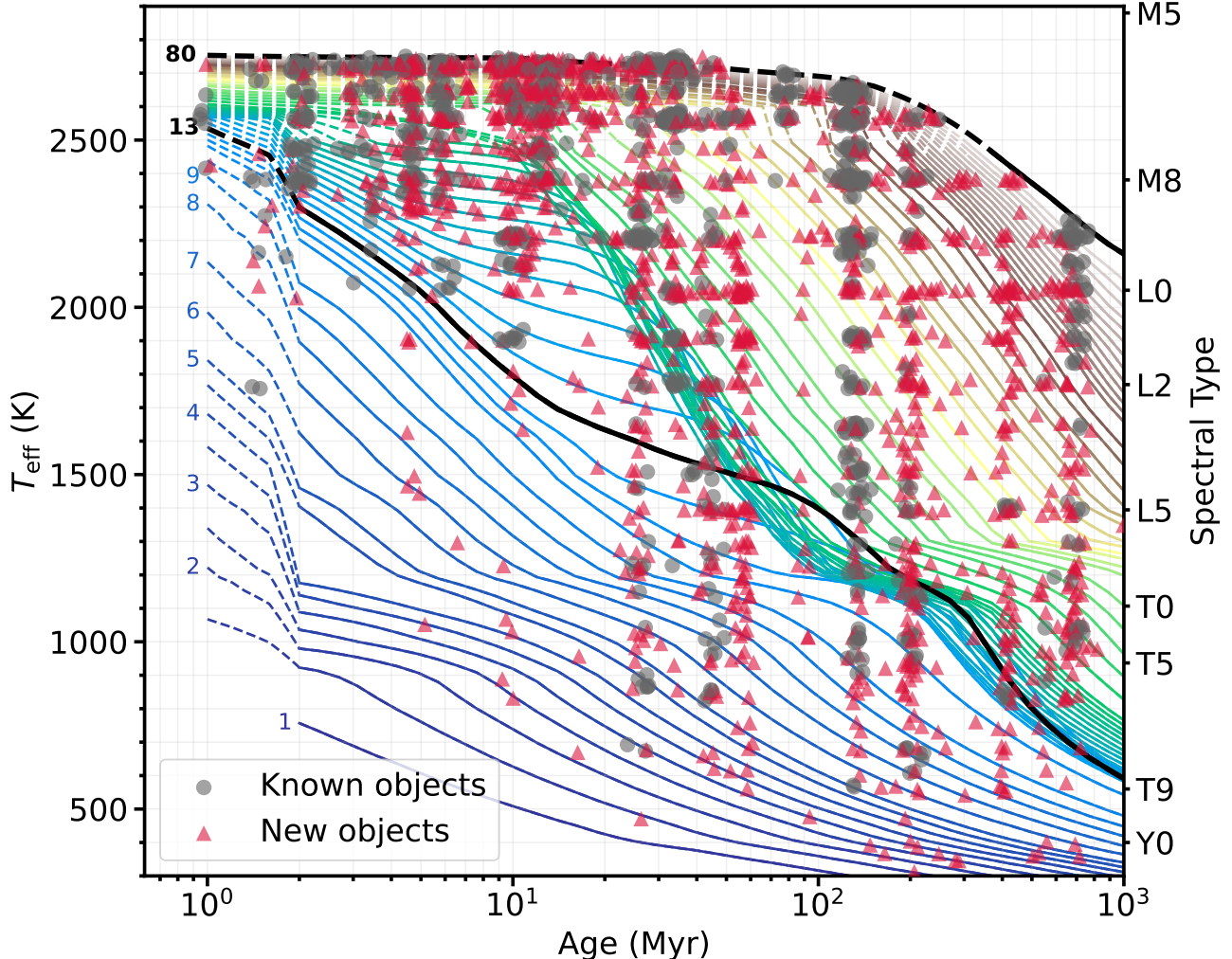


Figure 26. Age and T_{eff} of the current census of candidate age-calibrated substellar objects listed in Table 8, in cases where the host association currently benefits from an age estimate. Known candidate members of young association from the literature are shown as grey circles, and new candidate members are shown as red triangles. The Morley et al. (2024) isomass tracks are displayed in the background with thick lines, and their extensions onto the empirical mass tracks of Section 4.6.3 are shown as dashed lines. The $13 M_{\text{Jup}}$ and $80 M_{\text{Jup}}$ tracks highlighted in black, and model track masses are labeled in M_{Jup} . A horizontal jitter of 0.02 dex in age was added for clarity, as nearby associations have ages clustered around few distinct values. The isomass tracks overlap significantly around $13 M_{\text{Jup}}$, significantly complicating reliable estimates around the planetary-mass regime boundary. This figure outlines that the age and T_{eff} coverage of age-calibrated substellar objects has improved significantly in recent years, allowing for detailed studies of substellar atmospheres in a range of parameters. See Section 5.8 for more details.

- **A Sunburst graph** of the hierarchical structure of the MOCAdb associations with a dynamic interface.

Users can also directly communicate with the database contents using Python `pandas` dataframes with the publicly available `mocapy` package³⁷.

For more advanced queries, users can directly communicate with the MOCAdb MySQL server using a MySQL client with the following credentials:

```
MySQL database  : mocadb
MySQL host      : 104.248.106.21
MySQL username  : public
MySQL password  : z@nUg_2h7_%?31y88
```

7. CONCLUSIONS

We presented the Montreal Open Clusters and Associations (MOCA) MySQL database, systematically compiling all known stellar associations and their members within 500 pc, in addition to all known nearby substellar objects. A number of literature properties (e.g., proper motions, radial velocities, parallaxes, photometry, rota-

³⁷ Available at <https://github.com/jgagneastro/mocapy>

tion periods) are compiled, combined into high-precision averages, or used as a basis for additional calculations (e.g. UVW Galactic space velocities).

We used this updated census of nearby young associations with an updated Gaussian Mixture Model representation, based on automated outlier rejection and extreme deconvolution, to update the Bayesian membership classification tool BANYAN Σ , allowing its models to capture much more complex shapes of nearby young associations, and updated its total number of modeled associations to 8125. Using this updated tool, we have identified 11535 new candidate members of nearby associations that were previously overlooked.

The MOCAdb is publicly accessible at <https://mocadb.ca>, through direct MySQL clients, or through the `mocapy` Python package, and allows users to directly interface with the data in a number of ways. The MOCAdb will enable the rapid construction of custom samples for a wide range of uses, such as sample construction for telescope follow-up or exoplanet searches, the construction of training sets for future age-dating tools, the population-level study of open cluster properties, or the search for isolated planetary-mass objects in nearby, young associations.

The MOCAdb will be updated continuously as new data become available, and as new features are needed³⁸. The combination of MOCAdb with future data sets will enable the efficient identification of many more age-calibrated exoplanets. The fourth data release of Gaia will not only greatly improve the astrometric and radial velocity accuracy of stellar members especially at the low-mass end. Its enabling of large-scale searches for astrometric exoplanets will also greatly improve our census of exoplanets in age-calibrated associations cataloged in this work.

Combining future missions that enable large-scale discovery and characterization of substellar objects with MOCAdb will also enable the discovery of many new isolated planetary-mass objects. For example, the Vera Rubin Observatory will provide parallaxes for thousands of substellar objects that are too faint for Gaia astrometry (Gizis et al. 2022), the Euclid space mission’s Wide Survey (Laureijs et al. 2011) will allow the direct spectroscopic identification of many substellar objects, and its Deep Survey will even enable parallax measurements for additional substellar objects (Zhang et al. 2024) at further distances.

³⁸ The state of the MOCAdb at the moment of publication is available as a frozen version of CSV files on Zenodo at <https://zenodo.org/uploads/18166118> with DOI 10.5281/zenodo.18166118.

ACKNOWLEDGEMENTS

This project was developed in part at the Gaia FA²te, hosted by the Flatiron Institute Center for Computational Astrophysics in 2022 June. This work was carried out partially with a Banting grant from the Natural Sciences and Engineering Research Council of Canada (NSERC). This work has benefited from The UltracoolSheet (Best et al. 2024a) at <http://bit.ly/UltracoolSheet>, maintained by Will Best, Trent Dupuy, Michael Liu, Rob Siverd, and Zhoujian Zhang, and developed from compilations by Dupuy & Liu (2012), Dupuy & Kraus (2013), Liu et al. (2016), Best et al. (2018), and Best et al. (2021).

This research made use of: the SIMBAD database and VizieR catalog access tool, operated at the Centre de Données astronomiques de Strasbourg, France (Ochsenbein et al. 2000); data products from the Two Micron All Sky Survey (2MASS; Skrutskie et al. 2006), which is a joint project of the University of Massachusetts and the Infrared Processing and Analysis Center (IPAC)/California Institute of Technology (Caltech), funded by the National Aeronautics and Space Administration (NASA) and the National Science Foundation (Skrutskie et al. 2006); data products from the *Wide-field Infrared Survey Explorer* (WISE; and Wright et al. 2010), which is a joint project of the University of California, Los Angeles, and the Jet Propulsion Laboratory (JPL)/Caltech, funded by NASA; the WEBDA database, operated at the Department of Theoretical Physics and Astrophysics of the Masaryk University; and the Unified Cluster Catalogue (UCC; Perren et al. 2023). This work has made use of the SIMPLE Archive of low-mass stars, brown dwarfs, and directly imaged exoplanets: 10.5281/zenodo.13937301.

The Digitized Sky Surveys (DSS) were produced at the Space Telescope Science Institute under U.S. Government grant NAG W-2166. The images of these surveys are based on photographic data obtained using the Oschin Schmidt Telescope on Palomar Mountain and the UK Schmidt Telescope. The plates were processed into the present compressed digital form with the permission of these institutions. The Second Palomar Observatory Sky Survey (POSS-II) was made by the California Institute of Technology with funds from the National Science Foundation, the National Geographic Society, the Sloan Foundation, the Samuel Oschin Foundation, and the Eastman Kodak Corporation. The Oschin Schmidt Telescope is operated by the California Institute of Technology and Palomar Observatory.

This work presents results from the European Space Agency (ESA) space mission Gaia. Gaia data are being processed by the Gaia Data Processing and

Analysis Consortium (DPAC). Funding for the DPAC is provided by national institutions, in particular the institutions participating in the Gaia MultiLateral Agreement (MLA). The Gaia mission website is <https://www.cosmos.esa.int/gaia>. The Gaia archive website is <https://archives.esac.esa.int/gaia>. The Digitized Sky Surveys were produced at the Space Telescope Science Institute under U.S. Government grant NAG W-2166. This research has benefitted from the SpeX Prism Spectral Libraries, maintained by Adam

Burgasser at <https://cass.ucsd.edu/~ajb/brown dwarfs/spexprism>. Part of this research was carried out at the Jet Propulsion Laboratory, California Institute of Technology, under a contract with the National Aeronautics and Space Administration (80NM0018D0004).

Software: BANYAN Σ (Gagné et al. 2018e), EA-GLES v2 (Jeffries & Jackson 2023; Weaver et al. 2024), BAFFLES (Stanford-Moore et al. 2020), ChronoFlow (Van-Lane et al. 2025), EVA (Barber & Mann 2023).

REFERENCES

Abbott, T. M. C., Adamów, M., Aguena, M., et al. 2021, *ApJS*, 255, 20

Abdurro'uf, Accetta, K., Aerts, C., et al. 2022, *The Astrophysical Journal Supplement Series*, 259.0, 35

Aberasturi, M., Caballero, J. A., Montesinos, B., et al. 2014, *The Astronomical Journal*, 148.0, 36

Abolfathi, B., Aguado, D. S., Aguilar, G., et al. 2018, *ApJS*, 235, 42

Abt, H. A. 1981, *Astrophysical Journal Supplement Series*, 45, 437

—. 1985, *The Astrophysical Journal Supplement Series*, 59.0, 95

Abt, H. A., & Cardona, O. 1983, *The Astrophysical Journal*, 272.0, 182

Abt, H. A., & Morrell, N. I. 1995, *Astrophysical Journal Supplement* v.99, 99, 135

Agüeros, M. A., Curtis, J. L., Núñez, A., et al. 2025, *Crowning the Queen: Membership, Age, Rotation, and Activity for the Open Cluster Coma Berenices*, doi:10.48550/arXiv.2509.03461

Ahumada, R., Allende Prieto, C., Almeida, A., et al. 2020, *The Astrophysical Journal Supplement Series*, 249.0, 3

Albert, L., Artigau, É., Delorme, P., et al. 2011, *The Astronomical Journal*, 141, 203

Alcalá, J. M., Spezzi, L., Chapman, N., et al. 2008, *The Astrophysical Journal*, 676.0, 427

Alessi, B. S., Moitinho, A., & Dias, W. S. 2003, *A&A*, 410, 565

Alexander, M. J., Hanes, R. J., Povich, M. S., & McSwain, M. V. 2016, *The Astronomical Journal*, 152.0, 190

Allen, P. R., Cruz, K. K., Koerner, D. W., McElwain, M. W., & Reid, N. I. 2007, *The Astronomical Journal*, 133, 971

Allende Prieto, C., Koesterke, L., Ludwig, H. G., Freytag, B., & Caffau, E. 2013, *A&A*, 550, A103

Aller, K. M. 2016, PhD thesis

Aller, K. M., Liu, M. C., Magnier, E. A., et al. 2016, *The Astrophysical Journal*, 821, 120

Allers, K. N., Gallimore, J. F., Liu, M. C., & Dupuy, T. J. 2016, *ApJ*, 819, 133, eprint: 1601.04717

Allers, K. N., & Liu, M. C. 2013, *The Astrophysical Journal*, 772, 79

—. 2020, *Publications of the Astronomical Society of the Pacific*, 132.0, 104401

Allers, K. N., Jaffe, D. T., Luhman, K. L., et al. 2007, *The Astrophysical Journal*, 657.0, 511

Alonso-Floriano, F. J., Morales, J. C., Caballero, J. A., et al. 2015, *Astronomy and Astrophysics*, 577, A128

Alves de Oliveira, C., & Casali, M. 2008, *Astronomy and Astrophysics*, 485.0, 155

Alves de Oliveira, C., Moraux, E., Bouvier, J., & Bouy, H. 2012, *Astronomy and Astrophysics*, 539, 151

Alves de Oliveira, C., Moraux, E., Bouvier, J., et al. 2010, *Astronomy and Astrophysics*, 515.0, A75

—. 2013, *Astronomy and Astrophysics*, 549.0, A123

Ardila, D., Martín, E., & Basri, G. 2000, *The Astronomical Journal*, 120, 479

Artigau, É., Doyon, R., Lafrenière, D., et al. 2006, *The Astrophysical Journal*, 651, L57

Artigau, É., Lafrenière, D., Doyon, R., et al. 2011, *The Astrophysical Journal*, 739, 48

Asiaín, R., Figueiras, F., Torra, J., & Chen, B. 1999, *A&A*, 341, 427

Aveni, A. F., & Hunter, Jr., J. H. 1969, *AJ*, 74, 1021

Azulay, R., Guirado, J. C., Marcaide, J. M., et al. 2017, *A&A*, 607, A10

Bagdonas, V., Drazdauskas, A., Tautvaišienė, G., Smiljanic, R., & Chorniy, Y. 2018, *A&A*, 615, A165

Bai, Y., Sun, Y.-C., He, X.-T., et al. 2012, *Research in Astronomy and Astrophysics*, 12.0, 443

Bailer-Jones, C. A. L., Rybizki, J., Fouesneau, M., Demleitner, M., & Andrae, R. 2021, *AJ*, 161, 147

Bailey, V., Meshkat, T., Reiter, M., et al. 2014, *The Astrophysical Journal*, 780.0, L4

Bally, J. 2008, in *Handbook of Star Forming Regions*, Volume I, ed. B. Reipurth, Vol. 4, 459

Bannister, N. P., & Jameson, R. F. 2007, *Monthly Notices of the Royal Astronomical Society: Letters*, 378, L24

Barber, M. G., & Mann, A. W. 2023, *ApJ*, 953, 127

Barber, M. G., Mann, A. W., Bush, J. L., et al. 2022, *AJ*, 164, 88

Bardalez Gagliuffi, D. C., Gagné, J., Faherty, J. K., & Burgasser, A. J. 2018, *The Astrophysical Journal*, 854.0, 101

Bardalez Gagliuffi, D. C., Burgasser, A. J., Gelino, C. R., et al. 2014, *ApJ*, 794, 143

Barnard, E. E., Frost, E. B., & Calvert, M. R. 1927, *A Photographic Atlas of Selected Regions of the Milky Way*, Vol. 0.0

Baroch, D., Morales, J. C., Ribas, I., et al. 2020, *A&A*, 641, A69

Barrado y Navascués, D. 1998, *A&A*, 339, 831

Barrado y Navascués, D., Béjar, V. J. S., Mundt, R., et al. 2003, *Astronomy and Astrophysics*, 404.0, 171

Barrado y Navascués, D., Zapatero Osorio, M. R., Béjar, V. J. S., et al. 2001, *Astronomy and Astrophysics*, 377.0, L9

Basri, G., & Martín, E. L. 1999, *The Astrophysical Journal*, 510.0, 266

Basri, G., Mohanty, S., Allard, F., et al. 2000, *The Astrophysical Journal*, 538, 363

Bayo, A., Barrado, D., Stauffer, J., et al. 2011, *Astronomy and Astrophysics*, 536.0, A63

Beamín, J. C., Minniti, D., Gromadzki, M., et al. 2013, *Astronomy and Astrophysics*, 557.0, L8

Beamín, J. C., Ivanov, V. D., Minniti, D., et al. 2015, *Monthly Notices of the Royal Astronomical Society*, 454.0, 4054

Beasor, E. R., Davies, B., Smith, N., Gehrzi, R. D., & Figer, D. F. 2021, *The Astrophysical Journal*, 912.0, 16

Becker, A. C., Bochanski, J. J., Hawley, S. L., et al. 2011, *The Astrophysical Journal*, 731.0, 17

Bedding, T. R., Robertson, J. G., & Marson, R. G. 1994, *A&A*, 290, 340

Béjar, V. J. S., Zapatero Osorio, M. R., Pérez-Garrido, A., et al. 2008, *The Astrophysical Journal*, 673, L185

Bell, C. P. M., Mamajek, E. E., & Naylor, T. 2015, *MNRAS*, 454, 593

Bell, C. P. M., Naylor, T., Mayne, N. J., Jeffries, R. D., & Littlefair, S. P. 2012, *Monthly Notices of the Royal Astronomical Society*, 424, 3178

—. 2013, *Monthly Notices of the Royal Astronomical Society*, 434, 806

Best, W. M. J., Dupuy, T. J., Liu, M. C., Siverd, R. J., & Zhang, Z. 2024a, *The UltracoolSheet: Photometry, Astrometry, Spectroscopy, and Multiplicity for 3000+ Ultracool Dwarfs and Imaged Exoplanets*, Zenodo, doi:10.5281/zenodo.4169085

Best, W. M. J., Liu, M. C., Magnier, E. A., & Dupuy, T. J. 2020, *AJ*, 159, 257

—. 2021, *AJ*, 161, 42

Best, W. M. J., Sanghi, A., Liu, M. C., Magnier, E. A., & Dupuy, T. J. 2024b, *The Astrophysical Journal*, 967.0, 115

Best, W. M. J., Liu, M. C., Magnier, E. A., et al. 2013, *The Astrophysical Journal*, 777, 84

—. 2015, *The Astrophysical Journal*, 814, 118

—. 2017, *The Astrophysical Journal*, 837, 95

Best, W. M. J., Magnier, E. A., Liu, M. C., et al. 2018, *ApJS*, 234, 1

Bianchi, L., Conti, A., & Shiao, B. 2014, *Advances in Space Research*, 53, 900

Bianchi, L., Shiao, B., & Thilker, D. 2017, *The Astrophysical Journal Supplement Series*, 230.0, 24

Bidelman, W. P. 1985, *Astrophysical Journal Supplement Series*, 59, 197

Bihain, G., Rebolo, R., Béjar, V. J. S., et al. 2006, *Astronomy and Astrophysics*, 458, 805

Bihain, G., Rebolo, R., Zapatero Osorio, M. R., Béjar, V. J. S., & Caballero, J. A. 2010, *Astronomy & Astrophysics*, 519, A93

Bihain, G., Scholz, R. D., Storm, J., & Schnurr, O. 2013, *Astronomy and Astrophysics*, 557.0, A43

Binks, A. S., Jeffries, R. D., & Maxted, P. F. L. 2015, *MNRAS*, 452, 173

Binks, A. S., Jeffries, R. D., & Ward, J. L. 2018, *MNRAS*, 473, 2465

Birky, J., Hogg, D. W., Mann, A. W., & Burgasser, A. 2020, *The Astrophysical Journal*, 892.0, 31

Blaauw, A. 1956, *ApJ*, 123, 408

—. 1964, *ARA&A*, 2, 213

Blaauw, A., Hiltner, W. A., & Johnson, H. L. 1959, *The Astrophysical Journal*, 130.0, 69

Blanco, V. M. 1949, *PASP*, 61, 183

Blomme, R., Frémat, Y., Sartoretti, P., et al. 2023, *A&A*, 674, A7

Bobylev, V. V., & Bajkova, A. T. 2007, *Astronomy Letters*, 33, 571

Bochanski, J. J., Gizis, J. E., Hawley, S. L., et al. 2005, *The Astronomical Journal*, 130, 1871

Bohn, A. J., Kenworthy, M. A., Ginski, C., et al. 2020, *The Astrophysical Journal*, 898.0, L16

Bonnefoy, M., Chauvin, G., Lagrange, A.-M., et al. 2014, *Astronomy & Astrophysics*, 562, A127

Bossini, D., Vallenari, A., Bragaglia, A., et al. 2019, *A&A*, 623, A108

Boudreault, S., & Bailer-Jones, C. A. L. 2009, *The Astrophysical Journal*, 706.0, 1484

Boudreault, S., Bailer-Jones, C. A. L., Goldman, B., Henning, T., & Caballero, J. A. 2010, *Astronomy and Astrophysics*, 510, A27

Boudreault, S., & Lodieu, N. 2013, *Monthly Notices of the Royal Astronomical Society*, 434, 142

Boudreault, S., Lodieu, N., Deacon, N. R., & Hambly, N. C. 2012, *Monthly Notices of the Royal Astronomical Society*, 426.0, 3419

Bouvier, J., Kendall, T. R., Meeus, G., et al. 2008, *Astronomy and Astrophysics*, 481, 661

Bouy, H., Brandner, W., Martín, E. L., et al. 2004, *Astronomy and Astrophysics*, 424.0, 213

Bouy, H., Huéamo, N., Barrado Y Navascués, D., et al. 2009, *Astronomy and Astrophysics*, 504.0, 199

Bouy, H., Bertin, E., Sarro, L. M., et al. 2015, *Astronomy and Astrophysics*, 577, A148

Bovy, J., Hogg, D. W., & Roweis, S. T. 2011, *Annals of Applied Statistics*, 5, 1657, *eprint*: 0905.2979

Bowler, B. P., Shkolnik, E. L., Liu, M. C., et al. 2015, *The Astrophysical Journal*, 806.0, 62

Bowler, B. P., Liu, M. C., Mawet, D., et al. 2017a, *The Astronomical Journal*, 153, 18

Bowler, B. P., Kraus, A. L., Bryan, M. L., et al. 2017b, *The Astronomical Journal*, 154.0, 165

Bowler, B. P., Hinkley, S., Ziegler, C., et al. 2019, *The Astrophysical Journal*, 877.0, 60

Braun, T. A. M., Yen, H.-W., Koch, P. M., et al. 2021, *ApJ*, 908, 46

Briceño, C., Calvet, N., Hernández, J., et al. 2019, *The Astronomical Journal*, 157.0, 85

Buder, S., Kos, J., Wang, X. E., et al. 2025, *Publications of the Astronomical Society of Australia*, 42.0, e051

Burgasser, A. 2014, *The SpeX Prism Library for Ultracool Dwarfs: A Resource for Stellar, Exoplanet and Galactic Science and Student-Led Research*, NASA Proposal id.14-ADAP14-149

Burgasser, A. J., Cruz, K. L., Cushing, M., et al. 2010, *ApJ*, 710, 1142

Burgasser, A. J., Geballe, T. R., Leggett, S. K., Kirkpatrick, J. D., & Golimowski, D. A. 2006, *ApJ*, 637, 1067

Burgasser, A. J.,Looper, D. L., & Kirkpatrick, J. D. 2017, *Research Notes of the American Astronomical Society*, 1.0, 42

Burgasser, A. J., Sheppard, S. S., & Luhman, K. L. 2013, *ApJ*, 772, 129

Burnham, K. P., & Anderson, D. R. 1998, On MAD and Comedians

Burningham, B., Pinfield, D. J., Leggett, S. K., et al. 2008, *Monthly Notices of the Royal Astronomical Society*, 391, 320

Burningham, B., Pinfield, D. J., Lucas, P. W., et al. 2010, *Monthly Notices of the Royal Astronomical Society*, 406, 1885

Burningham, B., Cardoso, C. V., Smith, L., et al. 2013, *MNRAS*, 433, 457

Burrows, A., Hubbard, W. B., Lunine, J. I., & Liebert, J. 2001, *Reviews of Modern Physics*, 73, 719

Burrows, A., Marley, M., Hubbard, W. B., et al. 1997, *ApJ*, 491, 856

Burssens, S., Simón-Díaz, S., Bowman, D. M., et al. 2020, *Astronomy and Astrophysics*, 639.0, A81

Béjar, V. J. S., Martín, E. L., Zapatero Osorio, M. R., et al. 2001, *The Astrophysical Journal*, 556.0, 830

Caballero, J. A., de Burgos, A., Alonso-Floriano, F. J., et al. 2019, *Astronomy and Astrophysics*, 629.0, A114

Cannon, A. J., & Pickering, E. C. 1993, *VizieR On-line Data Catalog*, 3135

Cantat-Gaudin, T., & Anders, F. 2020, *A&A*, 633, A99

Cantat-Gaudin, T., Jordi, C., Vallenari, A., et al. 2018, *A&A*, 618, A93

Cantat-Gaudin, T., Krone-Martins, A., Sedaghat, N., et al. 2019, *A&A*, 624, A126

Cantat-Gaudin, T., Anders, F., Castro-Ginard, A., et al. 2020, *A&A*, 640, A1

Capitanio, L., Lallement, R., Vergely, J. L., Elyajouri, M., & Monreal-Ibero, A. 2017, *Astronomy and Astrophysics*, 606, A65

Caratti o Garatti, A., Garcia Lopez, R., Antonucci, S., et al. 2012, *Astronomy and Astrophysics*, 538.0, A64

Carpenter, J. M., Hillenbrand, L. A., Skrutskie, M. F., & Meyer, M. R. 2002, *The Astronomical Journal*, 124.0, 1001

Castro, P. J., & Gizis, J. E. 2016, *The Astrophysical Journal*, 816.0, 78

Castro-Ginard, A., Jordi, C., Luri, X., et al. 2020, *A&A*, 635, A45

Cavallo, L., Spina, L., Carraro, G., et al. 2024, *The Astronomical Journal*, 167.0, 12

Chambers, K. C., Magnier, E. A., Metcalfe, N., et al. 2016, *arXiv.org*, arXiv:1612.05560

Chauvin, G., Lagrange, A.-M., Zuckerman, B., et al. 2005, *Astronomy & Astrophysics*, 438, L29

Chauvin, G., Desidera, S., Lagrange, A. M., et al. 2017, *Astronomy and Astrophysics*, 605.0, L9

Cheetham, A., Bonnefoy, M., Desidera, S., et al. 2018, *Astronomy and Astrophysics*, 615.0, A160

Cheetham, A. C., Kraus, A. L., Ireland, M. J., et al. 2015, *The Astrophysical Journal*, 813, 83

Chen, C. H., Mamajek, E. E., Bitner, M. A., et al. 2011, *The Astrophysical Journal*, 738, 122

Chereul, E., Crézé, M., & Bienaymé, O. 1999, *A&AS*, 135, 5

Chinchilla, P., Béjar, V. J. S., Lodieu, N., et al. 2020, *Astronomy and Astrophysics*, 633.0, A152

Chiu, K., Fan, X., Leggett, S. K., et al. 2006, *The Astronomical Journal*, 131, 2722

Chiu, K., Liu, M. C., Jiang, L., et al. 2008, *Monthly Notices of the Royal Astronomical Society: Letters*, 385, L53

Christy, J. W., & Walker, R. L. J. 1969, *Publications of the Astronomical Society of the Pacific*, 81, 643

Cioni, M. R. L., Clementini, G., Girardi, L., et al. 2011, *Astronomy and Astrophysics*, 527.0, A116

Collaboration, G., Babusiaux, C., van Leeuwen, F., et al. 2018, *Astronomy and Astrophysics*, 616.0, A10

Comerón, F., Fernández, M., Baraffe, I., Neuhauser, R., & Kaas, A. A. 2003, *Astronomy and Astrophysics*, 406.0, 1001

Comerón, F., Reipurth, B., Henry, A., & Fernández, M. 2004, *Astronomy and Astrophysics*, 417.0, 583

Comerón, F., Rieke, G. H., & Neuhauser, R. 1999, *Astronomy and Astrophysics*, 343.0, 477

Corbally, C. J. 1984, *Astrophysical Journal Supplement Series*, 55, 657

Couture, D., Gagné, J., & Doyon, R. 2023, *ApJ*, 946, 6

Covey, K. R., Agüeros, M. A., Green, P. J., et al. 2008, *The Astrophysical Journal Supplement Series*, 178.0, 339

Cowley, A., & Gugula, E. 1973, *Astronomy and Astrophysics*, 22.0, 203

Creevey, O. L., Sordo, R., Pailler, F., et al. 2023, *A&A*, 674, A26

Cropper, M., Katz, D., Sartoretti, P., et al. 2018, *A&A*, 616, A5

Crossfield, I. J. M., Waalkes, W., Newton, E. R., et al. 2019, *The Astrophysical Journal*, 883.0, L16

Cruz, K., Rodriguez, D., Alejandro, S., et al. 2025, *The SIMPLE Archive*, doi:10.5281/zenodo.13937301

Cruz, K. K., & Reid, N. I. 2002, *The Astronomical Journal*, 123, 2828

Cruz, K. K., Reid, N. I., Kirkpatrick, J. D., et al. 2007, *The Astronomical Journal*, 133, 439

Cruz, K. L., Kirkpatrick, J. D., & Burgasser, A. J. 2009, *The Astronomical Journal*, 137, 3345

Cruz, K. L., Núñez, A., Burgasser, A. J., et al. 2018, *AJ*, 155, 34

Cruz, K. L., Reid, I. N., Liebert, J., Kirkpatrick, J. D., & Lowrance, P. J. 2003, *AJ*, 126, 2421

Cummings, J. D., & Kalirai, J. S. 2018, *AJ*, 156, 165

Currie, T., Burrows, A., & Daemgen, S. 2014, *The Astrophysical Journal*, 787.0, 104

Currie, T., & Kenyon, S. J. 2009, *The Astronomical Journal*, 138.0, 703

Currie, T., Brandt, G. M., Brandt, T. D., et al. 2023, *Science*, 380.0, 198

Curtis, J. L., Agüeros, M. A., Mamajek, E. E., Wright, J. T., & Cummings, J. D. 2019, *AJ*, 158, 77

Curtis, J. L., Wolfgang, A., Wright, J. T., Brewer, J. M., & Johnson, J. A. 2013, *The Astronomical Journal*, 145.0, 134

Curtis, J. L., Agüeros, M. A., Matt, S. P., et al. 2020, *ApJ*, 904, 140

Cánovas, H., Cantero, C., Cieza, L., et al. 2019, *Astronomy and Astrophysics*, 626.0, A80

da Silva, L., Torres, C. A. O., de La Reza, R., et al. 2009, *Astronomy and Astrophysics*, 508, 833

Daemgen, S., Petr-Gotzens, M. G., Correia, S., et al. 2013, *Astronomy and Astrophysics*, 554.0, A43

Dahm, S. E., & Simon, T. 2005, *The Astronomical Journal*, 129.0, 829

Dahn, C. C., Harris, H. C., Subasavage, J. P., et al. 2017, *The Astronomical Journal*, 154.0, 147

Dai, D.-C., Li, Z., & Stojkovic, D. 2019, *ApJ*, 871, 119

Damiani, F., Prisinzano, L., Pillitteri, I., Micela, G., & Sciotino, S. 2019, *Astronomy and Astrophysics*, 623.0, A112

David, M., Blomme, R., Frémat, Y., et al. 2014, *A&A*, 562, A97

Davies, B., Clark, J. S., Trombley, C., et al. 2012, *Monthly Notices of the Royal Astronomical Society*, 419.0, 1871

Dawson, P., Scholz, A., & Ray, T. P. 2011, *Monthly Notices of the Royal Astronomical Society*, 418, 1231

Dawson, P., Scholz, A., Ray, T. P., et al. 2014, *Monthly Notices of the Royal Astronomical Society*, 442.0, 1586

Day-Jones, A. C., Marocco, F., Pinfield, D. J., et al. 2013, *Monthly Notices of the Royal Astronomical Society*, 430, 1171

de Burgos, A., Simón-Díaz, S., Urbaneja, M. A., & Negueruela, I. 2023, *Astronomy and Astrophysics*, 674.0, A212

De Rosa, R. J., Nielsen, E. L., Wahhaj, Z., et al. 2023, *Astronomy and Astrophysics*, 672.0, A94

De Rosa, R. J., Patience, J., Ward-Duong, K., et al. 2014, *Monthly Notices of the Royal Astronomical Society*, 445.0, 3694

de Zeeuw, P. T., Hoogerwerf, R., de Bruijne, J. H. J., Brown, A. G. A., & Blaauw, A. 1999, *AJ*, 117, 354

Deacon, N. R., Liu, M. C., Magnier, E. A., et al. 2011, *The Astronomical Journal*, 142, 77

—. 2014, *The Astrophysical Journal*, 792, 119

Delorme, P., Gagné, J., Malo, L., et al. 2012, *Astronomy and Astrophysics*, 548, 26

Delorme, P., Dupuy, T., Gagné, J., et al. 2017, *Astronomy and Astrophysics*, 602.0, A82

Desrochers, M.-E., Artigau, É., Gagné, J., et al. 2018, *The Astrophysical Journal*, 852, 55

Dhital, S., West, A. A., Stassun, K. G., & Bochanski, J. J. 2010, *The Astronomical Journal*, 139, 2566

Dias, W. S., Alessi, B. S., Moitinho, A., & Lépine, J. R. D. 2002, *A&A*, 389, 871

Dias, W. S., Monteiro, H., Moitinho, A., et al. 2021, *Monthly Notices of the Royal Astronomical Society*, 504.0, 356

Dieterich, S. B., Henry, T. J., Jao, W.-C., et al. 2014, *The Astronomical Journal*, 147, 94

Distler, A., Soares-Furtado, M., Vanderburg, A., et al. 2025, *AJ*, 169, 166

Douglas, S. T., Agüeros, M. A., Covey, K. R., et al. 2014, *The Astrophysical Journal*, 795.0, 161

Downes, J. J., Román-Zúñiga, C., Ballesteros-Paredes, J., et al. 2015, *Monthly Notices of the Royal Astronomical Society*, 450.0, 3490

Dressing, C. D., Newton, E. R., Schlieder, J. E., et al. 2017, *The Astrophysical Journal*, 836.0, 167

Dressing, C. D., Hardegree-Ullman, K., Schlieder, J. E., et al. 2019, *The Astronomical Journal*, 158.0, 87

Drilling, J. S., & Bergeron, L. E. 1995, *Publications of the Astronomical Society of the Pacific*, 107.0, 846

Ducourant, C., Teixeira, R., Krone-Martins, A., et al. 2017, *Astronomy and Astrophysics*, 597, A90

Dupuy, T. J., & Kraus, A. L. 2013, *Science*, 341, 1492

Dupuy, T. J., & Liu, M. C. 2012, *ApJS*, 201, 19

Dutra, C. M., & Bica, E. 2002, *Astronomy and Astrophysics*, 383.0, 631

Dye, S., Lawrence, A., Read, M. A., et al. 2018, *MNRAS*, 473, 5113

Edge, A., Sutherland, W., Kuijken, K., et al. 2013, *The Messenger*, 154.0, 32

Edwards, T. W. 1976, *Astronomical Journal*, 81, 245

Eggen, O. J. 1958, *Monthly Notices of the Royal Astronomical Society*, 118.0, 154

Eggen, O. J. 1958, *Journal of the British Astronomical Association*, 78, 21

—. 1971, *PASP*, 83, 251

—. 1975, *PASP*, 87, 37

Eggen, O. J. 1983, *The Astronomical Journal*, 88.0, 642

Eggl, S., Pilat-Lohinger, E., Funk, B., Georgakarakos, N., & Haghjhipour, N. 2013, *MNRAS*, 428, 3104

Eisenhauer, F., Perrin, G., Brandner, W., et al. 2009, in *Astrophysics and Space Science Proceedings*, Vol. 9, *Science with the VLT in the ELT Era*, ed. A. Moorwood, 361

Eldridge, J. J. 2009, *Monthly Notices of the Royal Astronomical Society*, 400.0, L20

Engle, S. G., & Guinan, E. F. 2023, *ApJL*, 954, L50

Epcstein, N., de Batz, B., Copet, E., et al. 1994, *Ap&SS*, 217, 3

Esplin, T. L., & Luhman, K. L. 2017, *The Astronomical Journal*, 154.0, 134

—. 2019, *The Astronomical Journal*, 158.0, 54

—. 2020, *The Astronomical Journal*, 159.0, 282

—. 2022, *The Astronomical Journal*, 163.0, 64

Esplin, T. L., Luhman, K. L., Faherty, J. K., Mamajek, E. E., & Bochanski, J. J. 2017, *The Astronomical Journal*, 154.0, 46

Esplin, T. L., Luhman, K. L., & Mamajek, E. E. 2014, *The Astrophysical Journal*, 784, 126

Esplin, T. L., Luhman, K. L., Miller, E. B., & Mamajek, E. E. 2018, *The Astronomical Journal*, 156, 75

Evans, Neal J., I., Dunham, M. M., Jørgensen, J. K., et al. 2009, *The Astrophysical Journal Supplement Series*, 181.0, 321

Fabricius, C., Høg, E., Makarov, V. V., et al. 2002, *Astronomy & Astrophysics*, 384, 180

Faherty, J. K., Cruz, K. K., Burgasser, A. J., et al. 2009, *The Astronomical Journal*, 137, 1

Faherty, J. K., Rice, E. L., Cruz, K. L., Mamajek, E. E., & Núñez, A. 2013, *The Astronomical Journal*, 145.0, 2

Faherty, J. K., Burgasser, A. J., Cruz, K. K., et al. 2012, *The Astrophysical Journal*, 752, 56

Faherty, J. K., Riedel, A. R., Cruz, K. L., et al. 2016, *ApJS*, 225, 10

Falk, M. 1997, *On MAD and Comedians*, doi:10.1023/A:1003258024248

Fang, M., Hillenbrand, L. A., Kim, J. S., et al. 2020, *The Astrophysical Journal*, 904.0, 146

Fang, M., van Boekel, R., Wang, W., et al. 2009, *Astronomy and Astrophysics*, 504.0, 461

Fang, M., Kim, J. S., Pascucci, I., et al. 2017, *The Astronomical Journal*, 153.0, 188

Feigelson, E. D., Lawson, W. A., & Garmire, G. P. 2003, *ApJ*, 599, 1207

Fekel, F. C., J. 1979, PhD thesis

Feltzing, S., & Holmberg, J. 2000, *Astronomy and Astrophysics*, 357.0, 153

Filippazzo, J. C., Rice, E. L., Faherty, J., et al. 2015, *ApJ*, 810, 158

Fitzpatrick, E. L. 1999, *The Publications of the Astronomical Society of the Pacific*, 111, 63

Flaherty, K. M., & Muzerolle, J. 2008, *The Astronomical Journal*, 135.0, 966

Fleming, T. A., Liebert, J., Gioia, I. M., & Maccacaro, T. 1988, *The Astrophysical Journal*, 331, 958

Flewelling, H. 2018, Pan-STARRS Data Release 2

Folkes, S. L., Pinfield, D. J., Jones, H. R. A., et al. 2012, *Monthly Notices of the Royal Astronomical Society*, 427, 3280

Forbrich, J., Dupuy, T. J., Reid, M. J., et al. 2016, *The Astrophysical Journal*, 827.0, 22

Fouesneau, M., Frémat, Y., Andrae, R., et al. 2023, *A&A*, 674, A28

Frasca, A., Guillout, P., Klutsch, A., et al. 2018, *Astronomy and Astrophysics*, 612.0, A96

Frasca, A., Molenda-Żakowicz, J., De Cat, P., et al. 2016, *Astronomy and Astrophysics*, 594.0, A39

Frémat, Y., Royer, F., Marchal, O., et al. 2023, *A&A*, 674, A8

Frinchaboy, P. M., & Majewski, S. R. 2008, *The Astronomical Journal*, 136.0, 118

Frye, R. L., MacConnell, D. J., & Humpherys, R. M. 1970, *Publications of the Astronomical Society of the Pacific*, 82.0, 1360

Fürnkranz, V., Meingast, S., & Alves, J. 2019, *Astronomy and Astrophysics*, 624.0, L11

Gagné, J., Allers, K. N., Theissen, C. A., et al. 2018a, *ApJL*, 854, L27

Gagné, J., Burgasser, A. J., Faherty, J. K., et al. 2015a, *ApJL*, 808, L20

Gagné, J., David, T. J., Mamajek, E. E., et al. 2020a, *ApJ*, 903, 96

Gagné, J., & Faherty, J. K. 2018, *ApJ*, 862, 138

Gagné, J., Faherty, J. K., Cruz, K. L., et al. 2014, *The Astrophysical Journal Letters*, 785, L14

Gagné, J., Faherty, J. K., & Mamajek, E. E. 2018b, *ApJ*, 865, 136

Gagné, J., Faherty, J. K., Moranta, L., & Popinchalk, M. 2021, *ApJL*, 915, L29

Gagné, J., Faherty, J. K., & Popinchalk, M. 2020b, *Research Notes of the American Astronomical Society*, 4, 92

Gagné, J., Fontaine, G., Simon, A., & Faherty, J. K. 2018c, *ApJL*, 861, L13

Gagné, J., Lafrenière, D., Doyon, R., Malo, L., & Artigau, É. 2014, *ApJ*, 783, 121

—. 2015b, *ApJ*, 798, 73

Gagné, J., Roy-Loubier, O., Faherty, J. K., Doyon, R., & Malo, L. 2018d, *ApJ*, 860, 43

Gagné, J., Faherty, J. K., Cruz, K. L., et al. 2015, *The Astrophysical Journal Supplement Series*, 219, 33

Gagné, J., Faherty, J. K., Mamajek, E. E., et al. 2017a, *ApJS*, 228, 18

Gagné, J., Faherty, J. K., Burgasser, A. J., et al. 2017b, *ApJL*, 841, L1

Gagné, J., Mamajek, E. E., Malo, L., et al. 2018e, *ApJ*, 856, 23

Gagné, J., Moranta, L., Faherty, J. K., et al. 2023, *The Astrophysical Journal*, 945.0, 119

Gaia Collaboration, Brown, A. G. A., Vallenari, A., et al. 2016a, *A&A*, 595, A2

Gaia Collaboration, Prusti, T., de Bruijne, J. H. J., et al. 2016b, *A&A*, 595, A1

Gaia Collaboration, Brown, A. G. A., Vallenari, A., et al. 2018, *A&A*, 616, A1

—. 2021, *A&A*, 649, A1

Gaia Collaboration, Vallenari, A., Brown, A. G. A., et al. 2023, *A&A*, 674, A1

Gaidos, E., Mann, A. W., Lépine, S., et al. 2014, *Monthly Notices of the Royal Astronomical Society*, 443, 2561

Gaidos, E. J. 1998, *PASP*, 110, 1259

Galindo-Guil, F. J., Barrado, D., Bouy, H., et al. 2022, *A&A*, 664, A70

Galli, P. A. B., Moraux, E., Bouy, H., et al. 2017, *Astronomy & Astrophysics*, 598, A48

Gálvez-Ortiz, M. C., Kuznetsov, M., Clarke, J. R. A., et al. 2014, *Monthly Notices of the Royal Astronomical Society*, 439, 3890

Gandolfi, D., Alcalá, J. M., Leccia, S., et al. 2008, *The Astrophysical Journal*, 687.0, 1303

Gao, X.-h. 2019, *Monthly Notices of the Royal Astronomical Society*, 486.0, 5405

Garcia, B. 1993, *The Astrophysical Journal Supplement Series*, 87.0, 197

Garrison, R. F., & Gray, R. O. 1994, *The Astronomical Journal*, 107, 1556

Geers, V., Scholz, A., Jayawardhana, R., et al. 2011, *ApJ*, 726, 23

Gennaro, M., Prada Moroni, P. G., & Tognelli, E. 2012, *MNRAS*, 420, 986

Gianninas, A., Bergeron, P., & Ruiz, M. T. 2011, *The Astrophysical Journal*, 743, 138

Gigoyan, K. S., & Mickaelian, A. M. 2012, *Monthly Notices of the Royal Astronomical Society*, 419.0, 3346

Ginestet, N., & Carquillat, J. M. 2002, *The Astrophysical Journal Supplement Series*, 143.0, 513

Gizis, J. E. 2002, *The Astrophysical Journal*, 575, 484

Gizis, J. E., Monet, D. G., Reid, I. N., et al. 2000, *The Astronomical Journal*, 120.0, 1085

Gizis, J. E., & Reid, I. N. 1997, *Publications of the Astronomical Society of the Pacific*, 109.0, 849

Gizis, J. E., & Reid, N. I. 2005, *The Publications of the Astronomical Society of the Pacific*, 117, 676

Gizis, J. E., Reid, N. I., & Monet, D. G. 1999, *The Astronomical Journal*, 118, 997

Gizis, J. E., Yoachim, P., Jones, R. L., Hilligoss, D., & Ji, J. 2022, *ApJS*, 263, 23

Gontcharov, G. A. 2006, *Astronomy Letters*, 32, 759

González-Payo, J., Cortés-Contreras, M., Lodieu, N., et al. 2021, *Astronomy and Astrophysics*, 650.0, A190

Gossage, S., Conroy, C., Dotter, A., et al. 2018, *ApJ*, 863, 67

Gray, R. O., Corbally, C. J., Garrison, R. F., et al. 2006, *The Astronomical Journal*, 132, 161

Gray, R. O., Corbally, C. J., Garrison, R. F., McFadden, M. T., & Robinson, P. E. 2003, *AJ*, 126, 2048

Gray, R. O., & Garrison, R. F. 1987, *Astrophysical Journal Supplement Series*, 65, 581

Gray, R. O., Napier, M. G., & Winkler, L. I. 2001, *The Astronomical Journal*, 121, 2148

Greco, J. J., Schneider, A. C., Cushing, M. C., Kirkpatrick, J. D., & Burgasser, A. J. 2019, *The Astronomical Journal*, 158.0, 182

Grieves, N., Ge, J., Thomas, N., et al. 2018, *Monthly Notices of the Royal Astronomical Society*, 481.0, 3244

Guetter, H. H. 1977, *The Astronomical Journal*, 82.0, 598

Guidry, J. A., Vanderbosch, Z. P., Hermes, J. J., et al. 2021, *ApJ*, 912, 125

Guieu, S., Dougados, C., Monin, J.-L., Magnier, E., & Martín, E. L. 2006, *Astronomy and Astrophysics*, 446, 485

Gunn, J. E., Griffin, R. F., Griffin, R. E. M., & Zimmerman, B. A. 1988, *AJ*, 96, 198

Guo, Y. X., Luo, A. L., Zhang, S., et al. 2019, *Monthly Notices of the Royal Astronomical Society*, 485.0, 2167

Gutermuth, R. A., Megeath, S. T., Myers, P. C., et al. 2009, *The Astrophysical Journal Supplement Series*, 184.0, 18

Gutermuth, R. A., Myers, P. C., Megeath, S. T., et al. 2008, *The Astrophysical Journal*, 674.0, 336

Hanbury Brown, R., Davis, J., & Allen, L. R. 1974, *MNRAS*, 167, 121

Hardegree-Ullman, K. K., Cushing, M. C., Muirhead, P. S., & Christiansen, J. L. 2019, *The Astronomical Journal*, 158.0, 75

Hariri, S., Carrasco Kind, M., & Brunner, R. J. 2018, *arXiv e-prints*, arXiv:1811.02141

Harlan, E. A. 1969, *The Astronomical Journal*, 74.0, 916

Hawley, S. L., Covey, K. R., Knapp, G. R., et al. 2002, *The Astronomical Journal*, 123, 3409

He, Z., Luo, Y., Wang, K., et al. 2023, *The Astrophysical Journal Supplement Series*, 267.0, 34

He, Z., Wang, K., Luo, Y., et al. 2022, *The Astrophysical Journal Supplement Series*, 262.0, 7

Heckmann, O., & Lübeck, K. 1958, *Zeitschrift für Astrophysik*, 45, 243

Henry, T. J., Subasavage, J. P., Brown, M. A., et al. 2004, *The Astronomical Journal*, 128, 2460

Henry, T. J., Walkowicz, L. M., Barto, T. C., & Goliowski, D. A. 2002, *The Astronomical Journal*, 123, 2002

Henry, T. J., Jao, W.-C., Winters, J. G., et al. 2018, *The Astronomical Journal*, 155.0, 265

Hernández, J., Morales-Calderon, M., Calvet, N., et al. 2010, *The Astrophysical Journal*, 722.0, 1226

Hernández, J., Calvet, N., Perez, A., et al. 2014, *The Astrophysical Journal*, 794.0, 36

Herpich, F. R., Almeida-Fernandes, F., Oliveira Schwarz, G. B., et al. 2024, *Astronomy and Astrophysics*, 689.0, A249

Hillenbrand, L. A. 1997, *The Astronomical Journal*, 113.0, 1733

Hillenbrand, L. A., Hoffer, A. S., & Herczeg, G. J. 2013, *The Astronomical Journal*, 146.0, 85

Hillenbrand, L. A., & White, R. J. 2004, *ApJ*, 604, 741

Hinkley, S., Bowler, B. P., Vigan, A., et al. 2015, *The Astrophysical Journal Letters*, 805, L10

Hoffmeister, C. 1962, *ZA*, 55, 290

Homeier, D., Koester, D., Hagen, H. J., et al. 1998, *Astronomy and Astrophysics*, 338.0, 563

Hoogerwerf, R., de Bruijne, J. H. J., Brown, A. G. A., et al. 1997, in , 571

Houk, N. 1978, Ann Arbor : Dept. of Astronomy

—. 1982, Michigan Catalogue of Two-dimensional Spectral Types for the HD stars. Volume 3. Declinations -40 to -26.

Houk, N., & Cowley, A. P. 1975, University of Michigan Catalogue of two-dimensional spectral types for the HD stars. Volume I. Declinations -90 to -53., I

Houk, N., & Smith-Moore, M. 1988, Michigan Catalogue of Two-dimensional Spectral Types for the HD Stars. Volume 4, 4

Houk, N., & Swift, C. 1999, Michigan Spectral Survey, 5, 0

Hsu, W.-H., Hartmann, L., Allen, L., et al. 2012, The Astrophysical Journal, 752.0, 59

Humphreys, A., Meisner, A. M., Burgasser, A. J., et al. 2023, Research Notes of the American Astronomical Society, 7.0, 184

Hunt, E. L., & Reffert, S. 2023, A&A, 673, A114

Hurt, S. A., Liu, M. C., Zhang, Z., et al. 2024, The Astrophysical Journal, 961.0, 121

Huélamo, N., Nürnberger, D. E. A., Ivanov, V. D., et al. 2010, Astronomy and Astrophysics, 521.0, L54

Häufeler, B., Jarvis, M., & Cross, N. J. G. 2022, Research Notes of the American Astronomical Society, 6.0, 109

Ingraham, P., Albert, L., Doyon, R., & Artigau, É. 2014, The Astrophysical Journal, 782, 8

Isaacson, H., & Fischer, D. 2010, ApJ, 725, 875

Ivezić, Ž., Kahn, S. M., Tyson, J. A., et al. 2019, ApJ, 873, 111

Jackson, J., & Stoy, R. H. 1955, Ann. Cape Obs., 18, 0

Janes, K. A., & Hoq, S. 2011, The Astronomical Journal, 141.0, 92

Janson, M., Jayawardhana, R., Girard, J. H., et al. 2012, The Astrophysical Journal Letters, 758, L2

Janson, M., Durkan, S., Bonnefoy, M., et al. 2018, A&A, 620, A33

Jayawardhana, R., & Ivanov, V. D. 2006, The Astrophysical Journal, 647.0, L167

Jeffries, R., & Jackson, R. 2023, in EAS2023, European Astronomical Society Annual Meeting, 193

Jeffries, R. D. 2007, Monthly Notices of the Royal Astronomical Society, 376.0, 1109

Jeffries, R. D., Jackson, R. J., Cottaar, M., et al. 2014, A&A, 563, A94

Jerabkova, T., Boffin, H. M. J., Beccari, G., & Anderson, R. I. 2019, MNRAS, 489, 4418

Jerabkova, T., Boffin, H. M. J., Beccari, G., et al. 2021, A&A, 647, A137

Jiménez-Esteban, F. M., Torres, S., Rebassa-Mansergas, A., et al. 2023, Monthly Notices of the Royal Astronomical Society, 518.0, 5106

Jones, J., White, R. J., Boyajian, T. S., et al. 2015, in American Astronomical Society Meeting Abstracts, Vol. 225, American Astronomical Society Meeting Abstracts #225, 112.03

Jönsson, H., Holtzman, J. A., Allende Prieto, C., et al. 2020, AJ, 160, 120

Kapteyn, J. C. 1914, ApJ, 40, 43

Kastner, J. H., Zuckerman, B., Weintraub, D. A., & Forveille, T. 1997, Science, 277, 67

Katz, D., Sartoretti, P., Guerrier, A., et al. 2023, A&A, 674, A5

Keenan, P. C., & McNeil, R. C. 1989, Astrophysical Journal Supplement Series (ISSN 0067-0049), 71, 245

Kellogg, K., Metchev, S., Miles-Páez, P. A., & Tannock, M. E. 2017, The Astronomical Journal, 154.0, 112

Kendall, T. R., Lodieu, N., Hambly, N. C., et al. 2007, Monthly Notices of the Royal Astronomical Society, 374, 372

Kendall, T. R., Mauron, N., Azzopardi, M., & Gigoyan, K. 2003, Astronomy & Astrophysics, 403, 929

Kenyon, S. J., & Hartmann, L. 1995, Astrophysical Journal Supplement v.101, 101, 117

Kerr, R., Kraus, A. L., Murphy, S. J., et al. 2022a, ApJ, 941, 143

—. 2022b, ApJ, 941, 49

Kerr, R., Kraus, A. L., & Rizzuto, A. C. 2023, ApJ, 954, 134

Kerr, R. M. P., Rizzuto, A. C., Kraus, A. L., & Offner, S. S. R. 2021, ApJ, 917, 23

Kharchenko, N. V. 2001, Kinematika i Fizika Nebesnykh Tel, 17, 409

Kharchenko, N. V., Piskunov, A. E., Röser, S., Schilbach, E., & Scholz, R. D. 2005, A&A, 440, 403

Kharchenko, N. V., Piskunov, A. E., Schilbach, E., Röser, S., & Scholz, R. D. 2013, A&A, 558, A53

Kharchenko, N. V., Scholz, R. D., Piskunov, A. E., Röser, S., & Schilbach, E. 2007, Astronomische Nachrichten, 328, 889

Kiman, R., Schmidt, S. J., Angus, R., et al. 2019, The Astronomical Journal, 157.0, 231

King, J. R., Villarreal, A. R., Soderblom, D. R., Gulliver, A. F., & Adelman, S. J. 2003, AJ, 125, 1980

Kirkpatrick, D. J., Henry, T. J., & Simons, D. A. 1995, Astronomical Journal, 109, 797

Kirkpatrick, D. J., Gizis, J. E., Reid, N. I., et al. 1999, The Astrophysical Journal, 519, 802

—. 2000, The Astronomical Journal, 120, 447

Kirkpatrick, D. J., Lowrance, P., Cruz, K. K., et al. 2008, The Astrophysical Journal, 689, 1295

Kirkpatrick, D. J., Kellogg, K., Schneider, A. C., et al. 2016, The Astrophysical Journal Supplement Series, 224, 36

Kirkpatrick, D. J., Martin, E. C., Smart, R. L., et al. 2019, The Astrophysical Journal Supplement Series, 240, 19

Kirkpatrick, J. D., Cushing, M. C., Gelino, C. R., et al. 2013, The Astrophysical Journal, 776, 128

Kirkpatrick, J. D., Looper, D. L., Burgasser, A. J., et al. 2010, ApJS, 190, 100

Kirkpatrick, J. D., Cushing, M. C., Gelino, C. R., et al. 2011, ApJS, 197, 19

Kirkpatrick, J. D., Gelino, C. R., Cushing, M. C., et al. 2012, *ApJ*, 753, 156

Kirkpatrick, J. D., Schneider, A., Fajardo-Acosta, S., et al. 2014, *ApJ*, 783, 122

Kirkpatrick, J. D., Gelino, C. R., Faherty, J. K., et al. 2021, *ApJS*, 253, 7

Kirkpatrick, J. D., Marocco, F., Gelino, C. R., et al. 2024, *The Astrophysical Journal Supplement Series*, 271.0, 55

Klutsch, A., Frasca, A., Guillout, P., et al. 2020, *Astronomy and Astrophysics*, 637.0, A43

Knapp, G. R., Leggett, S. K., Fan, X., et al. 2004, *The Astronomical Journal*, 127, 3553

Koen, C., Kilkenny, D., van Wyk, F., & Marang, F. 2010, *MNRAS*, 403, 1949

Koen, C., Miszalski, B., Väistö, P., & Koen, T. 2017, *Monthly Notices of the Royal Astronomical Society*, 465.0, 4723

Koenig, X. P., & Allen, L. E. 2011, *The Astrophysical Journal*, 726.0, 18

Kounkel, M., & Covey, K. 2019, *AJ*, 158, 122

Kounkel, M., Covey, K., & Stassun, K. G. 2020, *AJ*, 160, 279

Kounkel, M., Hartmann, L., Calvet, N., & Megeath, T. 2017, *The Astronomical Journal*, 154.0, 29

Kounkel, M., Stassun, K. G., Covey, K., & Hartmann, L. 2022, *Monthly Notices of the Royal Astronomical Society*, 517.0, 161

Kraus, A. L., Herczeg, G. J., Rizzuto, A. C., et al. 2017, *ApJ*, 838, 150

Kraus, A. L., & Hillenbrand, L. A. 2007a, *The Astrophysical Journal*, 662, 413

—. 2007b, *The Astronomical Journal*, 134, 2340

Kraus, A. L., Shkolnik, E. L., Allers, K. N., & Liu, M. C. 2014, *AJ*, 147, 146

Lachapelle, F.-R., Lafrenière, D., Gagné, J., et al. 2015, *The Astrophysical Journal*, 802, 61

Lallement, R., Vergely, J. L., Valette, B., et al. 2014, *Astronomy and Astrophysics*, 561, A91

Lallement, R., Capitanio, L., Ruiz-Dern, L., et al. 2018, *Astronomy and Astrophysics*, 616, A132

Latyshev, I. N. 1977, Wide physical pairs among bright A and B stars.

Laureijs, R., Amiaux, J., Arduini, S., et al. 2011, arXiv e-prints, arXiv:1110.3193

Lawrence, A., & Warren, S. 2005, *The Messenger*, 119, 56

Lawrence, A., Warren, S. J., Almaini, O., et al. 2007, *MNRAS*, 379, 1599

Lawrence, A., Warren, S. J., Almaini, O., et al. 2013, *VizieR Online Data Catalog: UKIDSS-DR9 LAS, GCS and DXS Surveys* (Lawrence+ 2012)

Leão, I. C., Pasquini, L., Ludwig, H. G., & de Medeiros, J. R. 2019, *MNRAS*, 483, 5026

Lee, S. G. 1984, *The Astronomical Journal*, 89.0, 702

Leggett, S. K., & Tremblin, P. 2025, *ApJ*, 979, 145

Lépine, S., Hilton, E. J., Mann, A. W., et al. 2013, *The Astronomical Journal*, 145, 102

Levine, J. L., Steinhauer, A., Elston, R. J., & Lada, E. A. 2006, *The Astrophysical Journal*, 646.0, 1215

Li, J. Z., & Hu, J. Y. 2000, *Acta Astrophysica Sinica*, 20.0, 25

Liebing, F., Jeffers, S. V., Reiners, A., & Zechmeister, M. 2021, *A&A*, 654, A168

Liu, J., Fang, M., & Liu, C. 2020, *The Astronomical Journal*, 159, 105

Liu, J., Fang, M., Tian, H., et al. 2021, *ApJS*, 254, 20

Liu, M. C., Dupuy, T. J., & Allers, K. N. 2016, *ApJ*, 833, 96

Liu, M. C., Deacon, N. R., Magnier, E. A., et al. 2011, *The Astrophysical Journal*, 740.0, L32

Liu, M. C., Magnier, E. A., Deacon, N. R., et al. 2013, *ApJL*, 777, L20

Lodieu, N. 2013, *Monthly Notices of the Royal Astronomical Society*, 431, 3222

Lodieu, N., Boudreault, S., & Béjar, V. J. S. 2014, *Monthly Notices of the Royal Astronomical Society*, 445, 3908

Lodieu, N., Birmingham, B., Hambly, N. C., & Pinfield, D. J. 2009, *Monthly Notices of the Royal Astronomical Society*, 397, 258

Lodieu, N., Deacon, N. R., & Hambly, N. C. 2012a, *Monthly Notices of the Royal Astronomical Society*, 422, 1495

Lodieu, N., Deacon, N. R., Hambly, N. C., & Boudreault, S. 2012b, *Monthly Notices of the Royal Astronomical Society*, 426, 3403

Lodieu, N., Dobbie, P. D., Cross, N. J. G., et al. 2013, *Monthly Notices of the Royal Astronomical Society*, 435, 2474

Lodieu, N., Dobbie, P. D., & Hambly, N. C. 2011, *Astronomy and Astrophysics*, 527, 24

Lodieu, N., Espinoza Contreras, M., Zapatero Osorio, M. R., et al. 2012c, *Astronomy & Astrophysics*, 542, A105

—. 2017, *Astronomy and Astrophysics*, 598.0, A92

Lodieu, N., Hambly, N. C., & Jameson, R. F. 2006, *Monthly Notices of the Royal Astronomical Society*, 373, 95

Lodieu, N., Scholz, R. D., McCaughrean, M. J., et al. 2005, *Astronomy & Astrophysics*, 440, 1061

Lodieu, N., Smart, R. L., Pérez-Garrido, A., & Silvotti, R. 2019, *Astronomy and Astrophysics*, 623.0, A35

Lodieu, N., Zapatero Osorio, M. R., Béjar, V. J. S., & Peña Ramírez, K. 2018, *Monthly Notices of the Royal Astronomical Society*, 473.0, 2020

Lodieu, N., Burningham, B., Day-Jones, A., et al. 2012d, *Astronomy & Astrophysics*, 548, A53

Löhner-Böttcher, J., Schmidt, W., Schlichenmaier, R., Steinmetz, T., & Holzwarth, R. 2019, *A&A*, 624, A57

Looper, D. L. 2011, ProQuest Dissertations And Theses; Thesis (Ph.D.)–University of Hawai'i at Manoa

Looper, D. L., Burgasser, A. J., Kirkpatrick, J. D., & Swift, B. J. 2007, *The Astrophysical Journal*, 669.0, L97

Luhman, K. L. 2004a, *The Astrophysical Journal*, 602, 816

—. 2004b, *The Astrophysical Journal*, 614.0, 398

—. 2006, *The Astrophysical Journal*, 645, 676

—. 2007, *The Astrophysical Journal Supplement Series*, 173, 104

Luhman, K. L. 2014, *ApJL*, 786, L18

Luhman, K. L. 2018, *The Astronomical Journal*, 156, 271

—. 2020, *The Astronomical Journal*, 160.0, 186

—. 2022a, *The Astronomical Journal*, 164.0, 151

—. 2022b, *The Astronomical Journal*, 163.0, 24

—. 2023a, *The Astronomical Journal*, 165.0, 37

—. 2023b, *The Astronomical Journal*, 165.0, 269

—. 2024, *The Astronomical Journal*, 168.0, 159

Luhman, K. L., Alves de Oliveira, C., Baraffe, I., et al. 2024, *The Astronomical Journal*, 167.0, 19

Luhman, K. L., & Esplin, T. L. 2020, *The Astronomical Journal*, 160.0, 44

Luhman, K. L., Herrmann, K. A., Mamajek, E. E., Esplin, T. L., & Pecaut, M. J. 2018, *The Astronomical Journal*, 156.0, 76

Luhman, K. L., & Mamajek, E. E. 2012, *The Astrophysical Journal*, 758, 31

Luhman, K. L., Mamajek, E. E., Allen, P. R., & Cruz, K. K. 2009, *The Astrophysical Journal*, 703, 399

Luhman, K. L., Mamajek, E. E., Shukla, S. J., & Loutrel, N. P. 2017, *The Astronomical Journal*, 153, 46

Luhman, K. L., & Muench, A. A. 2008, *The Astrophysical Journal*, 684, 654

Luhman, K. L., & Sheppard, S. S. 2014, *The Astrophysical Journal*, 787, 126

Luhman, K. L., Stauffer, J. R., Muench, A. A., et al. 2003, *The Astrophysical Journal*, 593.0, 1093

Luhman, K. L., Wilson, J. C., Brandner, W., et al. 2006, *The Astrophysical Journal*, 649.0, 894

Lépine, S., & Shara, M. M. 2005, *The Astronomical Journal*, 129.0, 1483

López Martí, B., Eislöffel, J., & Mundt, R. 2005, *Astronomy and Astrophysics*, 440.0, 139

Mace, G. N., Kirkpatrick, J. D., Cushing, M. C., et al. 2013, *ApJS*, 205, 6

Madsen, S., Dravins, D., & Lindegren, L. 2002, *A&A*, 381, 446

Magnier, E. A., Schlafly, E. F., Finkbeiner, D. P., et al. 2020, *The Astrophysical Journal Supplement Series*, 251.0, 6

Maia, F. F. S., Moraux, E., & Joncour, I. 2016, *MNRAS*, 458, 3027

Maire, A. L., Bonnefoy, M., Ginski, C., et al. 2016, *Astronomy and Astrophysics*, 587.0, A56

Majidi, F. Z., Desidera, S., Alcalá, J. M., et al. 2020, *Astronomy and Astrophysics*, 644.0, A169

Majidi, F. Z., Alcalá, J. M., Frasca, A., et al. 2023, *Astronomy and Astrophysics*, 671.0, A46

Malo, L., Artigau, É., Doyon, R., et al. 2014, *ApJ*, 788, 81

Malo, L., Artigau, É., Doyon, R., et al. 2014, *\apj*, 788, 81, eprint: 1402.6053

Malo, L., Doyon, R., Feiden, G. A., et al. 2014, *ApJ*, 792, 37

Malo, L., Doyon, R., Lafrenière, D., et al. 2013, *ApJ*, 762, 88

Mamajek, E. E. 2006, *The Astronomical Journal*, 132, 2198

Mamajek, E. E. 2007, in IAU Symposium, Vol. 237, Triggered Star Formation in a Turbulent ISM, ed. B. G. Elmegreen & J. Palous, 442–442

—. 2015, *Young Stars & Planets Near the Sun*, 314, 21

Mamajek, E. E., Lawson, W. A., & Feigelson, E. D. 1999, *The Astrophysical Journal*, 516, L77

Manara, C. F., Testi, L., Natta, A., & Alcalá, J. M. 2015, *Astronomy and Astrophysics*, 579, A66

Manjavacas, E., Goldman, B., Reffert, S., & Henning, T. 2013, *Astronomy & Astrophysics*, 560, A52

Marigo, P., Cummings, J. D., Curtis, J. L., et al. 2020, *Nature Astronomy*, 4.0, 1102

Markowitz, A. H. 1969, PhD thesis

Marocco, F., Smart, R. L., Jones, H. R. A., et al. 2010, *Astronomy & Astrophysics*, 524, A38

Marocco, F., Andrei, A. H., Smart, R. L., et al. 2013, *The Astronomical Journal*, 146, 161

Marocco, F., Day-Jones, A. C., Lucas, P. W., et al. 2014, *Monthly Notices of the Royal Astronomical Society*, 439, 372

Marocco, F., Jones, H. R. A., Day-Jones, A. C., et al. 2015, *Monthly Notices of the Royal Astronomical Society*, 449, 3651

Marocco, F., Eisenhardt, P. R. M., Fowler, J. W., et al. 2021, *ApJS*, 253, 8

Martin, E. C., Kirkpatrick, J. D., Beichman, C. A., et al. 2018, *The Astrophysical Journal*, 867.0, 109

Martín, E. L., Delfosse, X., & Guieu, S. 2004, *The Astronomical Journal*, 127, 449

Martín, E. L., Rebolo, R., & Zapatero Osorio, M. R. 1996, *Astrophysical Journal v.469*, 469, 706

Martín, E. L., Phan-Bao, N., Bessell, M., et al. 2010, *Astronomy and Astrophysics*, 517, 53

Martín, E. L., Brandner, W., Bouvier, J., et al. 2000, *The Astrophysical Journal*, 543.0, 299

Masana, E., Jordi, C., & Ribas, I. 2006, *A&A*, 450, 735

Maucó, K., Manara, C. F., Ansdell, M., et al. 2023, *Astronomy and Astrophysics*, 679.0, A82

McConnell. 19931, IRAS Point Sources of flux at 12 microns greater than flux at 25 microns and falling within about 7 degrees of the Galactic Plane

McInnes, L., & Healy, J. 2017, arXiv e-prints, arXiv:1705.07321

McMahon, R. G., Banerji, M., Gonzalez, E., et al. 2013, *The Messenger*, 154, 35

Meingast, S., & Alves, J. 2019, *A&A*, 621, L3

Meingast, S., Alves, J., & Fürnkranz, V. 2019, *A&A*, 622, L13

Meingast, S., Alves, J., & Rottensteiner, A. 2021, *A&A*, 645, A84

Meisner, A. M., Caselden, D., Schlafly, E. F., & Kiwy, F. 2023, *AJ*, 165, 36

Meisner, A. M., Caselden, D., Kirkpatrick, J. D., et al. 2020, *ApJ*, 889, 74

Meisner, A. M., Faherty, J. K., Kirkpatrick, J. D., et al. 2020, *The Astrophysical Journal*, 899.0, 123

Melnikov, S., & Eisloffel, J. 2012, *Astronomy and Astrophysics*, 544.0, A111

Merin, B., Jørgensen, J., Spezzi, L., et al. 2008, *The Astrophysical Journal Supplement Series*, 177, 551

Mesa, D., Vigan, A., D’Orazi, V., et al. 2016, *Astronomy and Astrophysics*, 593.0, A119

Meshkat, T., Bonnefoy, M., Mamajek, E. E., et al. 2015, *Monthly Notices of the Royal Astronomical Society*, 453, 2378

Messina, S., Desidera, S., Turatto, M., Lanzafame, A. C., & Guinan, E. F. 2010, *A&A*, 520, A15

Messina, S., Nardiello, D., Desidera, S., et al. 2022, *A&A*, 657, L3

Metchev, S. A., Kirkpatrick, J. D., Berriman, G. B., &Looper, D. 2008, *The Astrophysical Journal*, 676, 1281

Metodieva, Y., Antonova, A., Golev, V., et al. 2015, *Monthly Notices of the Royal Astronomical Society*, 446.0, 3878

Meunier, N., Mignon, L., & Lagrange, A. M. 2017, *åp*, 607, A124, _eprint: 1711.02331

Miret-Roig, N., Galli, P. A. B., Brandner, W., et al. 2020, *åp*, 642, A179, _eprint: 2007.10997

Molenda-Žakowicz, J., Sousa, S. G., Frasca, A., et al. 2013, *Monthly Notices of the Royal Astronomical Society*, 434.0, 1422

Monet, D. G., Levine, S. E., Canzian, B., et al. 2003, *The Astronomical Journal*, 125.0, 984

Montes, D., López-Santiago, J., Gálvez, M. C., et al. 2001, *Monthly Notices of the Royal Astronomical Society*, 328.0, 45

Montet, B. T., Bowler, B. P., Shkolnik, E. L., et al. 2015, *ApJL*, 813, L11

Moranta, L., Gagné, J., Couture, D., & Faherty, J. K. 2022, *ApJ*, 939, 94

Morgan, W. W., & Keenan, P. C. 1973, *Annual Review of Astronomy & Astrophysics*, 11, 29

Morley, C. V., Mukherjee, S., Marley, M. S., et al. 2024, *ApJ*, 975, 59

Muench, A. A., Lada, C. J., Luhman, K. L., Muzerolle, J., & Young, E. 2007, *The Astronomical Journal*, 134, 411

Mugrauer, M., & Neuhauser, R. 2009, *Astronomy and Astrophysics*, 494.0, 373

Murphy, S. J., & Lawson, W. A. 2015, *MNRAS*, 447, 1267

Murphy, S. J., Lawson, W. A., & Bessell, M. S. 2013, *MNRAS*, 435, 1325

Naud, M.-È., Artigau, È., Malo, L., et al. 2014, *The Astrophysical Journal*, 787, 5

Naylor, T. 2009, *Monthly Notices of the Royal Astronomical Society*, 399.0, 432

Nesterov, V. V., Kuzmin, A. V., Ashimbaeva, N. T., et al. 1995, *Astronomy and Astrophysics*, 110, 367

Neuhauser, R., Walter, F. M., Covino, E., et al. 2000, *A&AS*, 146, 323

Neuhauser, R., & Comerón, F. 1999, *Astronomy and Astrophysics*, 350.0, 612

Newton, E. R., Charbonneau, D., Irwin, J., et al. 2014, *AJ*, 147, 20

Newton, E. R., Mann, A. W., Tofflemire, B. M., et al. 2019, *ApJL*, 880, L17

Newton, E. R., Rampalli, R., Kraus, A. L., et al. 2022, *AJ*, 164, 115

Nidever, D. L., Dey, A., Fasbender, K., et al. 2021, *AJ*, 161, 192

Nielsen, E. L., De Rosa, R. J., Wang, J., et al. 2016, *AJ*, 152, 175

Nilsson, R., Veicht, A., Giorla Godfrey, P. A., et al. 2017, *The Astrophysical Journal*, 838.0, 64

Ochsenbein, F., Bauer, P., & Marcout, J. 2000, *A&AS*, 143, 23

O’Donoghue, D., Kilkenny, D., Koen, C., et al. 2013, *Monthly Notices of the Royal Astronomical Society*, 431.0, 240

Oh, S., Price-Whelan, A. M., Hogg, D. W., Morton, T. D., & Spergel, D. N. 2017, *AJ*, 153, 257

Olivares. 2025

Onken, C. A., Wolf, C., Bessell, M. S., et al. 2024, Publications of the Astronomical Society of Australia, 41.0, e061

Opolski, A. 1957, Arkiv for Astronomi, 2.0, 55

Oreajo, S., Cieza, L. A., Gamen, R., & Peterson, D. 2019, Monthly Notices of the Royal Astronomical Society, 487.0, 2937

Ortiz-León, G. N., Loinard, L., Dzib, S. A., et al. 2018, The Astrophysical Journal, 869.0, L33

Pang, X., Li, Y., Tang, S.-Y., Pasquato, M., & Kouwenhoven, M. B. N. 2020, The Astrophysical Journal, 900.0, L4

Parihar, P., Messina, S., Distefano, E., Shantikumar, N. S., & Medhi, B. J. 2009, Monthly Notices of the Royal Astronomical Society, 400.0, 603

Pasquini, L., Melo, C., Chavero, C., et al. 2011, Astronomy and Astrophysics, 526.0, A127

Patience, J., King, R. R., De Rosa, R. J., et al. 2012, Astronomy & Astrophysics, 540, A85

Paunzen, E., Duffee, B., Heiter, U., Kuschnig, R., & Weiss, W. W. 2001, Astronomy and Astrophysics, 373, 625

Pecaut, M. J., & Mamajek, E. E. 2013, ApJS, 208, 9

—. 2016, MNRAS, 461, 794

Pegues, J., Czekala, I., Andrews, S. M., et al. 2021, ApJ, 908, 42

Peña Ramírez, K., Zapatero Osorio, M. R., & Béjar, V. J. S. 2015, Astronomy & Astrophysics, 574, A118

Pérez-Garrido, A., Lodieu, N., & Rebolo, R. 2017, Astronomy and Astrophysics, 599, A78

Perren, G. I., Pera, M. S., Navone, H. D., & Vázquez, R. A. 2023, MNRAS, 526, 4107

Perryman, M. A. C., Lindegren, L., Kovalevsky, J., et al. 1997, Astronomy and Astrophysics 323, 323, L49

Perryman, M. A. C., Brown, A. G. A., Lebreton, Y., et al. 1998, Astronomy & Astrophysics, 331, 81

Peterson, D. E., Megeath, S. T., Luhman, K. L., et al. 2008, The Astrophysical Journal, 685.0, 313

Phan-Bao, N., & Bessell, M. S. 2006, Astronomy and Astrophysics, 446, 515

Phan Bao, N., Bessell, M. S., Martín, E. L., et al. 2008, Monthly Notices of the Royal Astronomical Society, 383, 831

Pickles, A. J. 1998, PASP, 110, 863

Pineda, J. S., Hallinan, G., Kirkpatrick, D. J., et al. 2016, The Astrophysical Journal, 826, 73

Platais, I., Kozhurina-Platais, V., & van Leeuwen, F. 1998, AJ, 116, 2423

Pozzo, M., Jeffries, R. D., Naylor, T., et al. 2000, MNRAS, 313, L23

Prisinzano, L., Damiani, F., Sciortino, S., et al. 2022, A&A, 664, A175

Pérez-Garrido, A., Lodieu, N., Rebolo, R., & Chinchilla, P. 2018, Astronomy and Astrophysics, 620.0, A130

Qi, Z., Yu, Y., Bucciarelli, B., et al. 2015, The Astronomical Journal, 150, 137

Qin, S., Zhong, J., Tang, T., & Chen, L. 2023, ApJS, 265, 12

Rajan, A., Rameau, J., De Rosa, R. J., et al. 2017, The Astronomical Journal, 154.0, 10

Rajpurohit, A. S., Reylé, C., Allard, F., et al. 2013, Astronomy and Astrophysics, 556, 15

Ratzenböck, S., Großschedl, J. E., Möller, T., et al. 2023, A&A, 677, A59

Ratzenböck, S., Großschedl, J. E., Alves, J., et al. 2023, Astronomy and Astrophysics, 678.0, A71

Rayner, J. T., Cushing, M. C., & Vacca, W. D. 2009, ApJS, 185, 289

Rayner, J. T., Toomey, D. W., Onaka, P. M., et al. 2003, The Publications of the Astronomical Society of the Pacific, 115, 362

Reid, I. N., Cruz, K. L., Kirkpatrick, J. D., et al. 2008, AJ, 136, 1290

Reid, I. N., & Hawley, S. L. 1999, The Astronomical Journal, 117.0, 343

Reid, N. I., Cruz, K. K., & Allen, P. R. 2007, The Astronomical Journal, 133, 2825

Reid, N. I., Gizis, J. E., & Hawley, S. L. 1995, The Astronomical Journal, 110, 1838

Reid, N. I., Cruz, K. K., Lowrance, P., et al. 2004, The Astronomical Journal, 128, 463

Riaz, B., Gizis, J. E., & Harvin, J. 2006, The Astronomical Journal, 132, 866

Ricker, G. R., Winn, J. N., Vanderspek, R., et al. 2015, Journal of Astronomical Telescopes, Instruments, and Systems, 1, 014003

Riddick, F. C., Roche, P. F., & Lucas, P. W. 2007, Monthly Notices of the Royal Astronomical Society, 381.0, 1077

Riedel, A. R., DiTomasso, V., Rice, E. L., et al. 2019, The Astronomical Journal, 157.0, 247

Rizzuto, A. C., Ireland, M. J., & Kraus, A. L. 2015, Monthly Notices of the Royal Astronomical Society, 448, 2737

Rizzuto, A. C., Ireland, M. J., & Robertson, J. G. 2011, Monthly Notices of the Royal Astronomical Society, 416, 3108

Rizzuto, A. C., Mann, A. W., Vanderburg, A., Kraus, A. L., & Covey, K. R. 2017, The Astronomical Journal, 154.0, 224

Robert, J., Gagné, J., Artigau, É., et al. 2016, *The Astrophysical Journal*, 830, 144

Roberts, Lewis C., J., Rice, E. L., Beichman, C. A., et al. 2012, *The Astronomical Journal*, 144.0, 14

Roccatagliata, V., Franciosini, E., Sacco, G. G., Randich, S., & Sicilia-Aguilar, A. 2020, *Astronomy and Astrophysics*, 638.0, A85

Rodet, L., Bonnefoy, M., Durkan, S., et al. 2018, *A&A*, 618, A23

Röser, S., & Schilbach, E. 2019, *A&A*, 627, A4

Röser, S., Schilbach, E., & Goldman, B. 2016, *A&A*, 595, A22

—. 2019, *A&A*, 621, L2

Röser, S., Schilbach, E., Piskunov, A. E., Kharchenko, N. V., & Scholz, R. D. 2011, *Astronomy and Astrophysics*, 531, A92

Roslund, C. 1960, *PASP*, 72, 205

Rothermich, A., Faherty, J. K., Bardalez-Gagliuffi, D., et al. 2024, *The Astronomical Journal*, 167.0, 253

Rydstrom, B. A. 1978, *Astronomy and Astrophysics Supplement Series*, 32.0, 25

Sacco, G. G., Franciosini, E., Randich, S., & Pallavicini, R. 2008, *Astronomy and Astrophysics*, 488.0, 167

Sahlmann, J., & Lazorenko, P. F. 2015, *MNRAS*, 453, L103

Sahlmann, J., Lazorenko, P. F., Ségransan, D., et al. 2014, *Astronomy and Astrophysics*, 565.0, A20

Saito, R. K., Hempel, M., Minniti, D., et al. 2012, *Astronomy and Astrophysics*, 537.0, A107

Sanghi, A., Liu, M. C., Best, W. M. J., et al. 2023, *The Astrophysical Journal*, 959.0, 63

Sartoretti, P., Katz, D., Cropper, M., et al. 2018, *A&A*, 616, A6

Sartori, M. J., Lépine, J. R. D., & Dias, W. S. 2003, *Astronomy & Astrophysics*, 404, 913

Sato, K., & Kuji, S. 1990, *Astronomy and Astrophysics Supplement Series*, 85.0, 1069

Saydjari, A. K., Schlafly, E. F., Lang, D., et al. 2023, *ApJS*, 264, 28

Schild, R. E. 1966, *The Astrophysical Journal*, 146.0, 142

Schlieder, J. E., Lépine, S., & Simon, M. 2010, *The Astronomical Journal*, 140, 119

Schlieder, J. E., Lépine, S., & Simon, M. 2012, *AJ*, 143, 80

Schmidt, S. J., West, A. A., Hawley, S. L., & Pineda, J. S. 2010, *The Astronomical Journal*, 139, 1808

Schneider, A. C., Cushing, M. C., Kirkpatrick, J. D., et al. 2014, *AJ*, 147, 34

Schneider, A. C., Greco, J., Cushing, M. C., et al. 2016a, *The Astrophysical Journal*, 817, 112

Schneider, A. C., Munn, J. A., Vrba, F. J., et al. 2023a, *The Astronomical Journal*, 166.0, 103

—. 2023b, *The Astronomical Journal*, 166.0, 103

—. 2023c, *The Astronomical Journal*, 166.0, 103

Schneider, A. C., Shkolnik, E. L., Allers, K. N., et al. 2019, *The Astronomical Journal*, 157.0, 234

Schneider, A. C., Windsor, J., Cushing, M. C., Kirkpatrick, J. D., & Shkolnik, E. L. 2017, *The Astronomical Journal*, 153.0, 196

Schneider, A. C., Windsor, J., Cushing, M. C., Kirkpatrick, J. D., & Wright, E. L. 2016b, *The Astrophysical Journal Letters*, 822, L1

Schneider, A. C., Cushing, M. C., Kirkpatrick, J. D., et al. 2015, *The Astrophysical Journal*, 804, 92

Schneider, A. C., Burgasser, A. J., Gerasimov, R., et al. 2020, *The Astrophysical Journal*, 898.0, 77

Schneider, A. C., Vrba, F. J., Munn, J. A., et al. 2022, *The Astronomical Journal*, 163.0, 242

Schneider, A. C., Burgasser, A. J., Bruursema, J., et al. 2023, *ApJL*, 943, L16

Schneider, A. C., Cushing, M. C., Stiller, R. A., et al. 2024, *The Astronomical Journal*, 168.0, 165

Schneider, A. C., Vrba, F. J., Bruursema, J., et al. 2025, *The Astronomical Journal*, 170.0, 86

Scholz, A., Geers, V., Jayawardhana, R., et al. 2009a, *The Astrophysical Journal*, 702, 805

Scholz, A., Muzic, K., Geers, V., et al. 2012, *The Astrophysical Journal*, 744, 6

Scholz, R.-D., & Bell, C. P. M. 2018, *Research Notes of the American Astronomical Society*, 2.0, 33

Scholz, R. D., McCaughrean, M. J., Zinnecker, H., & Lodieu, N. 2005a, *Astronomy & Astrophysics*, 430, L49

Scholz, R. D., Meusinger, H., & Jahreiß, H. 2005b, *Astronomy and Astrophysics*, 442, 211

Scholz, R. D., Storm, J., Knapp, G. R., & Zinnecker, H. 2009b, *Astronomy & Astrophysics*, 494, 949

Schutte, M. C., Lawson, K. D., Wisniewski, J. P., et al. 2020, *The Astronomical Journal*, 160.0, 156

Schwartz, R. D. 1977, *ApJS*, 35, 161

Schwassmann, A., & van Rhijn, P. J. 1935, *Bergedorfer Spektral-Durchmusterung der 115 noerdlichen Kapteynschen Eichfelder - Bd.1: Eichfeld 1 bis 19, Deklination +90 deg., +75 deg., +60 deg., Vol. 0.0*

Scott, D. W. 1992, *Multivariate Density Estimation*

Shang, L.-H., Luo, A. L., Wang, L., et al. 2022, *The Astrophysical Journal Supplement Series*, 259.0, 63

Sharma, K., Kembhavi, A., Kembhavi, A., et al. 2020, *Monthly Notices of the Royal Astronomical Society*, 491.0, 2280

Sheikhi, N., Hasheminia, M., Khalaj, P., et al. 2016, *Monthly Notices of the Royal Astronomical Society*, 457.0, 1028

Shkolnik, E., Liu, M. C., & Reid, I. N. 2009, *ApJ*, 699, 649

Shkolnik, E. L., Allers, K. N., Kraus, A. L., Liu, M. C., & Flagg, L. 2017, *The Astronomical Journal*, 154, 69

Shkolnik, E. L., Anglada-Escudé, G., Liu, M. C., et al. 2012, *ApJ*, 758, 56

Silaj, J., & Landstreet, J. D. 2014, *A&A*, 566, A132

Silverberg, S. M., Wisniewski, J. P., Kuchner, M. J., et al. 2020, *The Astrophysical Journal*, 890.0, 106

Sim, G., Lee, S. H., Ann, H. B., & Kim, S. 2019, *Journal of Korean Astronomical Society*, 52, 145

Simon, M., Guilloteau, S., Beck, T. L., et al. 2019, *ApJ*, 884, 42

Skiff, B. A. 2014, *VizieR On-line Data Catalog*, 1

Skrutskie, M. F., Cutri, R. M., Stiening, R., et al. 2006, *AJ*, 131, 1163

Slesnick, C. L., Carpenter, J. M., & Hillenbrand, L. A. 2006a, *AJ*, 131, 3016

Slesnick, C. L., Carpenter, J. M., Hillenbrand, L. A., & Mamajek, E. E. 2006b, *AJ*, 132, 2665

Slesnick, C. L., Hillenbrand, L. A., & Carpenter, J. M. 2008, *The Astrophysical Journal*, 688, 377

Slettebak, A. 1975, *The Astrophysical Journal*, 197.0, 137

Smart, R. L., Tinney, C. G., Bucciarelli, B., et al. 2013, *Monthly Notices of the Royal Astronomical Society*, 433.0, 2054

Smart, R. L., Bucciarelli, B., Jones, H. R. A., et al. 2018, *Monthly Notices of the Royal Astronomical Society*, 481.0, 3548

Smethells, W. G. 1974, PhD thesis

Smith, L. C., Lucas, P. W., Kurtev, R., et al. 2018, *Monthly Notices of the Royal Astronomical Society*, 474.0, 1826

Song, I., Zuckerman, B., & Bessell, M. S. 2003, *ApJ*, 599, 342

Sota, A., Maíz Apellániz, J., Morrell, N. I., et al. 2014, *The Astrophysical Journal Supplement Series*, 211.0, 10

Soubiran, C., Jasniewicz, G., Chemin, L., et al. 2018, *A&A*, 616, A7

Soubiran, C., Cantat-Gaudin, T., Romero-Gómez, M., et al. 2018, *Astronomy and Astrophysics*, 619.0, A155

Spezzi, L., Alcalá, J. M., Covino, E., et al. 2008, *The Astrophysical Journal*, 680, 1295

Stancliffe, R. J., Fossati, L., Passy, J. C., & Schneider, F. R. N. 2015, *Astronomy and Astrophysics*, 575.0, A117

Stanford-Moore, S. A., Nielsen, E. L., De Rosa, R. J., Macintosh, B., & Czekala, I. 2020, *ApJ*, 898, 27

Stassun, K. G., Mathieu, R. D., & Valenti, J. A. 2006, *Nature*, 440, 311

Stauffer, J. R. 1980, *The Astronomical Journal*, 85.0, 1341

Stauffer, J. R., Schultz, G., & Kirkpatrick, J. D. 1998, *The Astrophysical Journal*, 499, L199

Stauffer, J. R., Barrado y Navascués, D., Bouvier, J., et al. 1999, *ApJ*, 527, 219

Stauffer, J. R., Hartmann, L. W., Fazio, G. G., et al. 2007, *The Astrophysical Journal Supplement Series*, 172, 663

Steinmetz, M., Matijević, G., Enke, H., et al. 2020, *The Astronomical Journal*, 160.0, 82

Stephenson, C. B. 1959, *PASP*, 71, 145

Stephenson, C. B. 1960, *The Astronomical Journal*, 65.0, 60

Stephenson, C. B. 1986, *AJ*, 91, 144

Stoy, R. H. 1966, *Annals of the Cape Observatory*, 21.0, 0

Strom, K. M., Strom, S. E., & Merrill, K. M. 1993, *ApJ*, 412, 233

Struve, O., & Franklin, K. L. 1955, *The Astrophysical Journal*, 121.0, 337

Sun, Q., Wang, S. X., Mann, A. W., et al. 2023a, *The Astrophysical Journal*, 952.0, 68

—. 2023b, *The Astrophysical Journal*, 952.0, 68

Tang, S.-Y., Pang, X., Yuan, Z., et al. 2019, *ApJ*, 877, 12

Tarricq, Y., Soubiran, C., Casamiquela, L., et al. 2021, *A&A*, 647, A19

Terada, H., & Tokunaga, A. T. 2012, *The Astrophysical Journal*, 753.0, 19

Thao, P. C., Mann, A. W., Barber, M. G., et al. 2024, *AJ*, 168, 41

Thao, P. C., Mann, A. W., Barber, M. G., et al. 2024, *The Astronomical Journal*, 168.0, 41

Theissen, C. A., & West, A. A. 2017, *The Astronomical Journal*, 153.0, 165

Theissen, C. A., West, A. A., Shippee, G., Burgasser, A. J., & Schmidt, S. J. 2017, *The Astronomical Journal*, 153, 92

Thompson, M. A., Kirkpatrick, D. J., Mace, G. N., et al. 2013, *Publications of the Astronomical Society of the Pacific*, 125, 809

Thorstensen, J. R., Vennes, S., & Shambrook, A. 1994, *The Astronomical Journal*, 108.0, 1924

Tian, X.-m., Wang, Z.-h., Zhu, L.-y., & Yang, X.-L. 2023, *The Astrophysical Journal Supplement Series*, 266.0, 14

Tinney, C. G., Kirkpatrick, J. D., Faherty, J. K., et al. 2018, *The Astrophysical Journal Supplement Series*, 236.0, 28

Tofflemire, B. M., Rizzuto, A. C., Newton, E. R., et al. 2021, *AJ*, 161, 171

Torres, C. A. O., Quast, G. R., da Silva, L., et al. 2006, *A&A*, 460, 695

Torres, C. A. O., Quast, G. R., Melo, C. H. F., & Sterzik, M. F. 2008, in *Handbook of Star Forming Regions*, Volume II, ed. B. Reipurth, Vol. 5, 757

Tremblay, P. E., Hollands, M. A., Gentile Fusillo, N. P., et al. 2020, *Monthly Notices of the Royal Astronomical Society*, 497.0, 130

Trifonov, T., Tal-Or, L., Zechmeister, M., et al. 2020, *A&A*, 636, A74

Turner, D. G., Mandushev, G. I., & Forbes, D. 1994, *The Astronomical Journal*, 107.0, 1796

van den Bergh, S., & Hagen, G. L. 1975, *AJ*, 80, 11

Van-Lane, P. R., Speagle, J. S., Eadie, G. M., et al. 2025, *ApJ*, 986, 59

van Leeuwen, F. 2007, *A&A*, 474, 653

van Leeuwen, F. 2007, *Astronomy and Astrophysics*, 474.0, 653

Vincent, O., Barstow, M. A., Jordan, S., et al. 2024, *Astronomy and Astrophysics*, 682.0, A5

Viswanath, G., Janson, M., Gratton, R., et al. 2023, *Astronomy and Astrophysics*, 675.0, A54

Voges, W., Aschenbach, B., Boller, T., et al. 1999, *A&A*, 349, 389

Vos, J. M., Faherty, J. K., Gagné, J., et al. 2022, *The Astrophysical Journal*, 924.0, 68

Vrba, F. J., Henden, A. A., Luginbuhl, C. B., et al. 2004, *The Astronomical Journal*, 127, 2948

Wagner, K., Apai, D., Kasper, M., et al. 2020, *The Astrophysical Journal*, 902.0, L6

Wahhaj, Z., Liu, M. C., Biller, B. A., et al. 2011, *The Astrophysical Journal*, 729, 139

Waisberg, I., Klein, Y., & Katz, B. 2025, *Research Notes of the American Astronomical Society*, 9, 71

Walter, F. M., Wolk, S. J., & Sherry, W. 1998, in *Astronomical Society of the Pacific Conference Series*, Vol. 154, Cool Stars, Stellar Systems, and the Sun, ed. R. A. Donahue & J. A. Bookbinder, 1793

Wang, W., Boudreault, S., Goldman, B., et al. 2011, *Astronomy and Astrophysics*, 531.0, A164

Wang, Y.-F., Luo, A. L., Chen, W.-P., et al. 2022, *Astronomy and Astrophysics*, 660.0, A38

Ward-Duong, K., Patience, J., Follette, K., et al. 2021, *The Astronomical Journal*, 161.0, 5

Weaver, G., Jeffries, R. D., & Jackson, R. J. 2024, *MNRAS*, 534, 2014

Webb, R. A., Zuckerman, B., Platais, I., et al. 1999, *The Astrophysical Journal*, 512, L63

Weinberger, A. J., Boss, A. P., Keiser, S. A., et al. 2016, *The Astronomical Journal*, 152, 24

Wenger, M., Ochsenbein, F., Egret, D., et al. 2000, *A&AS*, 143, 9

West, A. A., Hawley, S. L., Bochanski, J. J., et al. 2008, *The Astronomical Journal*, 135, 785

West, A. A., Weisenburger, K. L., Irwin, J., et al. 2015, *The Astrophysical Journal*, 812.0, 3

West, A. A., Morgan, D. P., Bochanski, J. J., et al. 2011, *AJ*, 141, 97

White, R. J., Gabor, J. M., & Hillenbrand, L. A. 2007, *The Astronomical Journal*, 133, 2524

Wilking, B. A., Gagné, M., & Allen, L. E. 2008a, *Handbook of Star Forming Regions*, I, 351

Wilking, B. A., Gagné, M., & Allen, L. E. 2008b, *VizieR Online Data Catalog: JKH photometry in LDN 1688* (Wilking+, 2008)

Wilking, B. A., Meyer, M. R., Greene, T. P., Mikhail, A., & Carlson, G. 2004, *The Astronomical Journal*, 127.0, 1131

Wilson, O. C. 1963, *The Astrophysical Journal*, 138.0, 832

Winston, E., Megeath, S. T., Wolk, S. J., et al. 2010, *The Astronomical Journal*, 140.0, 266

Winters, J. G., Sevrinsky, R. A., Jao, W.-C., et al. 2017, *The Astronomical Journal*, 153.0, 14

Wolk, S. J., Winston, E., Bourke, T. L., et al. 2010, *The Astrophysical Journal*, 715.0, 671

Wood, M. L., Mann, A. W., Barber, M. G., et al. 2023, *AJ*, 165, 85

Wood, M. L., Mann, A. W., Barber, M. G., et al. 2023, *The Astronomical Journal*, 165.0, 85

Wright, E. L., Eisenhardt, P. R. M., Mainzer, A. K., et al. 2010, *The Astronomical Journal*, 140, 1868

Wu, Y.-L., Close, L. M., Males, J. R., et al. 2015, *The Astrophysical Journal*, 801.0, 4

Yamashita, Y., & Norimoto, Y. 1981, *Annals of the Tokyo Astronomical Observatory*, 18.0, 124

Yao, Y., Meyer, M. R., Covey, K. R., Tan, J. C., & Da Rio, N. 2018, *The Astrophysical Journal*, 869.0, 72

Zacharias, N., Finch, C. T., Girard, T. M., et al. 2012, *VizieR On-line Data Catalog*, 1322, 0

Zacharias, N., Finch, C., Girard, T., et al. 2010, *The Astronomical Journal*, 139, 2184

Zapatero Osorio, M. R., Béjar, V. J. S., Martín, E. L., et al. 2000, *Science*, 290, 103

—. 2002a, *The Astrophysical Journal*, 578, 536

Zapatero Osorio, M. R., Béjar, V. J. S., Pavlenko, Y., et al. 2002b, *Astronomy & Astrophysics*, 384, 937

Zapatero Osorio, M. R., Gálvez Ortiz, M. C., Bihain, G., et al. 2014, *Astronomy and Astrophysics*, 568.0, A77

Zhang, J., Zhang, Y., Kang, Z., Li, C., & Zhao, Y. 2023a, *The Astrophysical Journal Supplement Series*, 267.0, 7

Zhang, J. Y., Lodieu, N., & Martín, E. L. 2024, *A&A*, 686, A171

Zhang, L.-y., Su, T., Misra, P., et al. 2023b, *The Astrophysical Journal Supplement Series*, 264.0, 17

Zhang, L.-Y., Long, L., Shi, J., et al. 2020, *MNRAS*, 495, 1252

Zhang, Z., Liu, M. C., Best, W. M. J., Dupuy, T. J., & Siverd, R. J. 2021, *ApJ*, 911, 7

Zhang, Z., Liu, M. C., Morley, C. V., et al. 2022, *The Astrophysical Journal*, 935.0, 15

Zhang, Z., Liu, M. C., Best, W. M. J., et al. 2018, *ApJ*, 858, 41

Zhang, Z. H., Pokorny, R. S., Jones, H. R. A., et al. 2009, *Astronomy & Astrophysics*, 497, 619

Zhang, Z. H., Pinfield, D. J., Day-Jones, A. C., et al. 2010, *Monthly Notices of the Royal Astronomical Society*, 404, 1817

Zhang, Z. H., Galvez-Ortiz, M. C., Pinfield, D. J., et al. 2018, *Monthly Notices of the Royal Astronomical Society*, 480.0, 5447

Zhong, J., Lépine, S., Hou, J., et al. 2015, *The Astronomical Journal*, 150.0, 42

Zuckerman, B. 2019, *ApJ*, 870, 27

Zuckerman, B., Bessell, M. S., Song, I., & Kim, S. 2006, *ApJL*, 649, L115

Zuckerman, B., Klein, B., & Kastner, J. 2019, *The Astrophysical Journal*, 887.0, 87

Zuckerman, B., Rhee, J. H., Song, I., & Bessell, M. S. 2011, *The Astrophysical Journal*, 732, 61

Zuckerman, B., & Song, I. 2004, *ARA&A*, 42, 685

Zuckerman, B., Song, I., & Bessell, M. S. 2004, *ApJL*, 613, L65

Zuckerman, B., Song, I., Bessell, M. S., & Webb, R. A. 2001, *ApJL*, 562, L87

Zuckerman, B., Vican, L., Song, I., & Schneider, A. C. 2013, *The Astrophysical Journal*, 778, 5

Zuckerman, B., & Webb, R. A. 2000, *ApJ*, 535, 959

APPENDIX

In this section, we provide a few examples of MySQL queries that can be used in the MOCAdb. Comments shown directly in the MySQL code blocks are preceded with the - symbols, which are ignored by MySQL upon execution.

In the first example, a user might aim to list all membership claims to the β Pic moving group (`moca_aid = BPMG`) for objects with spectral types T0 or later. This would be achieved by starting from the `data_spectral_types` table to filter on spectral types, and joining the resulting rows with the `data_memberships` table, which contains an exhausting list of all association members, with the associated reference and type of membership. The potentially multiple membership claims related to a single object will be combined using a MySQL GROUP BY statement.

```

SELECT
    -- Main object information
    mo.designation, mo.ra, mo.dec,
    -- Spectral type information
    spt.spectral_type, spt.moca_pid AS spt_ref,
    -- Membership information, stacked by moca_oid
    GROUP_CONCAT(CONCAT(dm.moca_mtid, ',', dm.moca_pid, ',')) AS all_mem
    -- Start from spectral types table to limit the spectral type range
    FROM data_spectral_types spt
    -- Join the main objects table to get the main designation
    JOIN moca_objects mo USING(moca_oid)
    -- Join the non-rejected memberships in BPMG
    -- This will duplicate some rows for multiple membership claims
    JOIN data_memberships dm ON(
        dm.moca_oid=spt.moca_oid AND
        dm.moca_mtid != 'R' AND
        dm.moca_aid='BPMG')
WHERE
    -- Only consider the best-available spectral type
    spt.adopted=1 AND
    -- Ignore spectral type estimates based on photometry
    spt.photometric_estimate=0 AND
    -- Limit the search to T0 or later (numeric spt = 20)
    spt.spectral_type_number >= 20
    -- Combine the duplicated rows caused by multiple membership claims
    GROUP BY spt.moca_oid;

```

If a user would instead aim to list the objects which are currently categorized as high-probability candidate members of β PMG using the latest version of the BANYAN Σ models with all available observables, regardless of literature membership claims, the following query would achieve this:

```

SELECT
    -- Main object information
    mo.designation, mo.ra, mo.dec,
    -- Spectral type information
    spt.spectral_type, spt.moca_pid AS spt_ref,
    -- Membership information
    cbs.ya_prob, cbs.observables, cbs.list_prob_yas
-- Start from spectral types table to limit the spectral type range
FROM data_spectral_types spt
-- Join the main objects table to get the main designation
JOIN moca_objects mo USING(moca_oid)
-- Join the BANYAN Sigma calculations that place an object in BPMG
-- with a probability above 90%
-- this table includes every combination of observables
-- and every available set of BANYAN models (moca_bsmdid)
JOIN calc_banyan_sigma cbs ON(
    -- Match the results with the moca_oid object
    cbs.moca_oid=spt.moca_oid AND
    -- Only consider BPMG
    cbs.moca_aid='BPMG' AND
    -- Only consider the rows using all available observables
    cbs.max_observables=1 AND
    -- Only consider objects with 90% membership or more
    cbs.ya_prob >= 90
)
-- Join the list of available BANYAN models
-- to restrain results to the latest one (adopted=1)
JOIN moca_banyan_sigma_models mbsm ON(
    -- Match using the model version id
    mbsm.moca_bsmdid=cbs.moca_bsmdid AND
    -- Restraine to currently adopted BANYAN model version
    mbsm.adopted=1)
WHERE
    -- Only consider the best-available spectral type
    spt.adopted=1 AND
    -- Ignore spectral type estimates based on photometry
    spt.photometric_estimate=0 AND
    -- Limit the search to T0 or later (numeric spt = 20)
    spt.spectral_type_number >= 20;

```

As a final example, let us consider a case where a user aims to gather all age-calibrated lithium equivalent width measurements as a function of the Gaia DR3 $G - G_{RP}$ color. This could be achieved by starting from the `calc_equivalent_widths_combined` table, which already combines all available individual measurements per star, and joining the Gaia photometry, individual references, memberships, and the age associated to the host association. In this specific example, the ages are based on the membership classifications as directed by the best-available BANYAN Σ membership probabilities.

```

SELECT
    -- Main object information
    mo.designation, mo.ra, mo.dec,
    -- Li EW information
    cewc.ew_angstrom*1000 AS ewli_milliangstrom,
    cewc.ew_angstrom_unc*1000 AS e_ewli_milliangstrom,
    -- Combine the EW Li references per object
    GROUP_CONCAT(ewref.bibcode) AS ew_refs,
    -- Gaia colors
    (gmag.magnitude - grpmag.magnitude) AS g_rp_color,
    -- Membership information
    cbs.moca_aid, cbs.ya_prob, cbs.observables,
    -- Age information
    daa.age_myr, ageref.bibcode AS age_ref
    -- Start from the table that contains combined equivalent widths per-object
FROM calc_equivalent_widths_combined AS cewc
    -- Join the main object table for generic information
JOIN moca_objects mo USING(moca_oid)
    -- Join the individual EW measurements to gather the references
    -- this will cause duplicated rows which will be re-combined
    -- with a GROUP BY statement
JOIN data_equivalent_widths AS ew ON(ew.junct_setid=cewc.junct_setid)
    -- Include the bibcodes for EW references
JOIN moca_publications AS ewref ON(ewref.moca_pid=ew.moca_pid)
    -- Include Gaia DR3 G-band photometry (dereddened when necessary)
    -- from the photometry table
JOIN data_photometry AS gmag ON(
    -- This constraint matches the EWs to the photometry with the moca_oid
    gmag.moca_oid=cewc.moca_oid AND
    -- This selects the Gaia DR3 G-band photometry
    gmag.moca_psid='gaiadr3_gmag' AND
    -- This restrains the selection to the best-available measurement
    gmag.adopted=1)
    -- Repeat with Gaia DR3 G_RP-band photometry
JOIN data_photometry AS grpmag ON(
    grpmag.moca_oid=cewc.moca_oid AND
    -- This selects the Gaia DR3 G_RP-band photometry
    grpmag.moca_psid='gaiadr3_rpmag' AND
    grpmag.adopted=1)
    -- Join membership information based on BANYAN Sigma
JOIN calc_banyan_sigma cbs ON(
    -- Match the results with the moca_oid object
    cbs.moca_oid=cewc.moca_oid AND
    -- Only consider the rows using all available observables
    cbs.max_observables=1 AND
    -- Only consider objects with 90% membership or more

```

```
cbs.ya_prob >= 90
)
-- Join the list of available BANYAN models
-- to restrain results to the latest one (adopted=1)
JOIN moca_banyan_sigma_models mbsm ON(
    -- Match using the model version id
    mbsm.moca_bsmdid=cbs.moca_bsmdid AND
    -- Restraine to currently adopted BANYAN model version
    mbsm.adopted=1)
-- Join the best-available association age
JOIN data_association_ages daa ON(
    -- Age is selected based on BANYAN Sigma membership
    daa.moca_aid=cbs.moca_aid AND
    -- Restraine to the adopted age
    daa.adopted=1
)
-- Include the bibcodes for age references
JOIN moca_publications AS ageref ON(ageref.moca_pid=daa.moca_pid)
-- This selects the Li equivalent widths
WHERE cewc.moca_spid='li'
-- Group by objects to combine the individual Li EW references
GROUP BY cewc.moca_oid;
```

Table 1. List of Associations Considered in this Work.

textttmoca_aid	Designation	Real	Suboptimal Definition	Disc. Ref.	Age (Myr)	Age Ref.
ABDMG	AB Doradus moving group	1	0	1	133^{+15}_{-20}	2
BPMG	β Pictoris moving group	1	0	3	26 ± 3	4
CAR	Carina association	1	0	5	$33.7^{+2.0}_{-1.9}$	6
CARN	Carina-Near moving group	1	0	7	200	7
CBER	Coma Berenices	1	0	—	675 ± 100	8
COL	Columba association	1	0	5	$33.7^{+2.0}_{-1.9}$	6
EPSC	ε Cha association	1	0	9	3.7	10
ETAC	η Cha association	1	0	11	6.5	10
HYA	Hyades open cluster	1	0	—	695^{+85}_{-67}	12
LCC	Lower Centaurus Crux OB association	1	0	13	21 ± 4	14
OCT	Octans association	1	0	5	30-40	15
PL8	Platais 8 open cluster	1	0	16	$33.7^{+2.0}_{-1.9}$	6
PLE	Pleiades association	1	0	—	$127.4 +6.3/-10$	12
THA	Tucana-Horologium association	1	0	17	40 ± 3	18
THOR	32 Ori association	1	0	19	21 ± 4	14
TWA	TW Hya association	1	0	20	10	21
UCL	Upper Centaurus Lupus OB association	1	0	13	21 ± 4	14
UMA	Ursa Major association	1	0	—	414	22
USCO	Upper Scorpius OB association	1	0	13	10	23
IC2602	IC 2602 open cluster	1	0	—	$40.0^{+1.9}_{-1.4}$	6
IC2391	IC 2391 open cluster	1	0	—	$51.0^{+5.6}_{-3.9}$	6
XFOR	χ 1 Fornacis cluster	1	0	24	$33.7^{+2.0}_{-1.9}$	6
ROPH	ρ Ophiuchi star-forming region	1	0	—	< 2	25
CRA	Corona Australis star-forming region	1	0	—	4-5	26
UCRA	Upper Corona Australis star-forming region	1	0	27	10	28

NOTE—Only the first 25 rows are shown here; the full table is available in the online version of this journal.

References—(1) Zuckerman et al. (2004), (2) Gagné et al. (2018c), (3) Zuckerman et al. (2001), (4) Malo et al. (2014), (5) Torres et al. (2008), (6) Luhman et al. (2024), (7) Zuckerman et al. (2006), (8) Agüeros et al. (2025), (9) Feigelson et al. (2003), (10) Murphy et al. (2013), (11) Mamajek et al. (1999), (12) Galindo-Guil et al. (2022), (13) Blaauw (1964), (14) Luhman (2022a), (15) Murphy & Lawson (2015), (16) Platais et al. (1998), (17) Zuckerman & Webb (2000), (18) Kraus et al. (2014), (19) Mamajek (2007), (20) Kastner et al. (1997), (21) Bell et al. (2015), (22) Jones et al. (2015), (23) Pecaut & Mamajek (2016), (24) Dias et al. (2002), (25) Wilking et al. (2008a), (26) Gennaro et al. (2012), (27) Neuhäuser et al. (2000), (28) Gagné et al. (2018e).

Table 2. New candidate members identified in this work.

Designation	Spectral Type	moca_aid	Banyan Σ P (%)	$\mu_\alpha \cos \delta$ (mas yr $^{-1}$)	μ_δ (mas yr $^{-1}$)	Distance (pc)	RV (km s $^{-1}$)	Refs ^a
Gaia DR2 1576589693004879616	A0	UMA	99.9	114 ± 2	2 ± 2	25.3 ± 0.1	...	1;2;−;3
Gaia DR3 1563590579347125632	A1.5Vs	UMA	99.9	122.5 ± 0.3	-22.7 ± 0.8	24.9 ± 0.3	-5.6 ± 0.9	4;5;−;5
Gaia DR3 3966634844566024960	M2.5	UMA	99.9	85.16 ± 0.04	-48.24 ± 0.02	24.83 ± 0.02	-10.7 ± 0.9	6;5;−;5
Gaia DR3 843042092397033472	M3	UMA	99.9	100.9 ± 0.4	23.5 ± 0.5	24.1 ± 0.3	-11.3 ± 0.8	7;5;−;5
2MASS J09161018+0153088	M4Ve	UMA	99.9	54.82 ± 0.03	-101.31 ± 0.02	15.652 ± 0.007	-12 ± 1	8;5;−;5
2MASS J16352740+3500577	M4Ve	UMA	99.9	139.4 ± 0.1	-143.6 ± 0.1	17.24 ± 0.03	3.0 ± 0.3	8;5;−;5
PM J07472+5020	M4Ve	UMA	99.9	-16.79 ± 0.02	79.62 ± 0.02	14.109 ± 0.005	-15.0 ± 0.8	8;5;−;5
2MASS J11430780+6220365	(M6.0)	UMA	99.9	65.61 ± 0.05	18.76 ± 0.06	36.90 ± 0.08	...	−;5;−;5
2MASS J10390493+4352266	(M6.0)	UMA	99.9	61.57 ± 0.03	11.54 ± 0.03	28.71 ± 0.03	-11 ± 2	−;5;−;5
Gaia DR3 1713327707813549696	M7e	UMA	99.9	73.8 ± 0.2	-3.1 ± 0.2	41.8 ± 0.3	...	9;5;−;5
2MASS J13445832+7715513	(M7.1)	UMA	99.9	73.8 ± 0.2	-3.1 ± 0.2	41.8 ± 0.3	...	−;5;−;5
2MASS J11240487+3808054	M8.5	UMA	99.9	125.7 ± 0.1	-9.2 ± 0.2	18.41 ± 0.05	-14 ± 3	10;5;−;5
2MASS J01474488+6351090	K0V	CARN	97.5	581.68 ± 0.03	-246.46 ± 0.04	10.041 ± 0.004	2.74 ± 0.06	11;5;−;5
HD 99279	K5-V	CARN	98.1	-525 ± 2	82 ± 2	12.1 ± 0.2	8 ± 5	12;13;−;13
TYC 8576-789-1	K6Ve	CARN	91.8	-48.11 ± 0.01	66.59 ± 0.01	70.08 ± 0.05	17 ± 1	14;5;−;5
Gaia DR3 5448465052078103040	(K7.0)	CARN	93.7	-101.2 ± 0.1	34.5 ± 0.1	55.4 ± 0.6	...	−;5;−;5
Gaia DR3 2489349339521604864	M1.5	CARN	94.6	193.06 ± 0.03	7.68 ± 0.02	30.71 ± 0.02	15.9 ± 0.3	15;5;−;5
Gaia DR3 3409167094776800384	M1.5V	CARN	96.4	102.36 ± 0.02	-135.32 ± 0.02	20.608 ± 0.010	...	16;5;−;5
Gaia DR3 5584660801498379264	(M1.6)	CARN	98.2	-37.77 ± 0.01	87.92 ± 0.02	47.71 ± 0.03	24.3 ± 0.7	−;5;−;5
LP 794-87	M3.5	CARN	98.0	-453 ± 4	-33 ± 4	...	7 ± 8	17;18;−;−

^aReferences for spectral types, proper motions, radial velocities, and distances, respectively.

NOTE—Only the first 20 rows are shown here; the full table, which also contains the right ascension, and declination columns, is available in the online version of this journal. Distances between parentheses are photometric rather than trigonometric. Spectral types between parentheses are estimated based on colors.

References—(1) King et al. (2003), (2) Schneider et al. (2025), (3) van Leeuwen (2007), (4) Gray et al. (2003), (5) Gaia Collaboration et al. (2023), (6) Bai et al. (2012), (7) Zhang et al. (2023b), (8) Lépine et al. (2013), (9) Gizis et al. (2000), (10) Cruz et al. (2003), (11) White et al. (2007), (12) Gray et al. (2006), (13) Gaia Collaboration et al. (2018), (14) Torres et al. (2006), (15) Reid et al. (2004), (16) Alonso-Floriano et al. (2015), (17) Reid et al. (2007), (18) Marocco et al. (2021).

Table 3. List of Tables in MOCAdb.

Table Name	Number of Columns	Number of Rows
moca_associations	18	10261
moca_changelog	11	61408
moca_companions	17	36887
moca_spectral_indices	15	78
moca_instruments	6	73
moca_missions	21	42
moca_banyan_sigma_models	16	1
moca_objects	18	3234191
moca_spectra_packages	30	28
moca_object_properties	10	22
moca_publications	19	5507
moca_extinction_by_spectral_reference	12	2093
moca_spectral_type_references	16	161
moca_sequences	35	7
moca_chemical_species	14	10
moca_spectra	69	4064
moca_photometry_systems	18	109
moca_object_types	5	13
moca_membership_types	7	6
cat_2mass	73	2152213
cat_apogeedr16_allstars	176	439475
cat_apogeedr16_allvisits	70	1679797
cat_allwise	305	1371102
cat_catwise	200	1769974
cat_decapsdr2	223	2004
cat_denisdr3	87	23366
cat_desdr1	184	22169
cat_desdr2	238	41963
cat_erassdr1	256	833615
cat_euclidq1	664	589
cat_gaiadr1	66	145784
cat_gaiadr2	103	3081410
cat_gaiadr3	164	3064316
cat_gaiaedr3	109	609388
cat_galahdr3	191	6583
cat_galex_gr67	103	43920
cat_hipparcos	33	118182
cat_gaiadr3_binary_masses	19	10549
cat_gaiadr3_vari_rotation_modulation	72	16433
cat_exoplanets_nasa	295	5154

NOTE—Only the first 40 rows are shown here; the full table is available in the online version of this journal.

Table 4. List of Columns in MOCAdb.

Table Name	Column Name	Data Type
moca_associations	id	int(11) unsigned
moca_associations	moca_aid	varchar(12)
moca_associations	moca_pid	varchar(20)
moca_associations	name	varchar(255)
moca_associations	simbad_id	varchar(255)
moca_associations	is_real	varchar(1)
moca_associations	coeval	varchar(1)
moca_associations	suboptimal_grouping	varchar(1)
moca_associations	in_banyan	tinyint(1)
moca_associations	in_banyan_sigma_2020	tinyint(1)
moca_associations	in_partiview	tinyint(1)
moca_associations	physical_nature	varchar(50)
moca_associations	comments	text
moca_associations	created_timestamp	timestamp
moca_associations	modified_timestamp	timestamp
moca_associations	bibcode	varchar(30)
moca_changelog	id	int(11) unsigned
moca_changelog	created_timestamp	datetime
moca_changelog	user	varchar(50)
moca_changelog	machine_name	varchar(50)
moca_changelog	modified_tables	text
moca_changelog	nrows_modified	int(11)
moca_changelog	user_description	text
moca_companions	moca_cid	int(11) unsigned
moca_companions	moca_oid_parent	int(11) unsigned
moca_companions	moca_oid_child	int(11) unsigned
moca_companions	moca_pid	varchar(20)
moca_companions	origin	varchar(255)
moca_companions	object_designation_parent	varchar(60)
moca_companions	object_designation_type_parent	varchar(20)
moca_companions	object_designation_child	varchar(60)
moca_companions	object_designation_type_child	varchar(20)
moca_companions	publication_comments	varchar(255)
moca_companions	comments	text
moca_companions	created_timestamp	timestamp
moca_companions	modified_timestamp	timestamp
moca_companions	ignored	tinyint(1)
moca_companions	bibcode	varchar(30)
moca_spectral_indices	id	int(11) unsigned
moca_spectral_indices	moca_siid	varchar(20)

NOTE—Only the first 40 rows are shown here; the full table is available in the online version of this journal.

Table 5. External Catalogs Cross-Matched with MOCAdb Entries.

MOCAdb Table	Mission Name	Reference
cat_2mass	2MASS PSC	1
cat_apogeedr16_allstars	APOGEE DR16	2
cat_decapsdr2	DECAPS DR2	3
cat_denisdr3	DENIS DR3	4
cat_desdr2	DES DR2	5
cat_gaiadr1	Gaia DR1	6
cat_gaiadr2	Gaia DR2	7
cat_gaiaedr3	Gaia EDR3	8
cat_gaiadr3	Gaia DR3	9
cat_galahdr3	GALAH DR3	10
cat_galex_gr67	Galex GR67	11
cat_hipparcos	Hipparcos 2007 reduction	12
cat_nscdr2	NSC DR2	13
cat_ps1dr2	PS1 DR2	14
cat_ravedr6	RAVE DR6	15
cat_rosat	ROSAT All-Sky	16
cat_splusdr4	S-PLUS DR4	17
cat_sdssdr17	SDSS DR17	18
cat_smssdr4	SMSS DR4	19
cat_uhsdr3	UHS DR3	20
cat_ukidssdxsdr11plus	UKIDSSDXS DR11PLUS	21
cat_ukidssgcsdr11plus	UKIDSSGCS DR11PLUS	21
cat_ukidssgpsdr11plus	UKIDSSGPS DR11PLUS	21
cat_ukidsslasdr11plus	UKIDSSLAS DR11PLUS	21
cat_vhsdr6	VHS DR6	22
cat_videodr5	VIDEO DR5	23
cat_vikingdr4	VIKING DR4	24
cat_viracdr4_plx	VIRAC DR4	25
cat_vmcdr5	VMC DR5	26
cat_vvvdr5	VVV DR5	27
cat_wise	WISE All-Sky SC	28
cat_allwise	WISE AllWISE	29
cat_catwise	WISE CatWISE	30

References—(1) Skrutskie et al. (2006), (2) Ahumada et al. (2020), (3) Saydari et al. (2023), (4) Epchtein et al. (1994), (5) Abbott et al. (2021), (6) Gaia Collaboration et al. (2016a), (7) Gaia Collaboration et al. (2018), (8) Gaia Collaboration et al. (2021), (9) Gaia Collaboration et al. (2023), (10) Buder et al. (2025), (11) Bianchi et al. (2017), (12) van Leeuwen (2007), (13) Nidever et al. (2021), (14) Chambers et al. (2016), (15) Steinmetz et al. (2020), (16) Voges et al. (1999), (17) Herpich et al. (2024), (18) Abdurro'uf et al. (2022), (19) Onken et al. (2024), (20) Schneider et al. (2025), (21) Lawrence et al. (2007), (22) McMahon et al. (2013), (23) Häußler et al. (2022), (24) Edge et al. (2013), (25) Smith et al. (2018), (26) Cioni et al. (2011), (27) Saito et al. (2012), (28) Wright et al. (2010), (29) Kirkpatrick et al. (2014), (30) Marocco et al. (2021).

Table 6. Age-calibrated exoplanets currently known.

Host Star Designation	N_{exo}	Method	<code>moca_aid</code>	Banyan Σ Prob. (%)	Mem. Ref.	Age (Myr)	Age Ref.
GJ 393	1	RV	ABDMG	99.3	1	133^{+15}_{-20}	2
GJ 849	2	RV	CRIUS197	94.8	3	...	—
HD 147513	1	RV	CRIUS135	95.2	3	100-700	4
GJ 163	3	RV	HSC1711	85.1	3	260 (-190,+670)	5
GJ 3021	1	RV	CRIUS203	97.3	3	$670.0^{+376.7/-241.1}$	—
LSPM J2116+0234	1	RV	CARN	92.7	3	200	6
bet Pic	2	RV	BPMG	99.0	7	26 ± 3	8
GJ 9714	1	RV	VELA	91.7	3	2-9960	—
HD 114783	2	RV	OCTN	89.8	3	30-100	9
HIP 12961	1	RV	CRIUS197	98.7	3	...	—
HD 179949	1	RV	VELA	85.2	3	2-9960	—
HD 142415	1	RV	CRIUS209	81.0	3	...	—
HS Psc	1	RV	ABDMG	99.4	10	133^{+15}_{-20}	2
30 Ari B	1	RV	CRIUS203	83.2	3	$670.0^{+376.7/-241.1}$	—
eps Tau	1	RV	HYA	99.9	11	695^{+85}_{-67}	12
HD 285507	1	RV	HYA	99.9	11	695^{+85}_{-67}	12
HD 212301	1	RV	MEL5	93.6	13	210 ± 27	14
HD 135625	1	RV	CRIUS209	97.4	3	...	—
HD 114082	1	RV	GRSCOS27C	99.5	3	14.6	15
TAP 26	1	RV	OH29	99.9	16	29.3 ± 1	17
V830 Tau	1	RV	L1529	99.9	18	3.4	15
CI Tau	1	RV	TAUMGLIU4	99.9	16	2.0	16
Pr0201	1	RV	PRA	99.9	19	617	20
Pr0211	2	RV	CPRA	99.9	21	617.0	20
NGC 2682 Sand 364	1	RV	NGC2682	99.7	22	4000	22
NGC 2682 YBP 401	1	RV	NGC2682	99.9	22	4000	22
NGC 2682 Sand 978	1	RV	NGC2682	99.9	22	4000	22
NGC 2682 Sand 1429	1	RV	NGC2682	99.9	22	4000	22
NGC 2682 YBP 1194	1	RV	NGC2682	99.8	22	4000	22
NGC 2682 YBP 1514	1	RV	NGC2682	99.9	22	4000	22

NOTE—Only the first 30 rows are shown here; the full table is available in the online version of this journal.

References—(1) da Silva et al. (2009), (2) Gagné et al. (2018c), (3) This Paper, (4) Moranta et al. (2022), (5) Hunt & Reffert (2023), (6) Zuckerman et al. (2006), (7) Zuckerman et al. (2001), (8) Malo et al. (2014), (9) Zuckerman et al. (2013), (10) Schlieder et al. (2010), (11) Perryman et al. (1998), (12) Galindo-Guil et al. (2022), (13) Thao et al. (2024), (14) Thao et al. (2024), (15) Kerr et al. (2021), (16) Liu et al. (2021), (17) Luhman et al. (2024), (18) Luhman (2023a), (19) Douglas et al. (2014), (20) Gossage et al. (2018), (21) Röser & Schilbach (2019), (22) Tarricq et al. (2021).

Table 7. Age-calibrated TESS exoplanets candidates.

Host Star Designation	N_{exo}	<code>moca_aid</code>	Banyan Σ Prob. (%)	Mem. Ref.	Age (Myr)	Age Ref.
TIC 141141249	1	ARG	93.1	1	45-50	2
TIC 278198753	1	CAR	81.3	1	$33.7^{+2.0}_{-1.9}$	3
TIC 325468685	1	CRIUS131	82.5	1	$569.1^{+619.1}_{-239.3}$	—
TIC 441420236	1	BPMG	98.1	4	26 ± 3	5
TIC 31374837	1	CRIUS197	93.0	1	...	—
TIC 192790476	1	MEL5	97.2	6	210 ± 27	7
TIC 299798795	1	MEL5	99.8	6	210 ± 27	7
TIC 51024887	1	OCEMG	90.1	1	500-600	8
TIC 27491137	1	CRIUS224	99.5	9	...	—
TIC 180695581	1	CRIUS224	99.6	9	...	—
TIC 437011608	1	CRIUS197	92.3	1	...	—
TIC 4070275	1	CHYA	99.9	10	695^{+85}_{-67}	11
TIC 434226736	1	HYA	99.9	12	695^{+85}_{-67}	11
TIC 244161191	1	COL	92.7	1	$33.7^{+2.0}_{-1.9}$	3
TIC 20182165	1	OCTN	97.5	13	30-100	13
TIC 77951245	1	COL	99.9	12	$33.7^{+2.0}_{-1.9}$	3
TIC 419957393	1	OCTN	96.3	1	30-100	13
TIC 464646604	1	ABDMG	96.6	14	133^{+15}_{-20}	15
TIC 18310799	1	HYA	99.9	16	695^{+85}_{-67}	11
TIC 311183180	1	CHYA	86.5	1	695^{+85}_{-67}	11
TIC 298981199	1	OCTN	99.2	1	30-100	13
TIC 311271011	1	CRIUS223	99.4	9	100-700	—
TIC 93125144	1	ABDMG	82.9	14	133^{+15}_{-20}	15
TIC 39200363	1	CRIUS205	99.9	9	...	—
TIC 391903064	1	ABDMG	99.3	1	133^{+15}_{-20}	15
TIC 360630575	1	MEL4	95.0	17	23-26	—
TIC 157081737	1	THEIA301	97.9	18	195.0	19
TIC 360156606	1	HSC2523	99.9	1	$7.0^{+4.2}_{-4.1}$	20
TIC 224225541	1	SUN1	99.6	21	204 ± 45	22
TIC 166053959	1	GRX	88.0	23	300 ± 60	24

NOTE—Only the first 30 rows are shown here; the full table is available in the online version of this journal.

References—(1) This Paper, (2) Zuckerman (2019), (3) Luhman et al. (2024), (4) Zuckerman et al. (2001), (5) Malo et al. (2014), (6) Thao et al. (2024), (7) Thao et al. (2024), (8) Gagné et al. (2023), (9) Moranta et al. (2022), (10) Röser & Schilbach (2019), (11) Galindo-Guil et al. (2022), (12) Gagné & Faherty (2018), (13) Zuckerman et al. (2013), (14) Messina et al. (2010), (15) Gagné et al. (2018c), (16) Meingast & Alves (2019), (17) Wood et al. (2023), (18) Kounkel & Covey (2019), (19) Kounkel et al. (2020), (20) Hunt & Reffert (2023), (21) Sun et al. (2023a), (22) Sun et al. (2023b), (23) Tang et al. (2019), (24) Messina et al. (2022).

Table 8. Candidate Age-Calibrated Substellar Objects.

Designation	Spectral Type	Cat.	BANYAN Σ <code>moca_aid</code>	Banyan Σ P (%)	Known Memberships	Distance (pc)	RV (km s $^{-1}$)	Mass (M_{Jup})	Refs ^a
CWISE J053644.83-305539.5	T9.5	new	BPMG	96.8	...	12.9 ± 0.6	...	$1.7_{-0.8}^{+1.4}$	1;1;−;1;2
WISEA J235402.79+024014.1	Y1	reclass.	HSC517	85.2	BPMG,LM	7.7 ± 0.2	...	$2.5_{-1.3}^{+2.0}$	3;1;−;1;4
CWISE J094005.45+523358.7	\geq Y1	new	CARN	50.2	...	17 ± 4	...	$2.8_{-1.6}^{+3.0}$	5;1;−;1;2
WISE J113949.24-332425.1	T7	reclass.	TWA	86.9	BPMG,LM	36 ± 4	...	$3.0_{-1.3}^{+2.2}$	6;1;−;1;4
CWISE J235644.87-481456.7	Y0.5	new	MEL5	93.5	$3.1_{-1.6}^{+2.3}$	5;7;−;−;2
WISEPC J225540.74-311841.8	T8	known	BPMG	92.8	BPMG,HM	13.8 ± 0.7	...	$3.4_{-1.4}^{+2.3}$	8;9;−;1;10
CWISE J213249.12+690113.8	T8.5	new	ARG	96.4	...	(23 ± 3)	...	$3.6_{-1.6}^{+2.2}$	5;2;−;2;2
ULAS J232600.40+020139.2	T8	new	CIC2391	77.4	...	22 ± 2	...	$3.8_{-0.6}^{+1.4}$	11;1;−;1;2
CWISE J201146.50-481259.8	Y0	new	MEL5	94.5	...	14.1 ± 0.7	...	$3.8_{-1.8}^{+2.6}$	5;1;−;1;2
WISE J035000.32-565830.2	Y1	new	CRIUS135	87.8	...	5.67 ± 0.07	...	$3.9_{-2.1}^{+3.7}$	12;1;−;1;2
ULAS J101721.40+011817.9	T8pec	new	ARG	92.6	...	(37 ± 19)	...	$4.3_{-1.7}^{+2.4}$	13;14;−;2;2
WISE J011952.75-450230.8	T8	new	ARG	95.5	...	(21 ± 4)	...	$4.3_{-1.8}^{+2.4}$	1;15;−;2;2
WISE J064723.23-623235.5	Y1	new	OCEMG	93.2	...	10.1 ± 0.2	...	$4.6_{-2.2}^{+3.0}$	16;1;−;1;2
CWISE J053512.02-773828.8	T9.5	new	CARN	98.0	...	(26 ± 9)	...	$4.6_{-2.2}^{+3.0}$	17;7;−;2;2
CWISE J125720.14+715349.2	Y1e	new	OCEMG	95.7	$4.7_{-2.2}^{+3.0}$	17;7;−;2
WISEPC J205628.90+145953.3	Y0	new	CHYA	55.7	...	7.1 ± 0.1	...	$4.9_{-2.5}^{+3.6}$	8;1;−;1;2
51 Eri b	T6.5:	known	BPMG	95.3	BPMG,HM	29.8 ± 0.1	20 ± 2	$5.0_{-1.8}^{+3.0}$	18;19;−;20;21
WISE J233226.49-432510.6	T9	known	ABDMG	99.6	ABDMG,HM	16.4 ± 0.6	...	$5.0_{-2.3}^{+3.0}$	12;1;−;1;10
S Ori J053804.65-021352.5	T5	new	CWNU1057	84.5	...	(92 ± 23)	...	$5.1_{-2.0}^{+3.0}$	22;22;−;2;2
PSO J159.2399-26.3885	T1.5	new	TWA	89.6	...	70 ± 16	...	$5.1_{-1.8}^{+2.5}$	23;24;−;24;2

^aReferences for spectral types, proper motions, radial velocities, distances, and memberships, respectively.

NOTE—Only the first 20 rows are shown here; the full table, which also contains the right ascension, declination, and proper motion columns, is available in the online version of this journal. Distances between parentheses are photometric rather than trigonometric.

References—(1) Kirkpatrick et al. (2021), (2) This Paper, (3) Schneider et al. (2015), (4) Best et al. (2024a), (5) Meisner et al. (2020), (6) Thompson et al. (2013), (7) Marocco et al. (2021), (8) Kirkpatrick et al. (2011), (9) Kirkpatrick et al. (2019), (10) Zhang et al. (2021), (11) Burningham et al. (2013), (12) Kirkpatrick et al. (2012), (13) Burningham et al. (2008), (14) Lawrence et al. (2007), (15) Nidever et al. (2021), (16) Kirkpatrick et al. (2013), (17) Meisner et al. (2020), (18) Rajan et al. (2017), (19) Gaia Collaboration et al. (2023), (20) Gaia Collaboration et al. (2018), (21) Zuckerman et al. (2001), (22) Peña Ramírez et al. (2015), (23) Best et al. (2015), (24) Best et al. (2020).

Table 9. Literature Planetary-Mass Objects which Membership is not Corroborated by BANYAN Σ .

Designation	Spectral Type	Banyan Σ P (%)	Lit. Memberships	Distance (pc)	RV (km s^{-1})	Refs ^a
[AKC2006] 17	L0	1.2	LUP,CM	305 ± 99	...	1;2;−;2;3
2MASS J00464841+0715177	L0 δ	0.0	BPMG,CM	37.8 ± 0.4	-2.8 ± 0.3	4;2;−;2;4
2MASS J01531463-6744181	L3 β	2.2	THA,CM	(25 ± 5)	...	4;5;−;6;4
2MASS J02411151-0326587	L0 γ	1.2	THA,CM	56 ± 7	6 ± 8	7;8;−;8;4
2MASS J04215450+2652315	M8.5	4.9	TAU,CM	9;10;−;−;11
2MASS J04311907+2335047	M7.75	4.6	TAU,HM	168 ± 8	32.3 ± 0.6	9;2;−;2;12
2MASS J04373705+2331080	L0	5.1	TAU,CM	(31 ± 7)	...	9;13;−;6;14
2MASS J06085283-2753583	L0 δ	10.0	COL,LM	44.2 ± 0.3	26.7 ± 0.6	4;2;−;2;4
2MASS J09553336-0208403	L7pec(red)	0.0	TWA,CM	(29 ± 6)	-20 ± 4	15;16;−;6;15
2MASS J10212570-2830427	L5 β	0.0	TWA,CM	(10 ± 2)	...	15;17;−;6;4
2MASS J11472421-2040204	L7pec(red)	6.0	TWA,CM	38 ± 3	7 ± 3	15;18;−;18;19
2MASS J12271545-0636458	M8.5 β	0.1	TWA,CM	39.1 ± 0.5	...	4;2;−;2;4
2MASS J12563961-2718455	L4 β	2.5	TWA,CM	(32 ± 8)	-19 ± 4	15;20;−;6;4
2MASS J16072342-3905099	L1	0.0	LUPIII,CM	$3,161 \pm 1,628$...	21;2;−;2;21
2MASS J16262218-2423523	M8.5	0.0	ROPH,CM	−;16;−;−;22
2MASS J16263252-2426354	M8	0.0	ROPH,CM	−;16;−;−;22
2MASS J16263991-2422334	M8.3	0.0	ROPH,CM	23;16;−;−;22
2MASS J16270592-2418402	L3	5.1	ROPH,CM	(22 ± 4)	...	24;16;−;6;22
2MASS J19350976-6200473	L1 γ	2.7	THA,CM	(31 ± 7)	...	4;25;−;6;4
2MASS J20113196-5048112	L3 γ	9.2	THA,CM	$2,042 \pm 1,315$...	4;17;−;2;4
2MASS J22134491-2136079	L0 γ	0.0	BPMG,LM	48 ± 2	-5 ± 4	7;2;−;2;4
2MASS J22163082+1953167	T3	0.0	BPMG,CM	$1,495 \pm 569$...	26;2;−;2;26
2MASS J22351658-3844154	L1.5 γ	0.0	THA,CM	41 ± 2	...	4;2;−;2;4

^aReferences for spectral types, proper motions, radial velocities, distances, and memberships, respectively.

NOTE—The right ascension, declination, and proper motion columns are available in the online version of this journal. Distances between parentheses are photometric rather than trigonometric.

References—(1) Jayawardhana & Ivanov (2006), (2) Gaia Collaboration et al. (2023), (3) Merín et al. (2008), (4) Gagné et al. (2015), (5) Gagné et al. (2015b), (6) This Paper, (7) Cruz et al. (2009), (8) Liu et al. (2016), (9) Luhman (2023a), (10) Zhang et al. (2018), (11) Luhman et al. (2009), (12) Slesnick et al. (2006b), (13) Schneider et al. (2025), (14) Best et al. (2017), (15) Gagné et al. (2017a), (16) Lawrence et al. (2007), (17) Nidever et al. (2021), (18) Best et al. (2020), (19) Schneider et al. (2016b), (20) Best et al. (2018), (21) López Martí et al. (2005), (22) Wilking et al. (2008a), (23) Geers et al. (2011), (24) Alves de Oliveira et al. (2012), (25) Marocco et al. (2021), (26) Best et al. (2015).